INTEGRATED NEUROVASCULAR COUPLING (NVC) MODEL: AN fNIRS STUDY ON MIGRAINE

by

Selin Taşdöğen

B.S. in Ch.E., Yıldız Technical University, 2005

Submitted to the Institude for Graduate Studies in
Science and Engineering in partial fulfillment of
the requirements for the degree of
Master of Science

Graduate Program in Chemical Engineering

Boğaziçi University

2007

ACKNOWLEDGEMENTS

I wish to express my deepest gratitude to my supervisor, Prof. Dr. Kutlu Ülgen, for her guidance and hospitality giving me the opportunity to do my thesis work under her supervision. Her everlasting enthusiasm and open mind have definitely encouraged me to complete this work. I owe my warmest thanks to Assist. Prof. Ata Akın, my co-supervisor, for his invaluable patience when I was stuck at dead-ends. Without his expert support and inspiration, this study would have been much harder and taken longer.

I also owe my sincere thanks to Burak Parlak, whose endless support and help in various technical matters and computer related problems has been of great value. I thank my dearest colleagues and lifetime partners, Elif Dereli and Arzu Uyar.

The last but not the least, I would like to thank my family for encouraging me to study and their strong belief on me. Without them I could never keep my calm in the hardest days and nights. This thesis is dedicated to them.

ABSTRACT

INTEGRATED NEUROVASCULAR COUPLING (NVC) MODEL: AN fNIRS STUDY ON MIGRAINE

Functional imaging techniques play a major role in monitoring the changes in brain hemodynamics. Migraine is one of the weirdest illnesses that have ever been described. It does not leave any symptom in patients like the other illnesses do, e.g. cancer. The most common symptom observed in migraine patients by the imaging techniques is the change in the brain hemodynamics. The existing mathematical model, Balloon Model, is described only for the hemodynamic changes in the venous compartment of the blood vessels in brain and it is thus not enough to describe the whole hemodynamic changes. The goal of this study was to improve the previous studies describing the venous compartment of the brain blood vessels by adding the arterial compartment hemodynamic changes as well as by integrating the CO_2 kinetics into these models. The partial pressure of CO_2 is the main parameter influencing cerebral blood flow, CBF, and was used as the input function since it is the driving force in the brain hemodynamics. Because the arterial compartment is rich in HbO_2, the oxygen kinetics was also modeled and integrated to Balloon model. The present integrated modeling of brain hemodynamics enables us to understand the facts underlying the migraine illness and its pathophysiology clearly.

ÖZET

ENTEGRE NÖROVASKÜLER EŞLEŞME MODELİ: MİGREN HASTALIĞI ÜZERİNE BİR fNIRS ÇALIŞMASI

İşlevsel görüntüleme teknikleri, beyin hemodinamiği değişiminin görüntülenmesinde önemli bir rol oynamaktadır. Migren şu ana kadar tanımlanan hastalıklar arasında en anlaşılmaz olanlardan biridir. Hastalarda diğer rahatsızlıklar, kanser vb gibi belirtiler bırakmaz. Görüntüleme teknikleri sayesinde migren hastalarında görülen ortak belirti beyin hemodinamiği değişimidir. Daha önce oluşturulan Balon Modeli ile beyindeki sadece toplardamar kısmının hemodinamik değişiminin modellenmiş olması bu modeli tüm hemodinamik değişimin tanımlanması açısından yetersiz kılmıştır. Bu çalışmanın amacı, daha önce beyin kan damarlarının toplardamar kısmı için tanımlanan modelin atardamar kısmının da eklenerek tamamlanması ve CO_2 kinetiğinin de bu modele entegrasyonudur. CO_2'in kısmi basıncının beyin hemodinamiğinde sürücü kuvvet olması nedeniyle, bu verinin giriş fonksiyonu olarak önemi bulunmaktadır. Atardamar kısmının HbO_2'ce zengin olması nedeniyle O_2 kinetiği incelenerek Balon Modeli'ne entegre edilmiştir. Bu tez çalışması kapsamında geliştirilen nörovasküler eşleşme modeli kullanılarak, beyin hemodinamiğinin modellenmesiyle birlikte migren hastalığının altında yatan gerçekler ve hastalığın patofizyolojisinin anlaşılabilmesi mümkün olmaktadır.

TABLE OF CONTENTS

LIST OF FIGURES

LIST OF TABLES

1. INTRODUCTION

Migraine is a neurovascular disorder, believed to affect nearly 12 per cent of the world's population. Migraine decreases the life quality of the patients drastically by knocking them out during attacks and forces them to restrict their daily activities between the attacks such as exercising, working, eating and sleeping in a way to avoid more frequent attacks. The disabling property of migraine also costs billions of dollars of economical loss to countries annually. Therefore, accurate diagnosis and treatment of migraine is important, which is only possible by understanding its dynamics [31].

This study aims to understand and explain the facts underlying the pathophysiology of migraine by identifying differences between a healthy subject's brain hemodynamics and a migraineur's (ST's data). It is intended to integrate the CO_2 kinetics into the conventional model, Balloon Model, which lacks the modelling of the arterial blood flow. Furthermore, a sensitivity analysis is also performed to show how the function parameters affect the integrated Neurovascular Coupling (NVC) Model. In addition to this the trapezoidal function time values are analyzed by ANOVA, which compares the means of two or more groups of data returning the p-value for the null hypothesis that the means of the groups are equal. A possible use of distinguishable parameters for migraineurs and healthy subjects will lead to migraine diagnosis. Although migraine has very unique symptoms, several test are applied before diagnosing a person with migraine in order to rule out a secondary headache causing migraine-like complaints which are not rare. These tests include general physical and neurological exams and for suspicious cases very expensive laboratory and radiological tests. Thus data from cerebrovascular dynamics confirming that a patient has migraineous response may at least decrease the need for costly examinations.

In chapter 2, a theoretical background about migraine are discussed in detail explaining the pathophysiology of migraine and the common theories of migraine pathogenesis including the symptoms and the phases of the illness. Furthermore, the

modeling approaches on the hemodynamic response and oxygen kinetics in the brain and finally the results in the literature are mentioned.

In chapter 3, the simulation process of NVC model is mentioned beginning from the collection of the data and ending up at the integration of oxygen and CO_2 kinetics into the conventional Balloon Model.

In chapter 4, the results of the conventional and integrated NVC model are explained with the figures which are followed by two analyses on the results (Sensitivity and ANOVA analysis) to compare the healthy subject's data with the migraineur's. Finally, the parameters underlying the migraine illness are discussed.

Chapters 5 gives the conclusions and puts forward some recommendations to give a new perspective for the improvement of the existing model and to get more precise and more close results to the normal behaviour of the brain hemodynamics.

2. THEORETICAL BACKGROUND

1. Migraine Pathophysiology

Although it is known to be mostly insensate, the brain has a pain system to signal tissue injury like other organs. It has been suggested that it is theoretically possible for all individuals to suffer a migraine attack. The occurrence and frequency of attacks in any individual will be governed by the sensitivity of their central nervous system to migraine specific triggers (e.g. certain foods, hormones, changes in levels of stress, consciousness and even exposure to light, sound and smell). It has been hypothesized that genetic abnormalities result in a lowered threshold of response to these specific trigger factors in migraineurs. The trigger factors can thus be conceptualized as modulators of the genetic set point that predisposes to migraine. Conversely, in normal individuals, who lack genetic deficits relevant to migraine, exposure to the same trigger factors would not breach the 'migraine threshold' and so an attack would not be initiated. It is possible that the abnormal hyperresponsivity of the brain of migraineurs, like familial hemiplegic migraine (FHM, type 1 indicates the point mutations in the Ca 2.1 channel whereas type 2 patients express mutations in the α subunit of the Na^+ ,K^+ pump [1]), may be a consequence of genetic abnormalities in ion channels that regulate neuronal excitability [2]. That sensitivity causes some scientists to identify migraine with a smoke alarm that will reliably wake a sleeping family in the event of any fire, giving false alarms every time the toast burns [3].

Migraine patients are characterized by increased amplitudes and reduced habituation of the contingent negative variation (CNV) response, especially before a migraine attack. Migraine provoking and precipitating agents can cause CNV abnormalities. However, it is unclear whether the temporal relation to the migraine attack determines how the brain reacts to a migraine precipitant. Experimentally induced achievement stress, one of the typical precipitants for migraine, was examined for its

effects upon the CNV response (Table 2.1). CNV was recorded during conditions of rest and stress, both before and after a migraine attack, as well as during a headache-free interval. The neurophysiological reactivity to stress in migraineurs was compared with those of healthy subjects. Before a migraine attack, migraine patients demonstrated significantly more pronounced neurophysiological reactivity to stress: the amplitude of the early CNV component was more increased and its habituation was more reduced in the stress condition, especially 1–3 days before an attack compared with changes of CNV amplitudes and habituation under stres obtained after an attack, during the headache-free interval, or in healthy controls. The study demonstrates that the brain of migraine patients is characterized by increased susceptibility to migraine provoking agents before an actual attack [4].

Table 2.1. CNV amplitudes and characteristics of the early CNV habituation (slope of habituation as a regression coefficient *a)* in migraineurs and healthy controls and for the rest and stress conditions [4].

	Before an attack		After an attack		During the interval		Healthy subjects	
	Rest	Stress	Rest	Stress	Rest	Stress	Rest	Stress
Total CNV (μV)	−8.9 ± 4.5	−16.2 ± 5.2	−11.7 ± 8.1	−12.5 ± 6.9	−9.2 ± 4.9	−13.8 ± 8.7	−6.1 ± 5.9	−10.8 ± 5.7
Early CNV (μV)	−11.3 ± 4.4	−17.4 ± 5.1	−12.6 ± 7.4	−12.9 ± 6.9	−10.6 ± 6.9	−13.7 ± 7.8	−6.2 ± 5.4	−9.8 ± 5.1
Late CNV (μV)	−9.5 ± 8.1	−19.4 ± 8.5	−14.4 ± 12.4	−15.2 ± 10.8	−11.1 ± 6.1	−16.4 ± 12.4	−9.5 ± 10.1	−16.6 ± 9.0
PINV (μV)	−0.9 ± 8.6	−6.9 ± 11.2	−7.0 ± 11.7	−3.4 ± 13.9	−1.5 ± 6.5	−4.6 ± 8.4	−1.3 ± 14.2	−3.5 ± 10.9
RT (ms)	294.8 ± 97	205.4 ± 52	291.6 ± 102	224.6 ± 59	249.8 ± 51	199.9 ± 47	259.9 ± 48	187.1 ± 41
Habituation (*a*)	0.04 ± 1.1	1.3 ± 1.5	0.39 ± 1.1	0.13 ± 1.2	0.26 ± 1.6	0.18 ± 1.3	−0.38 ± 1.4	−0.53 ± 1.4

Although exact mechanisms underlying migraine remain uncertain, several theories have been proposed. Various facts and observations about the disease acquired from both migraine research and clinical experiences have been the starting point for these hypothesis. Some essential information about migraine gathered by these studies and widely used by scientists to form hypothesis are the following [32] :

- Dietary, sleep, and hormonal changes can trigger a migraine.

- Migraine has a circadian rhythm similar to several diseases of vasoconstriction, such as myocardial infarction, angina pectoris, and ischemic stroke.
- Sleep is effective in aborting many migraines.
- Cerebral blood flow (CBF) is decreased during migraine aura.
- Both generalized systemic vasoconstriction and local cerebrovascular vasodilatation occur on the side where head pain occurs.
- Platelets release serotonin during a migraine attack.
- Levels of calcitonin gene-related peptide (CGRP), and probably substance P, are elevated during a migraine attack.

Some migraine models use the following concepts to explain the above phenomena:

- Similar to other internal organs, the brain has a pain system to signal tissue injury. The trigeminovascular system acts as a warning system, causing migraines to help "protect" the brain against insults such as ischemia, toxins, and intrinsic disease, just as angina pectoris "protects" the heart against ischemia.
- Neuronal and chemical activators – including prostaglandins, serotonin, and histamine – can stimulate the trigeminal nerve. Migraine triggers work either directly to alter these chemical mediators (e.g., fluctuating estrogen levels altering prostaglandins during menses), or indirectly through neural mediators (e.g., rapid eye movement [REM] sleep eliminating serotonin release from the dorsal raphe nucleus).
- When stimulated, the trigeminal nerve releases substance P and CGRP into dural and meningeal blood vessels. The release of substance P causes the degranulation of mast cells and the attraction of polymorphonuclear leukocytes. This leads to mast cell release of histamine and platelet release of serotonin, with consequent vasodilatation and exudation of plasma into the tissues. The resulting inflammation and swelling of the blood vessels represents the so-called sterile arteritis.
- The neurogenic inflammation and release of substance P causes both distention of cranial arteries and headache pain. It is likely that nitric oxide mediates the vasodilatation and may also act as a nociceptive neurotransmitter.
- Trigger factors either have direct actions on vasomotor tone (e.g., tyramine in certain foods) or mediate neurochemical release (e.g., sleep alters serotonin release from the

dorsal raphe nucleus; stress modifies catecholamine levels). Platelet changes, neurochemical mediators, and ischemia can also trigger the trigeminovascular system.

- Increases in platelet activity and catecholamine levels and in serotonin release from the dorsal raphe nucleus occur in early morning. Because these changes may trigger the trigeminovascular system, either directly or through ischemia, this might at least partially explain the circadian rhythm of migraine.
- Rapid eye movement (REM) sleep inhibits the release of serotonin from the dorsal raphe nucleus, and sleep may abort a migraine attack by inhibiting the serotonin-mediated stimulation of the trigeminovascular system.

2.2. Common Theories of Migraine Pathogenesis

Although not observed exactly by every migraineur, a migraine episode generally has four phases; the *prodrome,* the *aura,* the *attack* and the *postdrome*.

Even the *prodrome phase* occurs hours or even days before the headache begins, it is considered to be an integral component of the migraine process. It often acts as a warning sign that a migraine is imminent. About 60 per cent of people with migraine experience prodromal symptoms.

Typical symptoms can include:

Physical symptoms:

- Muscle stiffness, especially in the neck
- Altered perception of heat and cold
- Increased thirst
- Increased urination
- Food cravings
- Loss of appetite
- Yawning

- Constipation
- Diarrhea
- Fluid retention
- Sensitivity to light and/or sound

ii. Psychological symptoms:

- Depression
- Euphoria
- Irritability
- Restlessness
- Hyperactivity
- Fatigue
- Drowsiness
- Difficulty in concentration

Some patients are not always aware of these symptoms or may mistake them for migraine 'triggers'. A migraine diary (simple but effective migraine management tool that involves patients in their own care) can help patients discover their prodromal symptoms, thus giving them valuable time to prepare for the later stages of the attack [34].

The prodrome is followed by the *aura* phase, which involves the occurrence of one or more fully reversible focal neurological symptoms. It is experienced by about 20 per cent of migraine sufferers although not all patients with migraine with aura will experience the aura symptoms with every attack. This phase occurs just before the attack phase begins but in some patients, the aura phase can overlap with the later attack phase. Aura usually develops over 5-20 minutes and lasts for up to 1 hour. Aura symptoms are most commonly visual, though they can also be sensory or, more rarely, motor. The aura is generally associated with an electrical depolarization called 'Cortical Spreading Depression (CSD)' which will be mentioned later.

Aura symptoms include:

- Scintillation scotomas, e.g. bright rim around an area of visual loss (fortification spectra), flashing lights, jagged lines that block the visual field
- Visual resizing or reshaping of objects
- Blurred vision
- Unilateral sensory parasthesia that usually begins as numbness in the hand and migrates up the arm before moving into the face, lips and tongue
- Muscular weakness
- Partial paralysis on one side of the body
- Temporary dysphasia

The *attack (headache)* phase is the most disabling feature of a migraine attack and is the most common reason for consultation. Typically, the following characteristics apply:

- Headache lasts from 4-72 hours and causes moderate or severe pain.
- It is usually gradual in onset.
- It is throbbing, pounding or pulsating in character, although it may begin as a mild non-throbbing headache.
- It is unilateral in 70-80 per cent of patients (but can alternate from one side to the other in different attacks).
- It can be exacerbated by routine physical activity.
- It extends from the periorbital and frontal areas backwards to the temporo-parietal and occipital regions and can sometimes extend to the shoulder area.
- It frequently is present on awakening in the morning.

However, the headache is almost always accompanied by other symptoms, which generally intensify along with the headache (Figure 2.1):

- Nausea accompanies the headache in 70-90 per cent and leads to vomiting in 20-50 per cent.
- Vomiting may occur early or late in the headache phase and when it occurs after the headache is well established, it may result in a precipitious easing of the headache.

- Photophobia, phonophobia and osmophobia lead patients to seek seclusion in a dark, quiet room.
- The neck of the patient gets stiff or tender.
- Other possible symptoms during this phase can include blurry vision, diarrhea, abdominal cramps, facial pallor, sensations of heat or cold and localised edema of the scalp, the face, or the periorbital regions. Cranial autonomic symptoms such as nasal congestion, rhinorrhea, and lacrimation can also occur [34].

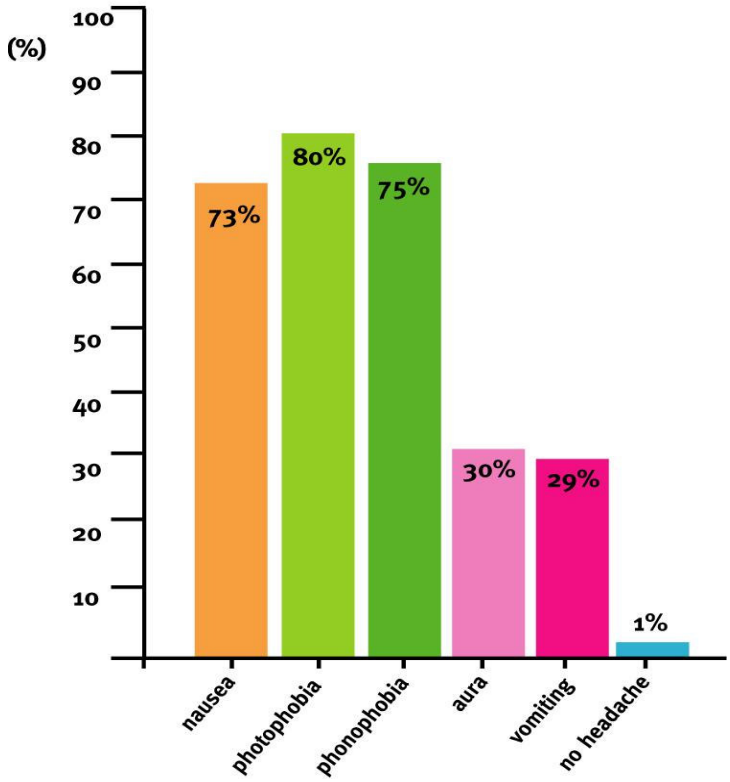

Figure 2.1. Migraine associated symptoms [32].

Some physicians can add a different phase between the attack (the headache) phase and the postdrome phases, the *resolution* phase. How migraine eventually resolve is still a mystery. Most of the time migraine resolves with sleep and an important brain communication chemical, serotonin, is restored in the brain and surrounding tissue.

Occasionally, and especially in children, vomiting will stop a migraine. This may be due to a release of serotonin that is stored in the intestinal track. Rarely, migraines terminate during an intense emotional response; seemingly during an emergency, the brain draws from its reserves to let the person manage the situation [34].

The *postdrome* phase is the phase, during which patients usually feel exhausted and mentally foggy for a while [32], but start to recover and crave for food [31, 5]. This phase consists of lingering symptoms that resemble a hangover or flu-like symptoms. Though not universally present, postdromes generally follow migraines that are long in duration. Common symptoms of a postdrome include fatigue, poor concentration, irritability, queasy stomach, and tender muscles [35].

Theories on the pathogenesis of migraine include:

- The Vascular Theory
- The Cortical Spreading Depression (CSD) Theory
- The Neurovascular Hypothesis
- The Serotonergic Abnormalities Hypothesis
- The Integrated Hypothesis

2.2.1. The Vascular Theory

H. Wolff developed the vascular theory of migraine pathogenesis during the 1940s and 1950s. According to this theory, migraine is a vasospastic disorder that is initiated by vasoconstriction in the cranial vasculature. The vasoconstriction stage appears to be associated with migraine aura.

Following the early vasoconstrictive stage, intracranial or extracranial blood vessels dilate. Whereas most of the brain is insensitive to pain, meningeal blood vessels show a high level of innervation. Thus, blood vessel dilatation activates the trigeminal sensory nerves that surround the meningeal blood vessels, causing pain. Activation of trigeminal nerves also causes the release of vasoactive neuropeptides that further contribute to dilatation and worsen pain.

Studies have documented the occurrence of oligemia during the aura phase of a migraine, and an increase in blood flow during the headache phase. Moreover, when a patient with a headache is given a vasodilator such as a nitrate, the headache intensifies, whereas when a patient is given a vasoconstrictor such as a 5-HT agonist, the headache is usually alleviated. These studies lend support to the vascular theory.

However, some researchers have questioned whether the measured decreases in CBF during the aura phase are sufficient to cause the aura symptoms (e.g., visual disturbances) that some migraineurs experience. Furthermore, vasodilatation alone cannot explain the local swelling and tenderness of the head that generally accompany migraine [31].

The development of new technologies allow scientist to investigate the vascular dynamics and the long standing theory more closely. Research has shown that during a migraine attack without aura, there are in fact only minor changes in cerebral blood flow, and the proposed initial vasoconstrictive phase may actually last several hours longer than the aura. It is also hypothesized that migraine sufferers have an inherent vasomotor instability and are more susceptible to the vasodilatory effects of certain chemical and physical agents [6]. Moreover, the vascular theory remains incapable of explaining the local swelling and tenderness of the head by only vasodilatation [31].

2.2.2. The Cortical Spreading Depression (CSD) Theory

Cortical spreading depression (CSD) is a relatively short-lasting wave of depolarization that spreads across the surface of the brain, moving from the back (occipital region) of the cerebral cortex toward the front at about 3-5 mm/minute (Figure 2.2). This electrical phenomenon can be induced in animals with noxious stimuli, and is frequently referred to in the literature as the “spreading depression of Leao.”

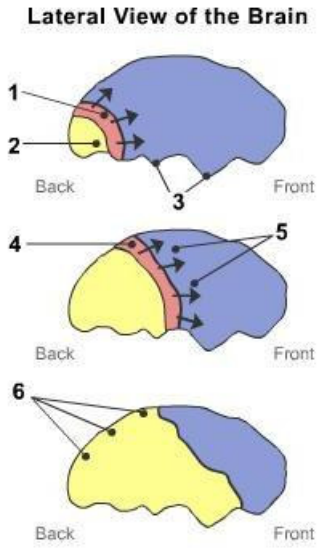

Figure 2.2. CSD (1) Spreading wave of cortical hyperexcitability, (2) CSD area suppressed neurological activity trailing the wave, (3) Area of normal brain activity, (4) Progression of the wave, (5) Expansion of the CSD area, (6) Area of CSD progressed from the occipital lobe, until terminated [7, 8].

According to the theory, CSD begins with a brief wave of excitation, followed by a prolonged period of neuronal depression, which is associated with disturbances in nerve cell metabolism and regional reductions in blood flow. It has been suggested that migraine aura results from this spreading depression that suppresses neuronal activity as it passes forward over the cerebral cortex. During migraine without aura, cerebral blood flow abnormalities usually are not seen, but recent data suggest that this may not always be the case.

Although CSD has been demonstrated only in animals, support for the CSD theory comes from observations that, in patients who have migraine with aura, a gradual spread of reduced blood flow that mimics the rate of progression of CSD in animals can be measured during the aura phase. One researcher who mapped his own scintillation scotomas (white hallucinations) noticed a relationship between the development and spread of the visual disturbance and the organization of the visual cortex of the brain. Thus, the aura symptoms

were consistent with a wave of intense excitation developing in the visual cortex, followed by a longer period of inhibition.

Wolf et al. [9] demonstrated Near Infrared Spectroscopy (NIRS) for the first time as capable of noninvasive on-line detection of CSD in the pentobarbital-anesthetized rat. CSD was accompanied by a brief and rapid increase of regional CBF (by laser-Doppler flowmetry) to 200-400 per cent baseline (Figure 2.3).

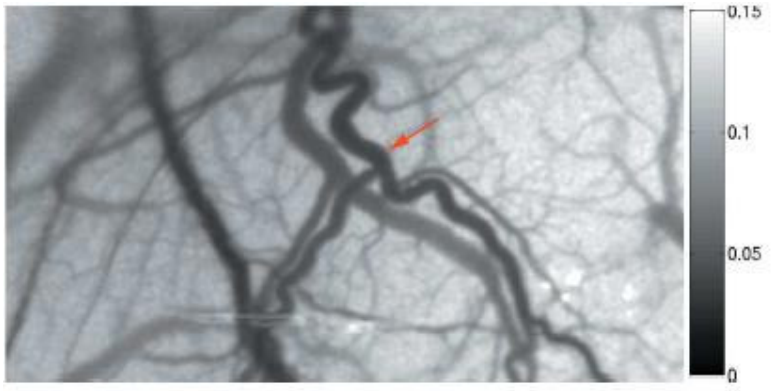

Figure 2.3. Spackle, contrast image demonstrating the spatial flow heterogeneities across the imaged area at a single time illustrating middle meningeal artery (MMA) and associated dural vein plus pial vessles and cerebral cortex. The darker values correspond to higher blood flow [10].

NIRS demonstrates that this hyperperfusion is associated with concentration increases of oxyhemoglobin, while deoxyhemoglobin decreases. Simultaneously, oxygen partial pressure, measured on the brain surface with a solid-state polarographic probe, was shown to be raised by at least 14 mm Hg during CSD. Oxygen-dependent phosphorescence life-time quenching measurements confirmed this finding. NIRS data on cytochrome aa3, however, showed a CSD-related shift toward a more reduced state, despite raised blood oxygenation. This may suggest either limited O_2 transport from the blood to mitochondria or decreased oxygen utilization during CSD as supposed by theories about compartmentalization of energy metabolism favoring glycolytic rather than aerobic energy supply during CSD. During most CSD episodes, a brief decrease in mean arterial blood

pressure (MABP) by 4-8 mm Hg was noted that might be caused by functional decortication during CSD [9].

2.2.2.1. Comparison Between Migraine Aura and Cortical Spreading Depression

Migraine auras are usually visual, apparently starting in area 17, i.e. the part of the brain with the highest neuronal density (Figure 2.4). This is consistent with the observation that CSD is much easier to elicit in brains with a high neuronal density. Functioning glial cells tend to decrease the probability of successful elicitation of a CSD. Both the migraine aura and CSD propagate along the cortical surface. Both tend to become extinct for reasons it is not yet understood. It is important that CSD tends to become extinct when propagating into a sulcus. The rate of spread of the migraine aura is usually 2±6 mm/min, while the rate of spread of CSD is variable, especially in gyrencephalic animals. CSD, as well as the aura, tends to be restricted to one hemisphere, both can repeat themselves, and both are accompanied by a transient neurological deficit [8].

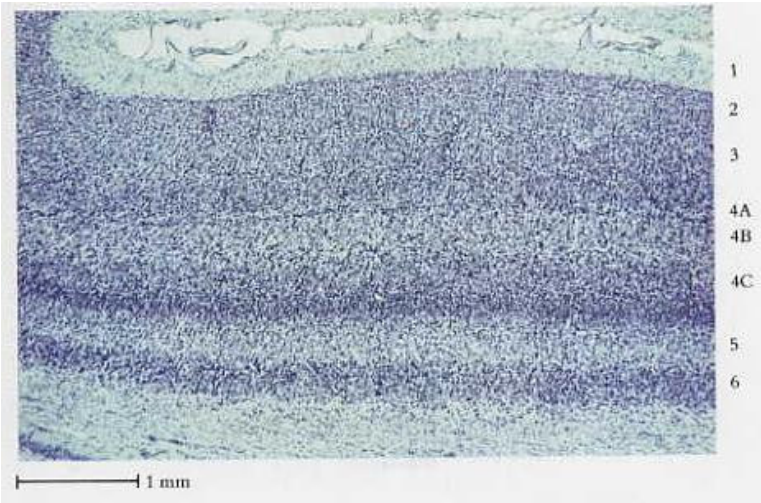

Figure 2.4. Area 17 of a macaque monkey's brain. A cross section of the striate cortex taken at higher magnification shows cells arranged in layers. Layers 2 and 3 are indistinguishable; layer 4A is very thin. The thick, light layer at the bottom is white matter.Layering pattern here is partly the result of variations in the staining and packing density of these cells. Layers 4C and 6 are densest and darkest; layers 1, 4B, and 5 are most loosely packed [36].

2.2.3. The Neurovascular Hypothesis

Fibers from the trigeminal nerve innervate blood vessels in the meninges, the extracranial arteries, and those in the circle of Willis. These nerve fibers contain nociceptors that are capable of generating pain impulses, and the endings of these nerve fibers contain peptide neurotransmitters (Figure 2.5).

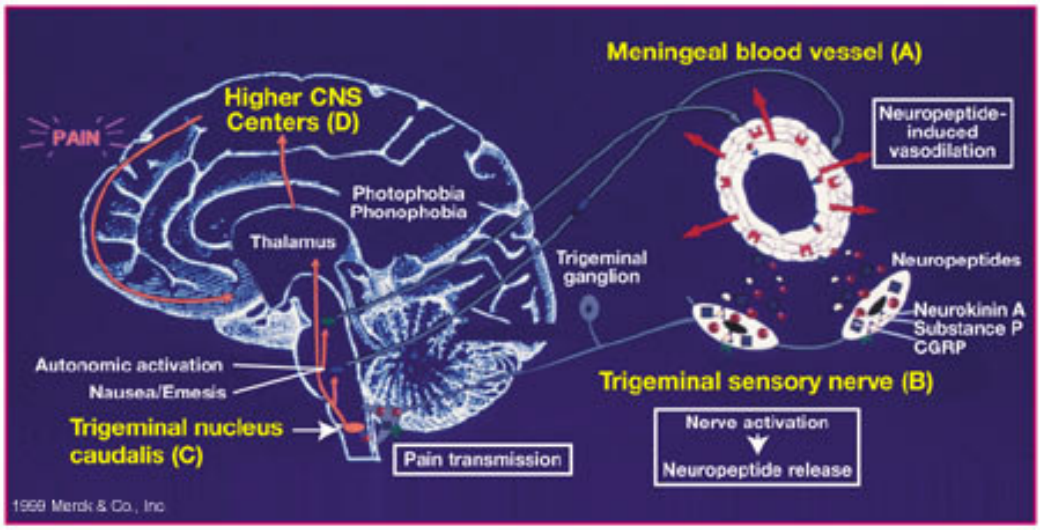

Figure 2.5. The trigeminovascular theory [32].

The neurovascular hypothesis proposes that either migraine triggers or CSD can activate trigeminal nerve axons, which then release neuropeptides (such as substance P, neurokinin A, and CGRP) from axon terminals near the meningeal and other blood vessels. Substance P and neurokinin A cause vasodilatation and promote the extravasation of plasma proteins and fluid from nearby meningeal blood vessels. Although CGRP does not promote plasma extravasation, it is a potent vasodilator. Together, these neuropeptides produce an inflammatory response in the area around the innervated blood vessels. This response is termed sterile neurogenic perivascular inflammation.

The neuropeptides may also sensitize nerve endings, providing a mechanism for sustaining the headache. When activated, the trigeminal nerve also transmits pain impulses

to the trigeminal nucleus caudalis, which relays pain impulses to higher centers of the brain.

According to the neurovascular theory, vasodilatation is not the cause of migraine headaches but is an accompanying phenomenon attributable to trigeminal nerve activation. Although the cause of this activation is not known, it may be due to ionic and metabolic disturbances in brain function, such as those associated with CSD. It has also been proposed that abnormal activity in brain stem sensory nuclei may cause antidromic activation of trigeminal sensory pathways.

2.2.4. The Serotonergic Abnormalities Hypothesis

Observations that both plasma and platelet levels of serotonin fluctuate during a migraine attack suggest that serotonin may be involved in the pathogenesis of migraine. When platelets are activated, they aggregate and release serotonin, thus increasing the plasma serotonin level. An increase in plasma serotonin level would be expected to cause vasoconstriction, whereas a decrease in serotonin would promote vasodilatation.

Platelet serotonin levels may drop precipitously during the headache phase of migraine. Also, urine levels of serotonin and its metabolites rise during headaches, suggesting that there is a large release of serotonin during such attacks. Moreover, drugs such as reserpine that cause the release and depletion of serotonin from tissue storage sites may precipitate migraine headaches.

An initial surge in plasma serotonin levels may cause constriction of cerebral blood vessels and a reduction in cerebral blood flow. If the blood flow is sufficiently reduced, migraine aura may result. A subsequent depletion and drop in serotonin levels may then lead to a marked dilatation of extracranial and intracranial arteries, precipitating migraine pain.

Several questions regarding the serotonin abnormalities hypothesis remain unanswered. It seems unlikely that changes in blood serotonin levels are solely responsible for the development of migraine. For instance, global changes in plasma serotonin levels do not explain the unilateral nature of migraine pain, and serotonin levels in patients with migraine may remain depressed long after the headache has resolved. It may be, however,

that changes in plasma serotonin levels reflect more important disturbances in brain serotonin levels.

One brain stem structure that has a high concentration of serotonin receptors is the dorsal raphe nucleus. This nucleus contains many serotonin-secreting neurons that terminate on cerebral blood vessels and various other brain areas that are involved in the production of migraine symptoms. It has been suggested that the raphe nucleus, which is responsive to changes in serotonin levels, may serve as a "migraine generator" [32].

2.2.5. The Integrated Hypothesis

The integrated hypothesis of migraine pathogenesis is an attempt to consolidate various theories and explain several observations related to migraine pain. According to this theory, triggers such as stress, glare, noise, the patient's internal clock, the dilatation of the internal or external carotid arteries, or other factors may activate specific centers in the brain stem.

One such center, the locus ceruleus, causes changes in epinephrine levels. Another center, the dorsal raphe nucleus, affects serotonin levels in the brain.

Constriction of cerebral blood vessels may cause a localized deficiency in blood flow, provoking CSD, which may, in turn, stimulate trigeminovascular fibers, eliciting neurogenic inflammation and headache pain.

Nerve fibers from the locus ceruleus, the dorsal raphe nucleus, and the trigeminal nerve cause a stimulation of cranial nerves that dilate both cerebral and extracranial blood vessels. The dilatation of meningeal vessels contributes to pain generation.

The locus ceruleus also sends fibers to higher centers of the cerebral cortex, where it influences a person's state of arousal and awareness, and descending projections interact with the body's pain control mechanisms.

Likewise, the dorsal raphe nucleus sends multiple fibers to blood vessels and upward toward the cerebral cortex. These serotonin-secreting fibers help regulate sleep and neuroendocrine functions. Other connections are made with lower brain stem areas and with the hypothalamus.

A disruption in the normal function of the hypothalamus may be responsible for prodromal signs and symptoms of migraine such as mood changes, food cravings, drowsiness, thirst, and yawning. These signs and symptoms may occur several hours, or even as long as 1 day, before headache pain begins [32].

2.3. Experimental Characterization of Hemodynamic Response

In recent years many NIRS studies have demonstrated that cerebral hemodynamic changes associated with functional brain activity can be assessed noninvasively in adult human subjects. It can capture cerebrovascular changes in the surface of the cortex. Functional Near Infrared Spectroscopy (fNIRS) can potentially detect and track cerebrovascular changes, called BOLD signals, by the use of optical methods. Similar to fMRI, fNIRS is sensitive to Hb while complimentarily it can measure the changes in oxyhemoglobin (HbO_2) [17].

Several types of brain activity have been studied, including motor activity, visual activation, auditory stimulation, and the performance of different cognitive tasks [18].

A temporal behavior model for human mental operation was presented as cerebral multi-phasic sustained response (CMSR) using fMRI. This CMSR indicates that different cerebral regions have differing temporal behavior of activation after a task period. Recently, this physiological behavior was observed in the language and visual system. In 1999 Kato et al. [37] developed the principal method of human functional spectroscopy using the scattering light NIR (lNIR). In this study, they tested the hypothesis that CMSR can observe a single-word speaking trial using lNIR which the output signals prove the relation between the HbO_2 and oxygen concentration (Figure 2.6).

Experimental characterization of the hemodynamic response is based on numerous experimental studies of the BOLD and CBF responses to brain activation, the followings are the key findings that motivate the modeling:

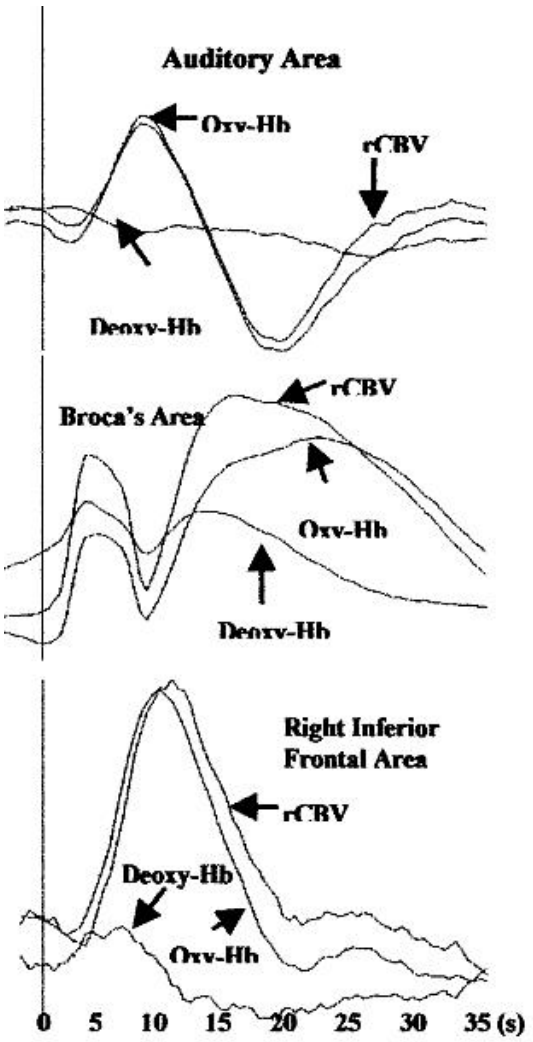

Figure 2.6. Kato's single-word speaking word trial [37].

1. CBF increases much more than $CMRO_2$ with brain activation, producing a reduction of the net cerebral oxygen extraction factor (E) and the total Hb present in an image voxel. This phenomenon is the primary cause of the BOLD signal change.

2. The CBF and BOLD responses to even a very brief stimulus are delayed by 1–2 seconds and have a temporal width on the order of 4–6 seconds. For a sustained stimulus of 20 seconds or longer, the response typically reaches a plateau value, although there can be substantial variation (e.g., an initial overshoot, a slow ramp, or an overshot at the end of the stimulus).

3. A post-stimulus undershoot of the BOLD signal is common and may last for 30 seconds or more, with longer duration stimuli tending to have longer post-undershoots. The CBF response typically shows only a shorter and weaker post-stimulus undershoot, or none at all [14].

4. Some investigators have reported an initial dip of the BOLD signal lasting 1–2 seconds before the standard BOLD signal increase, and a corresponding transient increase of Hb has been reported in optical imaging studies. The effect is small and not always present, but it has stirred interest because it may reflect a rapid increase of $CMRO_2$ before the CBF increase, and this phenomenon may be better localized to the area of increased metabolism (i.e., the CBF increase may cover a wider area).

5. The BOLD response typically exhibits a temporal nonlinearity such that an appropriately shifted and added response to a brief stimulus over-predicts the true response to an extended stimulus. This temporal nonlinearity is most pronounced when the brief stimulus is less than about 4 seconds and the extended stimulus is longer than 6 seconds. Comparing short and long duration stimuli that are both longer than about 4 seconds, the temporal nonlinearity is reduced.

6. Nonlinearity has also been reported as a "refractory period", such that two identical stimuli presented close together in time produce a net response with less than twice the integrated response of a single stimulus alone.

7. There is a growing body of evidence suggesting that the baseline CBF can have a strong effect on the magnitude of the BOLD response to the same stimulus. For example, if baseline CBF is increased by breathing CO_2, the BOLD response to the same task is reduced substantially. Interestingly, however, the CBF change (ΔCBF) appears to remain the same despite the baseline change. Similar results have been found with injection of acetazolamide, a carbonic anhydrase. Carbonic anhydrase catalyzes the conversion of CO_2 to bicarbonate ions, which increases the carrying capacity of the blood for removing CO_2. Inhibiting this enzyme may lead to increased CO_2 concentration in the brain, so the mechanism of action for increasing CBF may be the same as for CO_2 itself [16].

2.4. Modeling Approaches on the Hemodynamic Response and Oxygen Kinetics in the Brain

2.4.1. Modeling of the Brain Hemodynamic Responses

Lauritzen et al. [11] studied the regulation of the regional cerebral blood flow (rCBF) during and between the migraine attacks and concluded that regional blood flow increase in response to physiological activation was severely impaired in the hypoperfused brain areas, whereas neighboring normally perfused regions reacted normally. Confinement of the regulation abnormalities to the area of the oligemia supported their suggestion that the blood flow changes are caused by a change in local metabolism (hyperventilation, hypertension, and physiological activation tests). Between attacks of migraine, the patients had normal brain blood flow and regulation of brain circulation.

Several studies have reported changes in cerebrovascular reactivity during the interictal period of migraine. To characterize mechanisms of migraine, changes in total hemoglobin $(Hb)_T$ are compared with regional oxygen saturation (O_2^{sat}) of the right and left frontal lobes in response to intracranial pressure changes during the interictal period of migraine [12].

As the methods for measuring hemodynamic responses became more sophisticated with good time resolution, in particular as the functional magnetic resonance imaging (fMRI) technique was increasingly used as a means of inferring changes in neural activity, dynamic modeling of the hemodynamic responses became increasingly important as it could be used to uncover the neural signal which underlies the blood-oxygen-level-dependent (BOLD) signal as measured by fMRI. One of the first dynamic models linking the hemodynamic responses to neural activity was developed by Friston et al. (2000) [13]. They used (i) the Balloon/Windkessel model [14] which was a dynamic model linking normalised cerebral blood volume (CBV) to normalised CBF in the venous compartment, (ii) a second order linear dynamic system linking normalised CBF to stimulation, (iii) a conservation equation for the normalised deoxyhemoglobin in the venous compartment, and (iv) the steady state relationship between the oxygen extraction factor (OEF) and normalised CBF [14]. These were combined to produce a fourth order nonlinear dynamic system linking the normalised deoxyhemoglobin (Hb) in the venous compartment to

stimulation. Finally, a static nonlinear function was used [14] to link the normalised Hb and CBV to the BOLD signal.

Instead of using normalised quantities, a dynamic model using absolute quantities for the hemodynamic responses was used similar to the steady state model of Vafaee and Gjedde's Model. The model made full use of the oxygen diffusion equation, including nonzero tissue oxygen concentration. Hill's equation (1910) was used, and the dynamic equations were solved numerically to yield time series for cerebral oxygen metabolic rate ($CMRO_2$) as well as venous Hb in response to changes in CBF. The effects of the assumption of exponential decay of oxygen along the capillary was also examined [14,15].

Most, if not all, of the existing hemodynamic models assume either explicitly or tacitly that the measured CBF, CBV and BOLD signals originate from the venous compartment. Although the major contribution of the BOLD signal comes from the Hb which is primarily in the veins, the CBF and CBV measurements obtained via laser Doppler flowmetry (LDF) and optical imaging spectroscopy (OIS) are likely to come from the arterial, capillary and venous compartments. The adequate interpretation of the BOLD signal depends on an appropriate hemodynamic model taking into account the hemodynamic changes in all three compartments. For this purpose, the three-compartment hemodynamic model as an extension to the one-compartment model is developed [15].

In recent years four models considered were combined to provide a model of the full path from a temporal stimulus pattern to a measured CBF response and a BOLD response. The combined model includes; (i) the BOLD signal as a function of changes in oxygen extraction factor (E) and CBV, (ii) the balloon model, proposed to describe the transient dynamics of CBV and Hb and how they affect the BOLD signal, (iii) neurovascular coupling, relating the responses in CBF and $CMRO_2$ to the neural activity response, and (iv) a simple model for the temporal nonlinearity of the neural response itself. Recent experimental findings on the linearity of the BOLD response and the effect of the baseline physiological state on the BOLD response are considered in light of these models [16].

2.4.2. Dynamics of Blood Flow and Oxygenation Changes During Brain Activation

Despite the widespread use of functional neuroimaging techniques, the physiological changes in the brain that accompany neural activation are still poorly understood. During brain activation, a modest increase in the cerebral metabolic rate of oxygen ($CMRO_2$) is accompanied by a much larger increase in local blood flow. Because of this imbalance, local capillary and venous blood are more oxygenated during activation. The large increase in flow is the basis for mapping brain activation patterns with positron emission tomography (PET), and the decrease in local deoxyhemoglobin concentration is the basis for fMRI exploiting the BOLD effect. A possible explanation for the large flow increase could be the tight coupling of flow and oxygen metabolism in the presence of limited oxygen delivery. This oxygen limitation model is called "Balloon Model" and is based on the assumptions that essentially all of the oxygen leaving the capillary is metabolized and blood flow increases are accomplished by increased capillary blood velocity rather than capillary recruitment. Under these circumstances, increased blood flow leads to reduced oxygen extraction due to the decreased capillary transit time. The rate of delivery of oxygen, which is proportional to the product of flow and oxygen extraction fraction (OEF), therefore increases much less than the flow itself. In the context of this model, a large increase in flow is required to support a small increase in oxygen metabolism. The oxygen limitation model provides an interpretation of the mismatch between flow and oxygen metabolism changes during brain activation as evidence for tight coupling, rather than uncoupling, of flow and metabolism. However, detailed studies of the time course of Hb and HbO_2 changes during activation have revealed a complex pattern that may contain evidence of a transient uncoupling of flow and metabolism. In optical studies in a cat model, it is found that after a brief (4-s) visual stimulation, the total deoxyhemoglobin increased for the first 3 seconds, followed after a few seconds by the larger decrease associated with the BOLD effect. This "fast response" was interpreted as an initial increase in oxygen extraction, before the large flow increase (Figure 2.7).

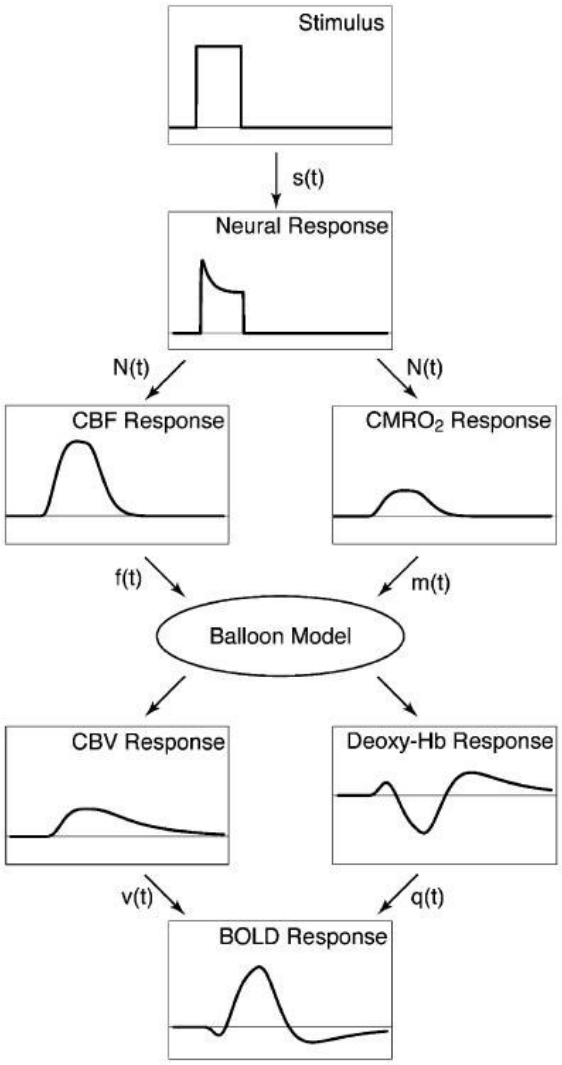

Figure 2.7. Diagram of the proposed model linking the applied stimulus to the resulting physiological responses and the measured BOLD response [16].

The conflicting effects of dynamic changes are incorporated in both blood oxygenation and blood volume. Calculations based on the Balloon model showed pronounced transients in the Hb content and the BOLD signal measured with fMRI, including initial dips and overshoots and a prolonged poststimulus undershoot of the BOLD signal. These transient effects were reported to occur in the presence of tight coupling CBF and $CMRO_2$ throughout the activation period [14].

Toronov [18] studied the behavior of cerebral physiological variables to improve the understanding of the BOLD-fMRI effect and simultaneously recorded the signals during motor functional activation in humans. The NIR data gave information on the changes in CBV and cerebral blood oxygenation (CBO). His data showed that the deoxy-Hb concentration was the major factor determining the time course of the BOLD signal. The increase in cerebral blood oxygenation during functional activation is due to the increase in the velocity of blood flow, and occurs without significant swelling of the blood vessels. Although NIRS cannot compete with fMRI in terms of spatial resolution, the unique biochemical specificity of NIRS makes it a perfect complementary method to resolve difficulties in the physiological interpretation of the BOLD signal. Particularly, using light sources at two different NIR wavelengths one can measure independently tissue oxy- and deoxy-Hb concentration [19]. Therefore, using NIRS data acquired simultaneously with BOLD fMRI, one can directly assess the role of the two major physiological variables underlying the BOLD signal, namely the regional cerebral oxygenation (rCBO) and regional cerebral blood volume (rCBV) [18].

The biomechanical model presented below (Balloon Model) describes the changes in physiological variables during brain activation. To connect the model with experimental fMRI data, first a quantitative expression for BOLD signal changes as a function of blood susceptibility and volume is needed. This relationship has been extensively explored using experimental data, numerical Monte Carlo simulations, and analytical calculations. Although the signal dependence is intrinsically a nonlinear function of susceptibility and blood volume due to the effects of diffusion, the situation is relatively simple for the case of gradient echo (GRE) signals affected by postcapillary blood vessels. In this initial analysis, there is a simplifying assumption that the GRE signal changes are primarily due to small postcapillary venous vessels and the contribution of capillaries are neglected. In this case, the role of diffusion is minor because of the larger size of the venous vessels, and the extravascular signal changes essentially depend just on the change in the total amount of Hb in the tissue voxel. In addition, the role of intravascular signal changes in BOLD experiments were investigated and concluded that at 1.5 T, these changes contribute more than half of the net observed signal change. Therefore both contributions are included in the model for the BOLD signal (Equation 2.1).

$$\frac{\Delta S}{S_0} = \frac{S - S_0}{S_0} = V_0\left[k_1(1-q) - k_2 v\left(\frac{q}{v} - 1\right) - k_3(1-v)\right] \tag{2.1}$$

To model the transient aspects of the BOLD signal, it is assumed that there is no capillary recruitment, in the oxygen limitation model mentioned above, and CBV changes occur primarily in the venous compartment. The arteriolar dilatation that produces a flow increase is assumed to cause a negligible change in blood volume. The vascular bed within a small volume of tissue is then shown as an expandable venous compartment (a balloon) that is fed by the output of the capillary bed. The volumetric flow rate (ml/s) into the tissue ($F_{in}(t)$) is assumed to be a function of time that drives the system. The volumetric flow out of the system ($F_{out}(t)$) is assumed to depend primarily on the pressure in the venous compartment. F_{out} is equal to $(P–P_{mixed})/R$, where P is the pressure in the venous compartment, P_{mixed} is the mixed venous pressure downstream from the tissue element, and R is the resistance of the vessels after the balloon. Then, the physical picture of activation is that after the arteriolar resistance is decreased producing an increase in F_{in}, the venous balloon swells, and the pressure increases until F_{out} matches F_{in} (a new steady state). The amount of swelling that occurs will depend on the biomechanical properties of the vessel as reflected in the pressure/volume curve of the venous balloon. However, rather than introducing pressures explicitly into the equations (and thus introducing more parameters), Buxton [14] assumed that F_{out} is a function of the venous volume, V. The rate of volume change of the balloon is the difference between F_{in} and F_{out}. They then considered the total deoxyhemoglobin Q(t) in the tissue element. For simplicity, they neglected the capillary contribution and assumed that all of the Hb is in the venous compartment. The rate of entry of Hb into the venous compartment is F_{in} E Ca, where E is the net extraction of O_2 from the blood as it passes through the capillary bed and C_a is the arterial O_2 concentration, (assumed to be due to a fully oxygenated deoxy-Hb concentration). The driving function of the system is the quantity $f_{in}(t)E(t)$ where f_{in} is the normalized F_{in}. If the balloon is treated as a well mixed compartment, the clearance rate of Hb from the tissue is F_{out} times its average venous concentration, Q(t)/V(t). The coupled equations for Q(t) and V(t) are then,

$$\frac{dQ}{dt} = \left[F_{in}(t) EC_a - F_{out}(v) \frac{Q(t)}{V(t)} \right] \tag{2.2}$$

$$\frac{dV}{dt} = \left[F_{in}(t) - F_{out}(v) \right] \tag{2.3}$$

By scaling each of these variables with their values at rest (t = 0), these equations can be written in terms of the dimensionless variables $q(t)=Q(t)/Q_0$, $v(t)=V(t)/V_0$, $f_{in}(t)=F_{in}(t)/F_0$ and $f_{out}(v)=F_{out}(v)/F_0$:

$$\frac{dq}{dt} = \frac{1}{\tau_0} \left[f_{in}(t) \frac{E(t)}{E_0} - f_{out}(t) \frac{q(t)}{v(t)} \right] \tag{2.4}$$

$$\frac{dv}{dt} = \frac{1}{\tau_0} \left[f_{in}(t) - f_{out}(t) \right] \tag{2.5}$$

where Q_0 is the resting deoxyhemoglobin content, V_0 is the resting volume, F_0 is the resting flow, $\tau_0 = F_0/V_0$ is the mean transit time through the venous compartment at rest, E_0 is the resting net extraction of O_2 by the capillary bed. T_0 simply sets the time scale for changes and E_0 is the only other parameter that appears explicitly. However, there are two functions that remain to be specified: E(t) and $f_{out}(v)$. At this point, the oxygen limitation model requires that the net extraction is equal to the unidirectional extraction. That is, $CMRO_2$ is assumed to increase as much as possible within the constraints set by limited oxygen delivery. Under these circumstances, a nonlinear expression for E(t) is a reasonable approximation for a wide range of transport conditions:

$$E(f_{in}) = 1 - (1 - E_0)^{1/f_{in}} \tag{2.6}$$

In equation 2.4, E(t) is then replaced with $E(f_{in}(t))$ from equation 2.6. Variable temporal patterns of response will then be created for different functional forms of $f_{out}(v)$, which is equivalent to different pressure/volume curves for the venous balloon. In constructing $f_{out}(v)$, we need to distinguish between the steady-state relationship of blood flow and volume and the transient relation $f_{out}(v)$ that controls the transition from one steady state to another. In early work using altered CO_2 pressure to change blood flow, Grubb [20] found that the steady-state total blood volume could be described empirically

by a power law relationship (Equation 2.7), where α was found to be about 0.4 from their data.

$$f_{out} = v^{1/\alpha} \tag{2.7}$$

The simplest assumption would be that $f_{out}(v)$ follows the same empirical relationship. However, experimental measurements, using a vascular contrast agent, suggested that although the steady-state relationship was in reasonable agreement with Grubb [20] , the transition periods were not. Therefore, Buxton [14] estimated the steady-state plateau level of volume change by a power law with exponent α, but the time course during the transition between steady-state levels followed a different pattern. In practical terms for the calculations, this means that the end points of the curve $f_{out}(v)$ are specified by the power law relation, but the shape of the curve between those end points is variable. For the calculations, they modeled $f_{out}(v)$ as a sum of a linear component and a power law (Equation 2.8).

$$f_{out} = v^{1/\alpha} + \tau . \frac{dv}{dt} \tag{2.8}$$

The essential feature of the balloon model is that it is assumed that the capillary volume is fixed but the venous volume can change (like a balloon) with a pressure/volume response curve that may vary.

According to Toronov [18], who used two different measurement techniques, fMRI and NIRS deoxy-Hb concentration is the major factor determining the time course of the BOLD signal. The increase in cerebral blood oxygenation during functional activation is due to an increase in the velocity of blood flow, and occurs without significant swelling of the blood vessels. The output signals of most measurement techniques depend upon many different interrelated parameters. For this reason, the behavior of such important cerebral parameters as rCBF, rCBV, rCBO, and $CMRO_2$ during cerebral activation remains controversial. It is concluded that both rCBF and $CMRO_2$ remain constant during cortical activation, while Buxton [14] have reported significant changes in these parameters [18].

2.4.3. The Rate of Oxygen Release and Its Effect on Capillary Tension

Mathematical modeling has been widely used in the past to characterize the process of tissue oxygenation since it was impossible to measure directly the intracapillary P_{O2}. These models range in complexity from the pioneer works to the model of Fletcher [21].

An assumption common to these models is the instantaneous release of oxygen by red blood cell (RBC) as it travels through the capillary. This assumption permits the direct calculation of the plasma P_{O2} profile from the known hemoglobin saturation (Hb^{sat}) and the oxyhemoglobin dissociation curve (ODC). However under certain conditions, the time required by the RBC to release its oxygen may be significant when compared to the capillary transit time. In 1964, it was speculated that with reduced O_2 supply, the unloading of oxygen may lead to an intracapillary P_{O2} gradient from the red blood cell to the plasma produced by the relatively slow rate of oxygen dissociation. This question was theoretically explored that normally the O_2 tension gradient across the red cell was less than 1 mm Hg. Under conditions of exercise with anemia this gradient could become as much as 18 per cent of the oxygen gradient from the capillary to the tissue. Their study assumed that the rate of oxygen release by the red blood cell equals the rate of O_2 consumption by the tissues but they neglected the effect of capillary transit time on the amount of oxygen released by the RBC.

The following equation is used to describe oxygenation of hemoglobin in red blood cells:

$$\frac{d[HbO_2]}{dt} = k_c'[O_2][Hb] - k_c[HbO_2] \tag{2.9}$$

where k_c'and k_c are pseudo-velocity constants that provide an empirical description of the combined chemical and diffusive processes seen in the reaction of oxygen with intact red blood cells. [Hb] is the concentration of reduced hemoglobin. This equation approximates the initial portion of the oxygen uptake curve with reasonable accuracy. However, when the complete reaction is examined, this equation is a poor model of O_2 uptake or release, since at equilibrium it describes a rectangular hyperbola and not the sigmoid-shaped ODC.

A more detailed model was developed using intermediate compound hypothesis according to which the reaction takes place in four stages sequentially as oxygen combines with hemoglobin. Although conceptually elegant, his hypothesis is not practical as a kinetic model of RBC oxygenation due to the many undetermined velocity constants required to define the time course of the reaction and the difficulty in solving a system of four simultaneous non-linear differential equations [22].

The time required by the RBCs to release the O_2 needed by the tissues may be rate-limiting under conditions of reduced O_2 supply (D_{O2}). A time-dependent mathematical model of capillary oxygen transport was developed by Gutierrez [22] to explore the effect that red blood cell-oxygen kinetics and capillary transit time have on the intracapillary plasma P_{O2}. The tissue capillaries were represented by a series of perfectly mixed compartments. In each compartment O_2 is removed by the tissues as a chemical reaction takes place between O_2 and HbO_2. A system of differential equations gives changes in the intracapillary concentration of HbO_2 and plasma O_2. These equations allow for changes in blood flow, arterial oxygenation, capillary transit time, rate of O_2 uptake, deoxy-Hb concentration and the position of the HbO_2 dissociation curve. The model is a mass transport analogy of the capillary; and it provides valuable insight into the time dependency of gas exchange in the peripheral tissue. The predicted capillary P_{O2} for conditions of normal O_2 supply is less than the P_{O2} calculated assuming an instantaneous rate of RBC deoxygenation. This difference in plasma P_{O2} is not present in the venous end of the capillary, since at this point HbO_2 and plasma O_2 have sufficient time to re-establish equilibrium. The end-capillary P_{O2} is significantly less than the venous P_{O2}. These results suggest that (1) the kinetics of RBC deoxygenation can play an important role in the delivery of O_2 to the tissues, and (2) the venous P_{O2} is not always an accurate measure of the end capillary P_{O2} [22].

Gutierrez [22] estimated the per cent hemoglobin saturation change with time in terms of P_{O2}, the parameters n, k_c' and k_c vary throughout the course of the oxygenation reaction since the combined effect of the chemical and diffusive processes cannot be completely described by constant terms.

$$\left(\frac{d(HbO_2\%)}{dt}\right)_R = k_c'\left[(\alpha P_{O2})^n(100 - HbO_2\%) - (\alpha P_{50})^n(HbO_2\%)\right] \tag{2.10}$$

where

$$n = \frac{2.635*(HbO_2\%)^2 - 274.042*(HbO_2\%)}{(HbO_2\%)^2 - 104.10*(HbO_2\%) - 31.32} \tag{2.11}$$

and

$$k_c' = 6325*\exp\left[(0.011537*(HbO_2\%))^{2.88697}\right] \tag{2.12}$$

In another model by Zheng et al. [15], they considered the oxygen diffusion equation including both the spatial and temporal partial derivatives, thus incorporating dynamics in the OEF and the capillary oxygen concentration. They also assumed a nonzero tissue oxygen tension that was related to an additional state variable. The result was a nonlinear dynamic model with seven state variables most of which were normalised quantities. The model was used to fit OIS data from a brief stimulation paradigm and was found to produce physiologically plausible model parameters [15].

2.4.4. The Hemodynamic Model for the Physiological Interpretation of *In Vivo* Measurements of the Concentration and Oxygen Saturation of Hemoglobin

Fantini [19] presented a model that describes the effect of physiological parameters such as the speed of blood flow, local oxygen consumption, capillary recruitment, and vascular dilatation/constriction on the concentration and oxygen saturation of hemoglobin in tissue (Figure 2.8). This model can be used to guide the physiological interpretation of hemodynamic and oximetric data collected in vivo with techniques such as optical imaging, NIRS and fMRI. A blood vessel of cross section area σ_{bv} intersects at a length L_{bv} with the volume V probed by the measurement technique of interest. The average blood speed within the vessel is given by $c^{(blood)}$, while O_2 represents the rate of oxygen diffusion from the blood vessel to the tissue within volume V. In addition to providing a formal description of well-established results (exercise-induced hyperemia, reperfusion hyperoxia, decrease in the deoxy-Hb concentration induced by brain activity, measurement of arterial

saturation by pulse oximetry, etc.), this model suggests that the superposition of asynchronous contributions from the arterial, capillary and venous hemoglobin compartments may be at the origin of observed out-of-phase oscillations of the [HbO_2] and deoxy-Hb concentration in tissue.

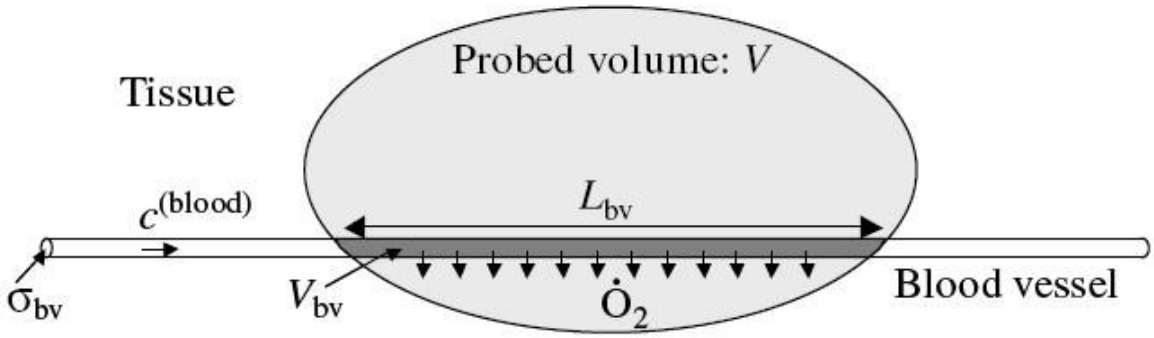

Figure 2.8. Schematic representation of Fantini model [19].

$$[O_2]^{(blood)}(l) = [O2]_0^{(blood)} \exp\left(-\frac{\alpha_{O2}}{c^{blood}} l\right) \tag{2.13}$$

The relation between the concentration of oxygen in the blood ($[O_2]^{(blood)}$) and its value at rest ($[O_2]^{(blood)}_0$) is given by equation 2.13 and it is based on the assumption that probability of oxygen extraction (α_{O2}) is not a function of l, where l is the line coordinate along the blood vessel. If $[O_2]^{(plasma)} >> [O_2]^{(tissue)}$, which is an approximation that has been used for brain tissue the spatial uniformity of α_{O2} implies that the ratio $[O_2]^{(plasma)}/[O_2]^{(blood)}$ is not a function of the blood oxygenation. Because of the nonlinear oxygen equilibrium curve of Hb, this assumption is not strictly correct, but Buxton [14] found that the nonlinear correction to that relation is not significant. However, the relation of $r \approx [O_2]^{(plasma)}/[O_2]^{(blood)}$ allowed for a variable diffusivity α_{O2} in their model for the regulation of cerebral oxygen delivery. In 2001, it was proposed that $[O_2]^{(tissue)}$ should not be neglected in r, so that an increased cellular utilization rate of oxygen can directly increase α_{O2} by decreasing $[O_2]^{(tissue)}$ and thereby increasing the oxygen concentration gradient across the blood vessel wall [19].

2.4.5. CO_2 Dynamics

As CO_2 is formed in the cells due to aerobic metabolism, it is transported through the blood stream by conversion to carbonic acid (H_2CO_3), which dissociates to hydrogen ion (H^+) and bicarbonate (HCO_3^-). The hydrogen ion binds to hemoglobin, and is transported to the lungs. In this case, hemoglobin is acting as a buffer for the acid, but is also acting as an effective "transportation vehicle" for ferrying carbon dioxide to the lungs. About two-thirds of the HCO_3^- will diffuse out into the plasma (and is replaced by chloride in the red cell). Only small amounts of carbon dioxide remain dissolved or attach to other compounds.

About 50 ml of CO_2 gas are contained in each 100 ml of arterial blood, almost all as HCO_3^-. As the blood goes through the capillaries, it picks up about 5 ml of additional CO_2. With this addition of acidic CO_2, the pH drops from 7.4 to 7.36. On reaching lungs, the process is reversed, and 5 ml of CO_2 is converted back from H^+ and HCO_3^- and discharged into the alveoli.

At rest, about 200 ml of CO_2 is produced and excreted through the lungs. Over 24 hours, this is the equivalent of 12,500 milliequivalents of acid produced by metabolism and eliminated through CO_2.

Special chemical receptors near the aorta and carotid arteries, called the aortic bodies and carotid bodies, are sensitive to an increase in carbon dioxide or acid concentration, or to a decrease in the pressure of oxygen (P_{O2}). When these receptors sense acidity or low oxygen, they stimulate the brain respiratory center to increase the speed and depth of breathing. The deep rapid breathing mixes alveolar air with increased amounts of low-CO_2 air, leading to a decrease in the carbon dioxide in the blood as it passes by the alveolus. The reduction in CO_2 raises the pH back towards normal.

When there is a rise in serum CO_2, such as with the increased metabolism of exercise, ventilation is stimulated until the CO_2 returns to normal levels.

Arterial carbon dioxide tension ($PaCO_2$) is well established as an important factor in the control of cerebral vascular resistance (CVR) and CBF in animals and man. The relationship between CBV, CBF, and cerebral vascular mean transit time (t_v) was investigated by Grubb et al. [20] during acute changes in $PaCO_2$ in rhesus monkeys and a significant linear relationship was found between CBF and $PaCO_2$ in the range of 15 and 76 torr. For each one torr change in $PaCO_2$, there was a corresponding change of 1.8 ml/100 gm per minute in the CBF. CBF and cerebral vascular mean transit time (t_v) have a nonlinear relationship [20].

A linear relationship between CBV and $PaCO_2$ was proposed by equation 2.14.

$$CBV = 0.041 * PaCO_2 + 2.0 \tag{2.14}$$

For each one torr change in $PaCO_2$ there is a change in CBV of 0.041 ml/100 gm of perfused tissue. At a normocarbic value of $PaCO_2$ (~37 torr), an average value of 3.5 ml/100 gm was found. He also obtained a significant linear relationship between CBF and $PaCO_2$ [20].

The complex relationships between $PaCO_2$, CBV, CBF and intracranial pressure (ICP) are investigated by Lodi et al. [23] using an original mathematical model. The model incorporates the incranial compliance, the cerebrospinal fluid production and the reabsorbtion processes, the collapse of the terminal cerebral veins, and the active response of the large and small cerebral arteries to perfusion cerebral changes (autoregulation) and to changes in $PaCO_2$ (chemical regulation) [23].

Gutierrez [24] has developed a two-compartment mass transport model of tissue CO_2 exchange to examine the relative contributions of blood flow and cellular hypoxia (dysoxia) to increases in tissue and venous blood CO_2 concentration (Figure 2.8). The model assumes perfectly mixed homogeneous conditions, steady-state equilibrium, and CO_2 production occurring exclusively at the tissues. The behavior of the model is compared with published data derived from an isolated dog hindlimb preparation subjected to either reductions in blood flow (ischemic hypoxia) or decreases in arterial P_{O2} (hypoxic

hypoxia). The results of the model corroborate the experimental finding of greater venous and tissue CO_2 concentrations with ischemic hypoxia than with hypoxic hypoxia. The model also predicts increases in tissue CO_2 concentration under conditions of adequate O_2 supply if CO_2 transfer from tissue to blood becomes impaired. Consequently, from a theoretical perspective, it appears that increases in the tissue or venous blood CO_2 concentration are neither sensitive nor specific markers of tissue dysoxia. The results of the model support the notion that changes in tissue and venous blood CO_2 concentration during dysoxia reflect primarily alterations in vascular perfusion and not scarcity in cellular energy supply.

There have been previous studies on simultaneous or dynamic transport and exchange of O_2 and CO_2 in the microcirculation. The kinetics of O_2 and CO_2 exchange have been studied through compartmental modeling by accounting for physical and biochemical processes including the acid–base balance. However, they did not account for convection and diffusion (and hence, concentration gradients) along the capillary length, a major aspect of determining tissue levels and understanding alveolar-arterial oxygen differences.

A quantitative model was developed for convective and diffusive gas (O_2 and CO_2) transport and acid–base regulation in blood flowing in microvessels and in oxygenators while accounting for Bohr and Haldane effects. They did not account for the permeation and subsequent consumption of O_2 within the tissue cells, or the production of CO_2. A more complete model of O_2 and CO_2 transport and exchange in the microcirculation is therefore needed for the analysis of experimental data [25].

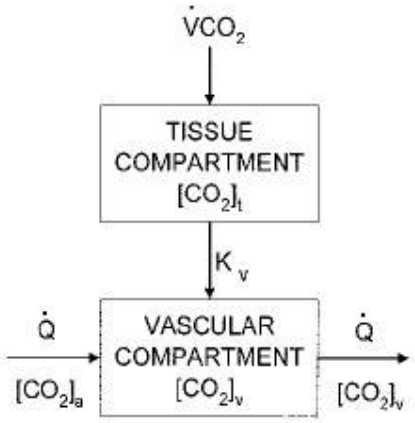

Figure 2.9. The tissue CO_2 exchange model consists of two perfectly mixed compartments: a tissue and a vascular compartment. Changes in tissue and vascular CO_2 concentrations, $[CO_2]_t$, and $[CO_2]_v$ depend on CO_2 production, V_{CO2}, arterial CO_2 concentration, $[CO_2]_a$, the diffusion term K_v, and tissue blood flow (Q) [24].

2.4.6. The Results of the Balloon Model

The Balloon Model is undoubtedly the simplistic biophysical model of the hemodynamic response to activation in the brain. The model is a concrete methematical representation of how blood volume changes in conjuction with blood oxygenation changes can create complex dynamics in the BOLD signal. A simple biomechanical model can produce blood volume changes that resolve very slowly, depending on the shape of the outflow curve as a function of volume.

The time profiles of deoxyhemoglobin content and volume are calculated by numerical integration of equations 2.4 and 2.5 using the Mathematica software package (Wolfram Research) [14]. However, the relationship between stimulus and flow response is poorly understood, and they did not attempt to model it. They referred to the “duration” of an activation as the time from the beginning of the up ramp of $f_{in}(t)$ to the beginning of the down ramp.

The response to a short, 8-s duration stimulus with a maximum flow change of 70 per cent is given in figure 2.10 when $f_{out}(v)$ is a linear function. The outflow lags slightly behind inflow (Figure 2.11). The model parameters in these calculations were $E_0 = 0.4$, $\alpha=0.5$ and $V_0 = 0.01$ [14].

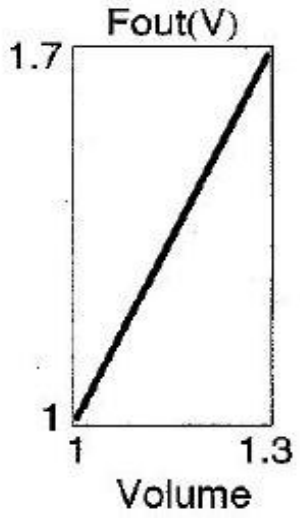

Figure 2.10. Balloon model curves for a linear form of $f_{out}(v)$, showing a simple pattern of response [14].

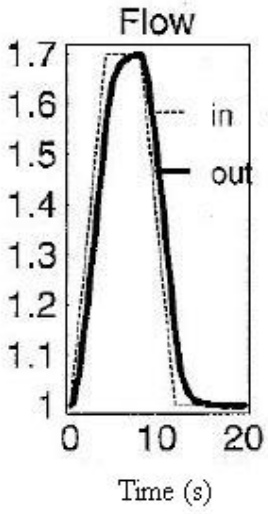

Figure 2.11. The trapezoidal $f_{in}(t)$ versus time plot [14].

A stimulation causes the blood volume to increase with a pattern like in figure 2.12. Its shape is trapezoidal; i.e. when the level of blood increases up to a certain value that it becomes saturated with CO_2. The figure represents the assumption that the capillary volume is fixed but the venous volume can change (like a balloon) with a pressure/volume response curve that may vary.

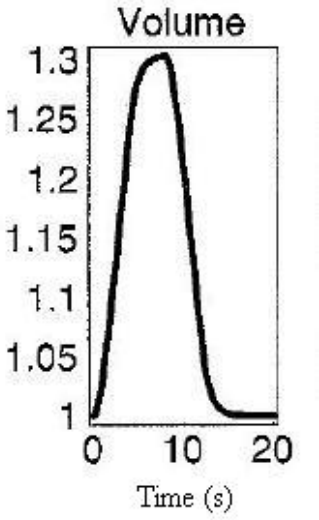

Figure 2.12. $f_{out}(v)$ versus time plot using Balloon model [14].

The total deoxyhemoglobin content increases slightly, then drops sharply, and finally returns to the resting level as shown in figure 2.13.

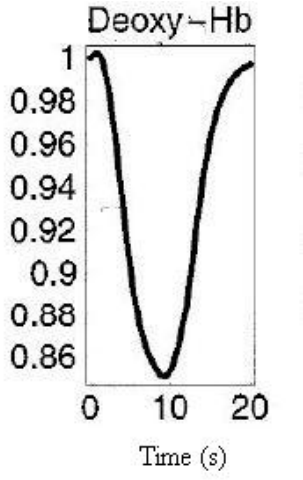

Figure 2.13. Deoxyhemoglobin concentration versus time plot using Balloon model [14]..

The BOLD response is qualitatively the inverse of the total deoxyhemoglobin response (Figure 2.14) [14].

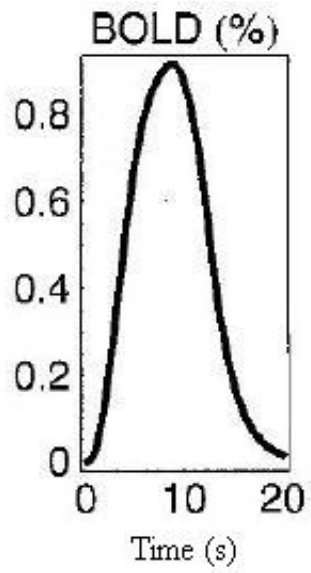

Figure 2.14. BOLD signal change as time elapses.

Furthermore, it can be seen from Figure 2.15 that BOLD signal lags the rCBF signal by about a second. The same point is mentioned by Friston et al. [13].

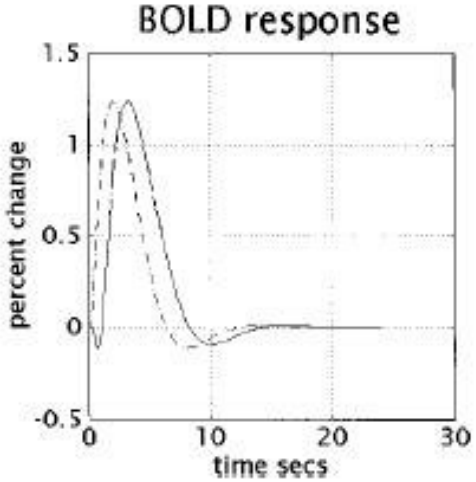

Figure 2.15. BOLD signal lagging the rCBF [13].

Friston et al. [13] combined the BOLD signal, deoxy-Hb concentration and venous volume (v) in a three dimensional plot (Figure 2.16).

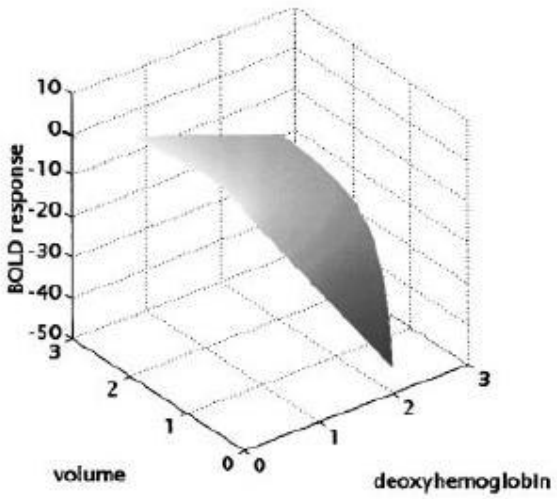

Figure 2.16. Plot of the nonlinear function of volume and deoxyhemoglobin that represents BOLD signal [13].

3. SIMULATION OF NEUROVASCULAR COUPLING (NVC) MODEL

3.1. Experimental Methods – fNIRS and Collection of Data

Functional near infrared sensor measures hemodynamic changes in the cortex using a portable, safe, affordable and negligibly intrusive NIR based optical brain imaging system. The hypothesis is that there is a positive correlation between blood oxygenation in the relevant areas of donolateral prefrontal cortex and cognitive effort defined as attention and working memory. In principle, brain activation causes an increase in local CBF that occurs within several seconds. This increase in CBF and oxygen delivery exceeds the increase in local oxygen consumption. Hence, cerebral blood oxygenation rises locally [26]. Oxygenated and deoxygenated hemoglobin have characteristic optical properties in the visible and near-infrared light range. Therefore, based on functional optical measurements, concentration changes of these molecules can be measured during functional brain activation (Figure 3.1) [27, 28].

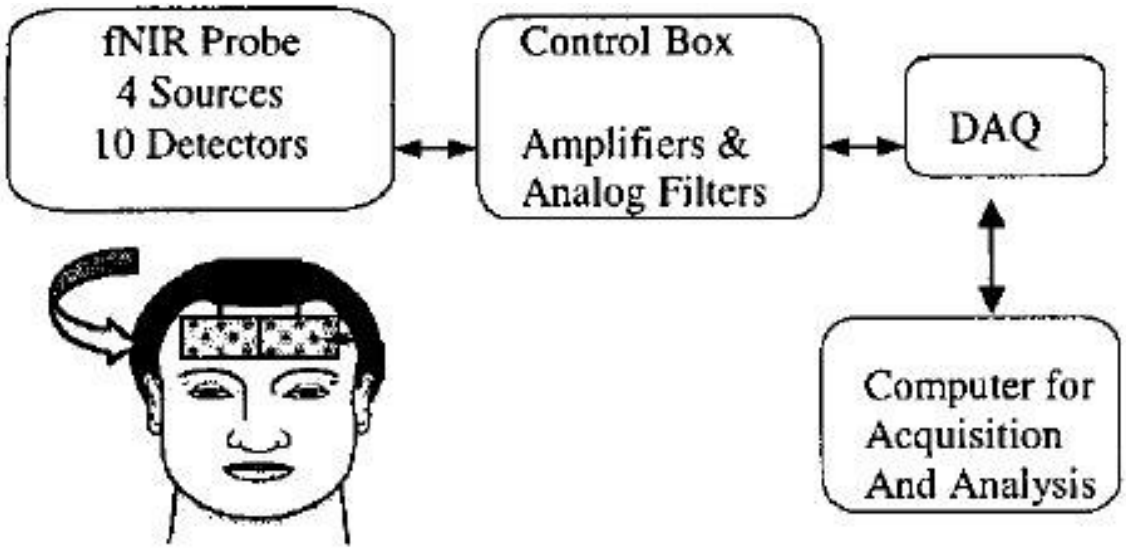

Figure 3.1. Data collection setup [26].

Brain hemodynamic data is collected by the NIROXCOPE 301, a continous wave fNIRS system, developed at the Biophotonics Laboratory of Institute of Biomedical Engineering. These systems house a probe that contains four light emitting diode (LED) sources (Epitex L4X730/4X805/4X850-40Q96 multi-wavelength LED, 50 mW optical power) each capable of emitting waves at three near-infrared wavelengths and twelve detectors (TI-Burr Brown, OPT101). The sources and detectors are equidistantly placed on the probe as seen in figure 3.2. The probe is positioned such that its base aligns with the eyebrows of the subject and the middle with the Fz location from EEG electrode placement. Each quadrant consists of four detectors separated from their centric source by 2.5 cm. There are four such quadrants made up of twelve detectors, hence the middle two quadrants share pairs of detectors as shown.

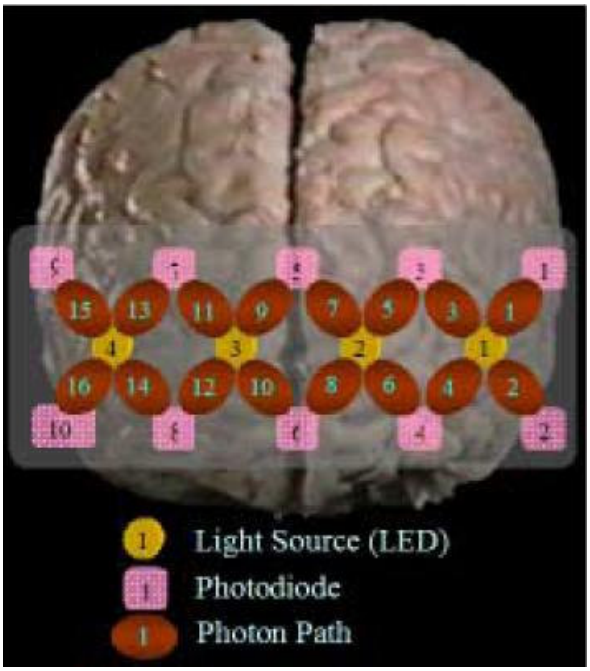

Figure 3.2. Source-detector configuration of the brain probe and nomenclature of detectors. The circles in the center of each quadrant are the multi-wavelength NIR LED light sources, while the squares around them are the fNIRS-sensitive detectors [3]. The balloons between source-detectors are the approximate brain regions where photons are traveling [17].

However, due to the time and wavelength multiplexing inherent in the system one ends up effectively with four non-overlapping quadrants of detectors. In other words, the multiplexing scheme guarantees that no two LEDs at adjacent quadrants and no two wavelengths within the same quadrant are ON at the same time, resulting in non-overlapping temporal and spatial measurements. Previous studies from the Biophotonics group have proved that breath holding task causes sufficient amount of cerebral oxygenation stress to induce a large increase in the cerebral blood flow specifically to the frontal region [17].

One healthy volunteer and one migraineur (ST) performed the breath holding experiment for 90 seconds rest and then 30 seconds breath holding followed by 90 seconds of rest. This 210 seconds cycle was repeated for four times. The Hb data obtained by breath holding experiment were in the form of a text file which could be opened in MATLAB® for further processing.

3.2. Simulation of the Neurovascular Coupling (NVC) Model

The balloon model developed by Buxton [14] was motivated by the observation in a cat study in which CBV returned to baseline more slowly than CBF at the end of the stimulus, this effect might explain the poststimulus undershoot of the BOLD signal that is often observed. A similar Windkessel model was proposed to embody the same concept and provide a biomechanical mechanism for a delayed CBV return to baseline. The balloon model has been refined and compared with experimental data, and some errors in the original parameter estimates were recently corrected. The model is capable of producing BOLD poststimulus undershoots that match well with experimental data. However, the central premise of the model, that the undershoot occurs when CBV returns slowly to baseline, has not been definitely established and focused experimental tests of this question are needed [18].

The total BOLD signal is assumed to be a volume-weighted sum of the extravascular (S_o) and intravascular (S_i) signal and given by equation (2.1).

$$\frac{\Delta S}{S_0} = \frac{S - S_0}{S_0} = V_0\left[k_1(1-q) - k_2 v\left(\frac{q}{v} - 1\right) - k_3(1-v)\right] \tag{2.1}$$

where V_0 is the resting blood volume fraction, v is the venous volume, q is the deoxyhemoglobin concentration and k_1, k_2 and k_3 are the constant parameters.

The central idea of the model is that the venous compartment is treated as a distensible balloon. The inflow to the balloon, f_{in}, is the cerebral blood, while the outflow from the balloon f_{out} is an increasing function of the balloon volume. The two dynamical variables are the total deoxyhemoglobin q(t) and the volume of the balloon v(t), the derivatives of which with respect to time are described by equations 2.4 and 2.5 respectively. The equations of the balloon model represent mass conservation for blood and deoxyhemoglobin as they pass through the venous balloon (Figure 3.3).

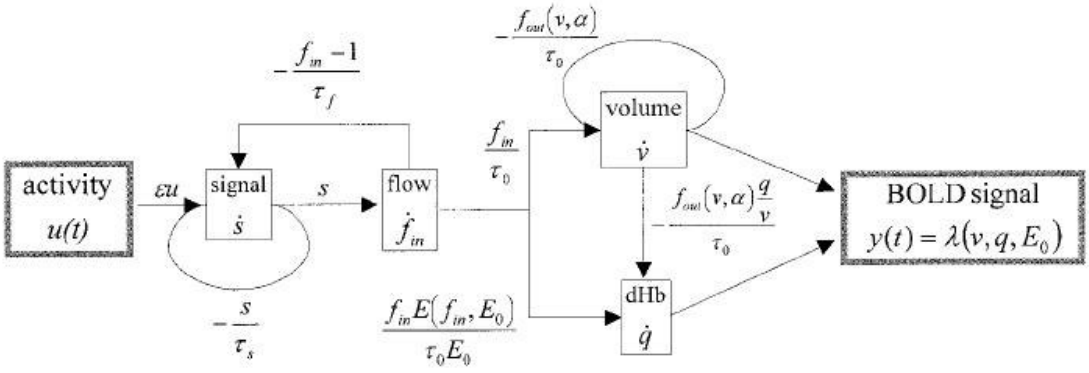

Figure 3.3. Schematic illustrating the organization of the hemodynamic model. This is a fully nonlinear single input $u(t)$, single output $y(t)$ state model with four state variables s, f_{in}, venous volume (v), and hemoglobin concentration (q)[13].

With this form, the balloon initially resists a change in volume, but eventually settles into a new steady-state that conforms with the power law model in equation 2.7. The time constant s controls how long this transient adjustment is required. A nonzero value for s produces hysteresis in the curve $f_{out}(v)$, so that the system follows a different

curve on inflation and deflation. To generalize this form and enable more fine tuning to data, s is allowed to take on different values during inflation (τ_+) and deflation (τ_-).

The net extraction fraction of oxygen is E(t), and the resting value is typically E_0=0.4. The time dimension of the equations is scaled by the time constant τ, the mean transit time through the balloon at rest. For a cerebral blood flow of 60 ml min^{-1}/100 ml^{-1} of tissue (equivalent to a rate constant of 0.01 s^{-1}) and a resting venous blood volume fraction of V_0 = 0.03, the mean transit time is τ = 3 s.

The driving function of the system is the quantity $f_{in}(t)E(t)$. In the original formulation of the balloon model, the extraction fraction was modeled as a fixed function of the inflow f with a tight coupling of flow and oxygen metabolism. The equations were generalized, treating E(t) as an independent quantity to be able to explore the dynamics that result from uncoupling of blood flow and oxygen metabolism.

In the original formulation of the balloon model [14], the outflow was modeled as a pure function of blood volume. Steady-state experiments [20], altering CBF with inhaled CO_2, indicated that the steady-state relationship between CBF and total blood volume was described by an empirical power law (Equation 2.7). However, interesting dynamics occur when the blood volume transiently lags behind this steady-state relationship, for example, due to viscoelastic effects. Therefore, that approach is not well suited to the modeling of data.

To that end, a simple model was proposed for these viscoelastic effects in which f_{out} is treated as a function of the balloon volume and the rate of change of that volume [14].

$$f_{out} = f_{in}^{1/\alpha} + \tau.\frac{dv}{dt} \tag{3.1}$$

For a specified driving function f(t)E(t), and values for the parameters τ, E_0 , α, τ_+ , and τ_- , equations 2.4-2.6 and 3.1 can be integrated numerically to yield dynamic time courses for q(t) and v(t). These dynamic physiological quantities can then be combined with the BOLD signal model (Equation 2.1) to generate MR signal curves. The equations and parameters used in the simulation of Balloon Model are given in Tables 3.1 and 3.2.

Table 3.1 The equations and parameters used in the simulation of the integrated neurovascular coupling model.

Name of the equations used	Parameter Values	Balance Equations
(1) BOLD signal	$k_1 = 2.8$ $k_2 = 0.57$ $k_3 = 0.43$	$\frac{\Delta S}{S_0} = \frac{S - S_0}{S_0} = V_0\left[k_1(1-q) - k_2 v\left(\frac{q}{v} - 1\right) - k_3(1-v)\right]$ (2.1)
(2) Cerebral Blood Volume (**CBV**) change	$\tau_0=2$	$\frac{dv}{dt} = \frac{1}{\tau_0}\left[f_{in}(t) - f_{out}(t)\right]$ (2.5)
(3) Deoxyhemoglobin (**Hb**) concentration change	$\tau_0=2$ $E_0=0.4$	$\frac{dq}{dt} = \frac{1}{\tau_0}\left[f_{in}(t)\frac{E(t)}{E_0} - f_{out}(t)\frac{q(t)}{v(t)}\right]$ (2.4)
(4) Oxygen extraction factor (**$E(f_{in})$**)	$E_0=0.4$	$E(f_{in}) = 1 - (1 - E_0)^{1/fin}$ (2.6)
(5) Output blood volume change during neural activation	$\alpha=0.4$	$f_{out} = f_{in}^{1/\alpha} + \tau.\frac{dv}{dt}$ (3.1)
(6) $PaCO_2$ versus f_{in}	h=50*trapmf(t,trap)+1	$f_{in} = 1 + \frac{0.7}{1 + 100000570.\exp(-5.251 * \log(h))}$ (3.3b)
(7) Trapezoidal function of f_{in}		$\text{trap} = [90 \;\; 118 \;\; 120 \;\; 210]$
(8) Oxyhemoglobin concentration (**HbO_2**)		$[HbO_2] = [Hb]_T - [Hb]$ (3.6)
(9) Relation between oxy-Hb concentration (**HbO_2**) and oxygen concentration (**O_2**)		$[\text{HbO}_2]^{\text{blood}} = 1/4 * [\text{O}_2]^{\text{blood}}$ (3.9)
(10) Oxygen concentration (**O_2**) change		$\frac{d[O_2]}{dt} = -\frac{d[HbO_2]}{dt}$ (3.10)

Table 3.2. Table of parameters used in integrated neurovascular coupling model.

Symbol	Name	Unit	Value
τ_0	Mean Transit Time Through the Venous Compartment at Rest	s^{-1}	τ_0 =2
E_0	Oxygen Extraction Factor at Rest		0.4
E	The Net Extraction of O_2 From the Blood as It Passes Through the Capillary Bed		-
f_{in}	Blood Flow Entering the Vessel	ml/s	-
f_{out}	Blood Flow Leaving the Vessel	ml/s	-
V(t)	Venous Volume	ml	-
V_0	Venous Volume at Rest	ml	
v	Normalized Venous Volume	ml	-
Q(t)	The total deoxyhemoglobin in the tissue element	micromoles	-
Q_0	The total deoxyhemoglobin in the tissue element at rest	ml/s	-
q	Normalized Deoxyhemoglobin Concentration	micromoles	-
α	Stiffness Factor	-	0.4
k_1	BOLD signal constant	-	2.8
k_2	BOLD signal constant	-	0.57
k_3	BOLD signal constant	-	0.43

3.3. Towards an integrated NVC Model

3.3.1 Integration of CO_2 Kinetics

In the present work, the main contribution is the addition of CO_2 kinetics into the conventional Balloon model. The previous studies did not include the modeling blood flow from arteries to capillaries as well as the input of CO_2 to the model.

The main parameter influencing the CBF is the arterial $PaCO_2$. Slowing down the breathing rate without enhancing the airflow or holding the breath can increase $PaCO_2$. The partial pressure of CO_2 is used as the input function to the integrated model, because the cerebral blood flow mechanism is regulated according to its concentration in the blood. When its concentration starts to increase, an increment in the flow occurs. So, a function expressing the relation between the partial pressure of CO_2 and the blood flow entering the capillaries had to be derived. In the previous works a linear relationship was defined which do not reflect the real attitude of the relationship.

$$Q_{brain} = \left(0.04 \frac{L}{mmHg.\min}\right) PaCO_2 - 0.93 \frac{L}{\min} \tag{3.2}$$

The validity range of Equation 3.2 is as 37 mmHg<$PaCO_2$<60 mmHg. Out of the range of inequality the CBF becomes much less sensitive to the changes of $PaCO_2$. For example, in hyperventilation, a more accurate and meaningful treatment is needed due to the individual changes.

A simple physical model, a simple four parameter formula, relating the CBF to $PaCO_2$ was developed by Gersten (2000) based on experiments with eight animals [32]. The parameters are: B_{max}, the maximal CBF corresponding to the maximal dilation of blood vessels, B_{min}, the minimal CBF corresponding to the maximal constriction of vessels, p_0 the value of arterial partial pressure of CO_2 at the average CBF and the parameter A, the slope at this point. The parameters can be extracted in an easy way, directly from the experimental data. After using the curve fitting method to the approximate values of the experimental data, the final equation obtained for the rhesus monkeys is as below (Equation 3.3a).

$$B(p) = 20.9 + \frac{92.8}{1 + 10570 \exp\left[-5.251.\log(p)\right]} \tag{3.3a}$$

In equation (3.3a), the CBF is represented by a sigmoid function. A sigmoid function is a mathematical function that produces a sigmoid curve — a curve having an "S" shape (Figure 3.4) [38].

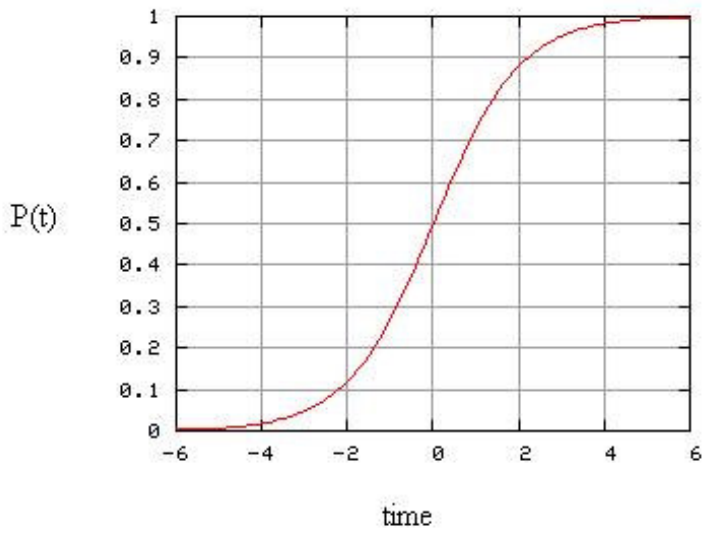

Figure 3.4. The "S" shaped sigmoid function plot [38].

Often, sigmoid function refers to the special case of the logistic function. Besides the logistic function, sigmoid functions include the ordinary arc-tangent, the hyperbolic tangent, and the error function. The integral of any smooth, positive, "bump-shaped" function will be sigmoidal, thus the cumulative distribution functions for many common probability distributions are sigmoidal (Equation 3.4).

$$P(t) = \frac{1}{1+e^{-t}} \tag{3.4}$$

In the present study, the parameters of the equation derived for the monkeys (Equation 3.3a) are changed by trial and error method to make it similar to the human brain hemodynamic behavior.

$$f_{in} = 1 + \frac{0.7}{1 + 100000570.\exp(-5.251 * \log(h))} \quad (3.3b)$$

Where h is the arterial partial pressure of CO_2 with the changing time values according to the trapezoidal values given in table 3.1.

3.3.2. Integration of Oxygen Kinetics (Hb and HbO_2)

A time-dependent mathematical model of capillary oxygen transport developed by Gutierrez ([22]) was used to estimate the oxyhemoglobin concentration. The tissue capillaries were represented by a series of perfectly mixed compartments (Figure 3.5). In each compartment O_2 is removed by the tissues as a chemical reaction takes place between O_2 and oxyhemoglobin. The system of differential equations gives changes in the intracapillary concentration of HbO_2 and plasma O_2. The model is a mass transport analogy of the capillary; and it provides valuable insight into the time dependency of gas exchange in the peripheral tissue.

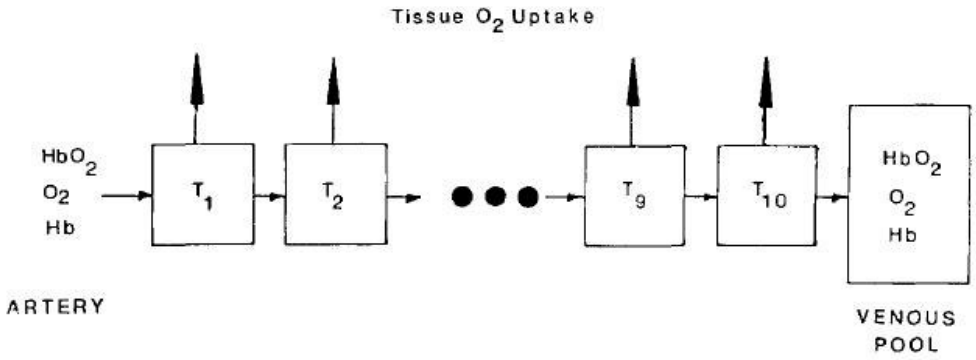

Figure 3.5. Capillary compartmental model [22].

Conceptual development of the model is based on the red blood cells which move along the capillary and release oxygen into the plasma. This process takes place in a progressive fashion from the arterial to the venous side. Assuming a constant O_2 tissue uptake (V_{O2}), and using Fick's equation, one can calculate the venous O_2 content and generate a linear O_2 saturation profile. The assumption of an instantaneous rate of deoxygenation by the RBC, allows the use of the oxyhemoglobin dissociation curve to

obtain the P_{O2} corresponding to any level of O_2 saturation along the capillary. With this method, the end-capillary P_{O2}, equals the venous Pv_{O2}. This equality of O_2 tensions is basic to the use of the mixed venous P_{O2} as a measure of tissue oxygenation.

Furthermore, oxygen in the RBC is in diffusional equilibrium with oxygen in plasma. Therefore, in arterial and venous blood, the plasma O_2 can be calculated from the oxyhemoglobin concentration using the oxyhemoglobin dissociation curve. As the cell moves along the capillary, a unidirectional process is set in motion where O_2 dissociates from HbO_2, diffuses into the plasma and it is taken up by the tissues. Here the assumption of chemical equilibrium within the capillary is no longer valid and the plasma P_{O2} cannot be calculated directly from the O_2 saturation (Equation 3.5).

$$\frac{d(HbO_2)}{dt} = \frac{Q}{V}\left([HbO_2]_{i-1} - [HbO_2]_i\right) + \left(\frac{d[HbO2]_i}{dt}\right)_R \tag{3.5}$$

where Q is the capillary blood flow in ml/min; V_i is the capillary compartment volume in ml; V_0, is the tissue O_2, uptake for that compartment in mM/min; and R is a subscript denoting the rate of change of $[HbO_2]$ by chemical reaction with O_2.

An important part of any mass transport model of tissue oxygenation is the mathematical description of the time dependent relationship between the plasma P_{O2} and the O_2, carried by the red blood cells traversing the capillary. This equation must accurately describe the dynamic process of oxygen uptake and release by the red blood cell from the onset of the reaction to equilibrium, and it must do so under all physiologically possible conditions.

Gutierrez (1986) [22] developed an empirical differential equation that described the kinetics of red blood cell oxygenation and deoxygenation from onset to equilibrium. The differential equation describing the rate of change of the $[HbO_2]$ in the intact RBC is assumed to be of the form:

$$\left(\frac{d[HbO_2]}{dt}\right)_R = k_c'[O_2]^n.[Hb] - k_c[HbO_2] \tag{3.6}$$

The parameters n, k_c' and k_c vary throughout the course of the oxygenation reaction since the combined effect of the chemical and diffusive processes cannot be completely described by constant terms. The equilibrium expression of equation 3.6, when $(d[HbO_2]/dt)_R = 0$;

$$\frac{k_c}{k_c'} = \frac{[HbO_2]}{[Hb][O_2]^n} \tag{3.7}$$

Assuming that hemoglobin not bound to oxygen is completely reduced, then the total amount of deoxy-Hb concentration equals [22];

$$[Hb]_T = [Hb] + [HbO_2] \tag{3.8}$$

The concentration of oxygen in the blood ($[O_2]^{(blood)}$)results from two contributions; (i) dissolved oxygen in the plasma ($[O_2]^{(plasma)}$) and (ii) oxygen bound to hemoglobin ($[O_2]^{(hemoglobin)}$). Because $[O_2]^{(plasma)}$ normally accounts for only 1–3 per cent of $[O_2]^{(blood)}$, $[O_2]^{(blood)}$ is considered to be equal to $[O_2]^{(hemoglobin)}$, and the $[HbO_2]$ in the blood (Equation 3.9);

$$[HbO_2]^{blood} = 1/4\,[O_2]^{blood} \tag{3.9}$$

where the factor 1/4 accounts for the four binding sites at each hemoglobin molecule for oxygen [9, 30].

Let *f* represent the fraction of hemoglobin bound to oxygen in the blood.

$$f = \frac{[HbO_2]}{[HbO_2] + [Hb]} \tag{3.10}$$

where $[HbO_2]$ is the concentration of the bound oxyhemoglobin, [Hb] is the deoxy-Hb concentration, i.e. the concentration of the free hemoglobin.

The summation of deoxy-Hb concentration and [HbO_2] is a biological constant known as blood capacity (for oxygen).

$$[Hb]+[HbO_2]=C \tag{3.11}$$

With the creation of an imbalance by the loss of dissolved oxygen into the tissue, the hemoglobin-bound oxygen undergoes a reversible chemical reaction that can be described empirically as:

$$Hb + O_2 \underset{k_2}{\overset{k_1}{\rightleftharpoons}} HbO_2$$

This chemical reaction can be formally described by the following differential equations [21]:

$$\frac{d[HbO_2]}{dt} = k_1[Hb][O_2]-k_2[HbO_2] \tag{3.12}$$

$$\frac{d[Hb]}{dt} = \frac{d[O_2]}{dt} = -\frac{d[HbO_2]}{dt} \tag{3.13}$$

4. RESULTS AND DISCUSSION

In the present study, the dynamics of blood flow and oxygenation changes during brain activation was investigated using an integrated biomechanical model. The present model takes the effects of dynamic changes in blood oxygenation and blood volume into consideration. The cerebral blood volume, CBV, in the model is taken as the total amount of blood containing Hb in oxidized and nonoxidized form. The results presented below give the relations between f_{out}, f_{in}, v, q, BOLD signal, $PaCO_2$, HbO_2 and O_2 concentrations and time.

4.1. Conventional (Buxton's) Balloon Model

For the viscoelastic effects, $f_{out}(v)$ is treated as an exponential function of the blood entering the venous vessel, f_{in}, with a power of 0.4 as given by equation 3.1. Figure 4.1 shows a similarity with the output of Buxton's Balloon Model (Figure 2.10) where f_{out} is treated as a function of the balloon volume and the rate of change of that volume. The pattern on the figure comes from the additional term of τ dv/dt at the end of the relation. The balloon initially resists a change in volume, but eventually settles into a new steady-state that conforms to the power law model.

Basically, the volume versus time graph (Figure 4.2) shows where the name 'Balloon Model' comes from. If the volume of the blood in the arterial part of the vessel increases, the venous part does not regulate itself very quickly. It only can increase its volume after a delay time, τ. The delay in the increase of the vessel diameter leads to an inflation which is observed as a balloon. Figure 4.2 shows these changes in the vessels.

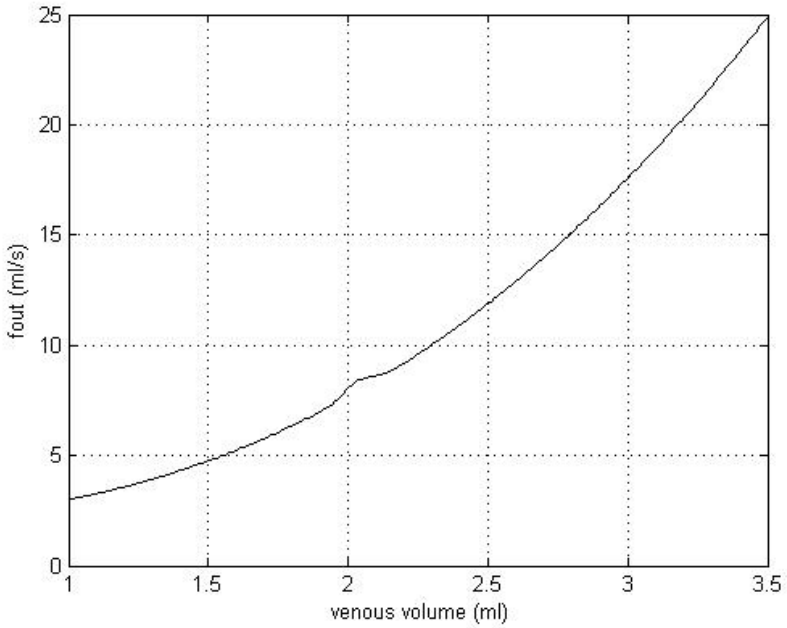

Figure 4.1. f_{out} versus f_{in}.

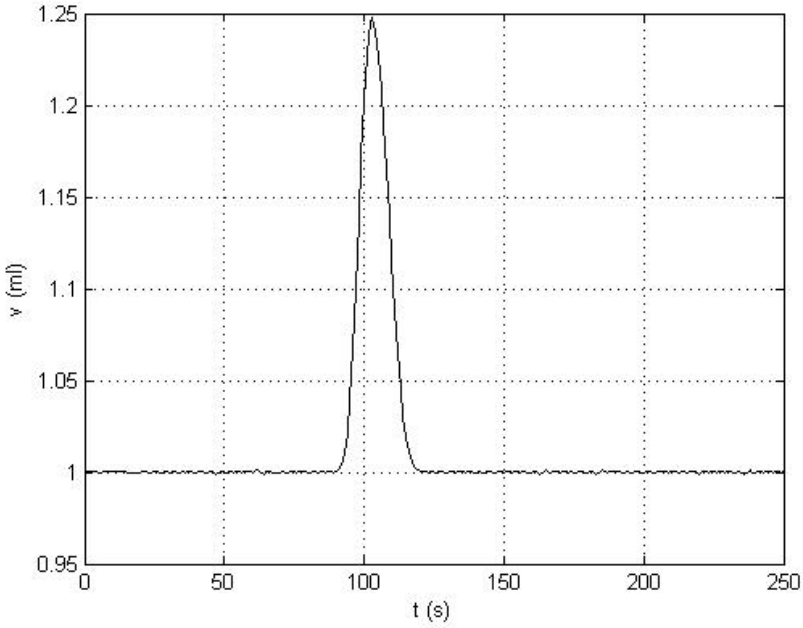

Figure 4.2. Venous volume versus time.

The increment in the venous volume, v, occurring after a stimulus causes a decrement in the concentration of Hb (Figure 4.3). In fact, the number of Hb molecules never increase or decrease in the blood. But the increment in the venous volume causes a decrement in its concentration per volume. Furthermore, the relation between the concentration of Hb and the venous blood volume is expressed by the equation 2.4. The second term on the right hand side of the relation shows the reverse ratio between q and v. Since the increment in v is much greater than the decrement in Hb it results with a net increment in BOLD signal (Figure 4.4).

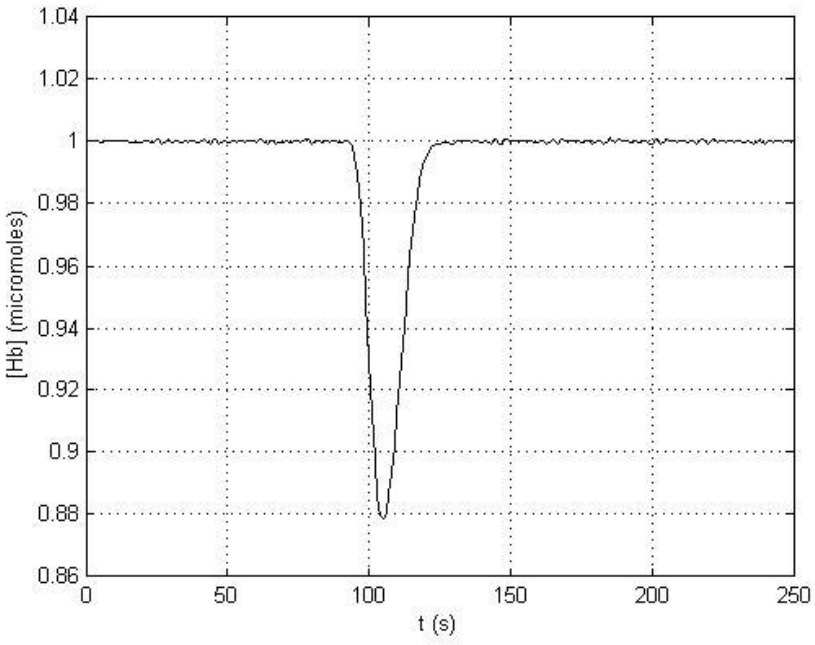

Figure 4.3. Deoxyhemoglobin concentration versus time.

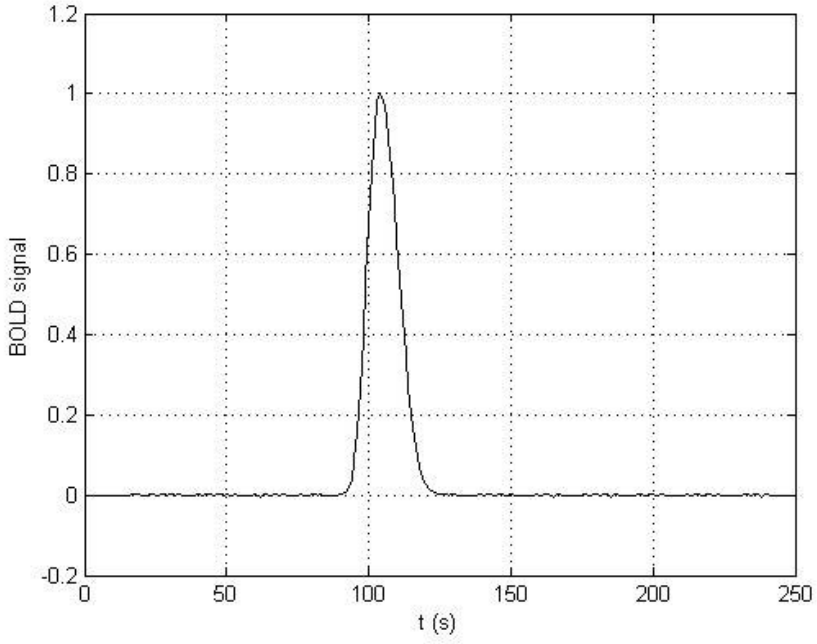

Figure 4.4. BOLD signal versus time.

4.2. Integrated Neurovascular Coupling (NVC) Model

Within the framework of the present study, CO_2 kinetics is added to conventional Balloon Model as the main improvement of the existing biomechanical model. f_{in} versus time graph indicates briefly how the experiment is performed. According to figure 4.5, the first 90 seconds is set as rest with a normal breathing pattern. Then the holding of breath was performed for 30 seconds after expiration of all the breath. Finally, 90 seconds were spent at rest. So, the input of the blood flow to the model is said to be a trapezoidal function by time (Figure 4.5).

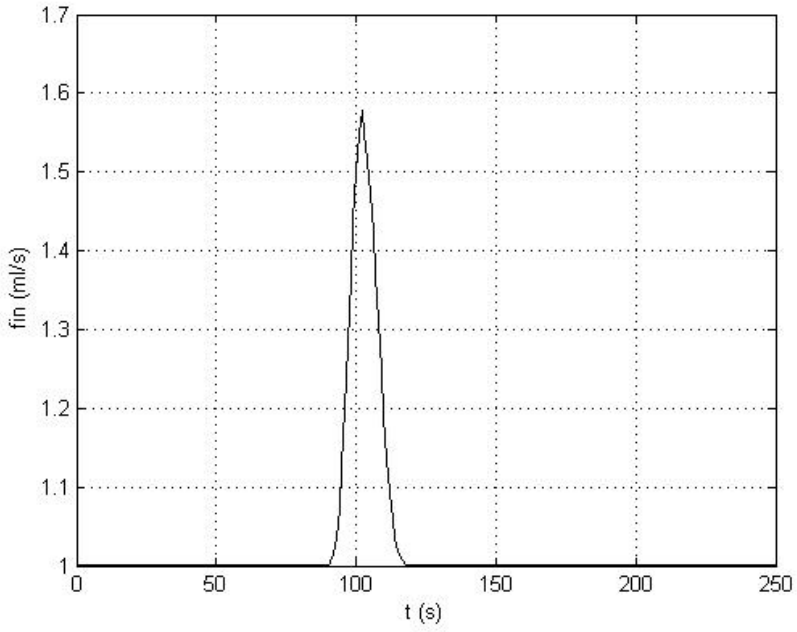

Figure 4.5. f_{in} versus time.

During a breath holding task, the partial pressure of CO_2 is known to be the driving force of the brain hemodynamics, because the cerebral blood volume CBV will be regulated with respect to this pressure change. The cerebral blood volume will increase until it is totally saturated with CO_2 (Figure 4.6). The derived sigmoid function shows the effect of the increment of the partial pressure of CO_2, $PaCO_2$, on the blood entering the capillary, f_{in}.

The blood coming from the arterial part carries Hb bounded to O_2, HbO_2. When a stimulus is given to the brain it will cause a change in the brain hemodynamics so that the brain cells need more oxygen. As a result, the increment in the blood flow on the arterial part of the vessel will cause an increment in the concentration of HbO_2 (Figure 4.7).

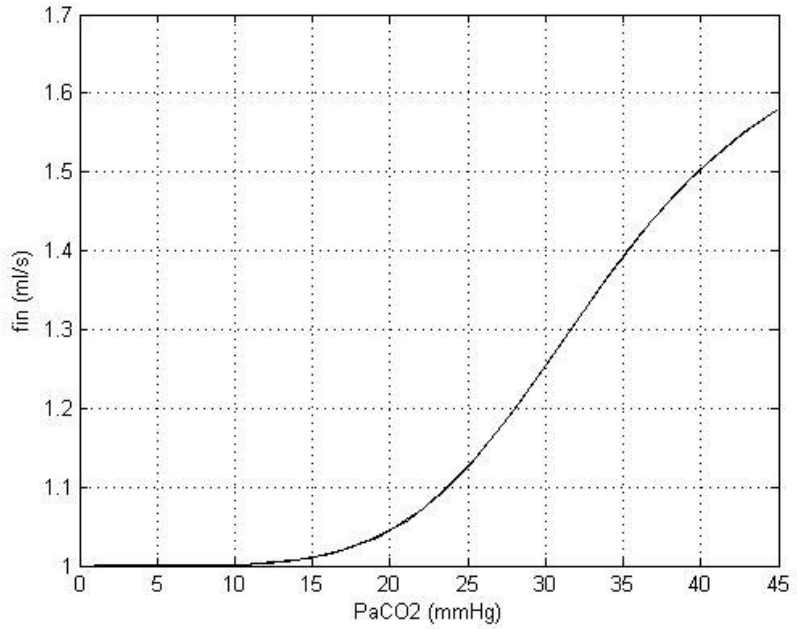

Figure 4.6. f_{in} versus partial pressure of CO_2.

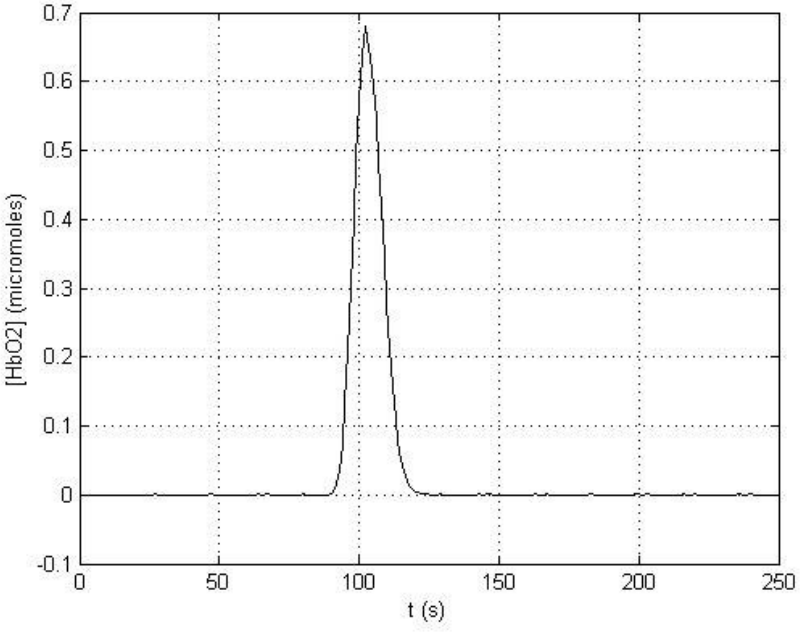

Figure 4.7. HbO_2 concentration versus time.

The carriage of more HbO_2 to the cells facilitates the chemical reaction in the cells which is a combustion reaction and needs O_2 to occur. So, when HbO_2 is carried to the capillaries by the arterial part of the vessel, oxygen will be separated from HbO_2 and it will be extracted by the cells with the oxygen extraction factor (OEF). So, the concentration of oxygen in the arterial part decreases (Figure 4.8).

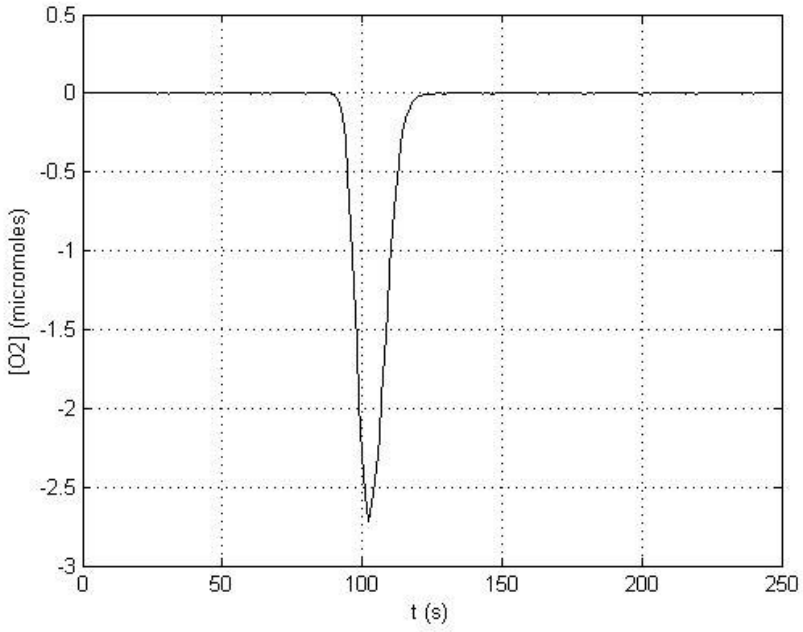

Figure 4.8. O_2 concentration versus time.

When a stimulus is applied, it causes an increment in the reaction mechanism which then causes an increment in the consumption rate of O_2 and decrement in O_2 concentration which in turn results in a decrement in the HbO_2 concentration in the arterial part of the vessel. So, as a conclusion the changes occurring in HbO_2 and O_2 concentrations are in opposite directions (Figure 4.9). Furthermore, the knowledge of the four binding sites for oxygen at each hemoglobin molecule expresses the ratio of the consumption rates of oxygen with respect to HbO_2.

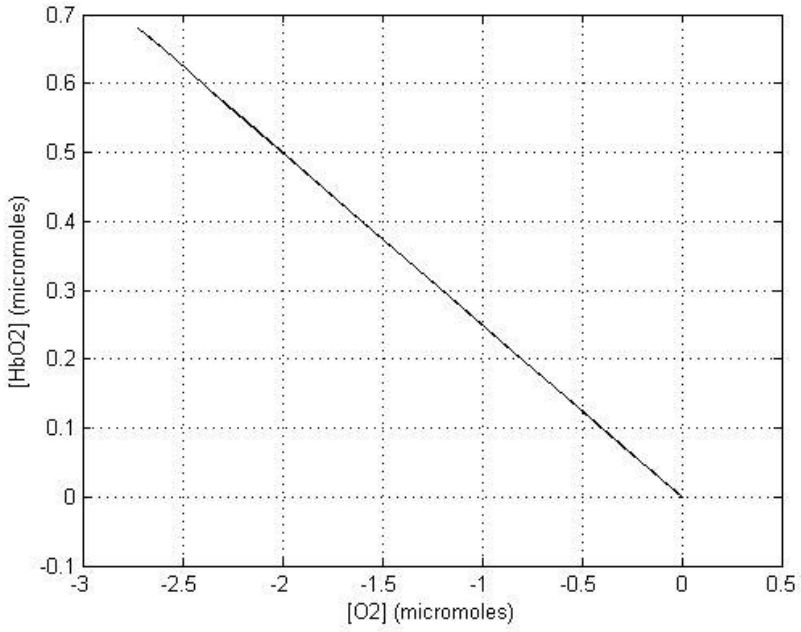

Figure 4.9. HbO_2 concentration versus O_2 concentration.

4.3. Application of the Integrated NVC Model to Volunteer's Data (Healthy Subject- Migraineur)

Several medical imaging, diagnostic and research tools are sensitive to the hemoglobin, in its oxygenated and/or deoxygenated forms, that is present in the blood. For example, near-infrared spectroscopy (NIRS) measures the optical absorption associated with oxyhemoglobin and deoxyhemoglobin, and BOLD (blood oxygen level-dependent) functional magnetic resonance imaging (fMRI) is based on magnetic susceptibility changes induced by paramagnetic deoxyhemoglobin. NIRS measurements of the concentration and oxygen saturation of hemoglobin in tissue, the fMRI BOLD signal and any measurement of blood oxygenation *in vivo* are the result of the interplay among a number of physiological parameters such as blood volume, blood flow and metabolic rate of oxygen. The conventional and integrated NVC Model graphs are the outputs from fMRI BOLD signals [19].

Figure 4.10 is one of the Hb outputs taken from a healthy subject during the breath holding experiment using NIROXCOPE 301. A healthy subject's typical Hb data begins with an initial dip then comes to a saturation value before it makes a post stimulus undershoot. Figure 4.11 is ST's fNIRS-Hb data obtained under the condition of a slight headache at Boğaziçi University Institute of Biomedical Engineering Biophotonics laboratory using NIROXCOPE 301. When the hemoglobin data of a migraineur is compared with that of a healthy subject's, the initial dip existing in the Hb data of healthy subject is greater than the dip seen in migraineur's Hb data (Figure 4.11). An additional difference between these graphs is that the healthy subject's hemoglobin concentration values reach to the baseline value after the post undershoot, but the migraineur's Hb data do not (Figure 4.11).

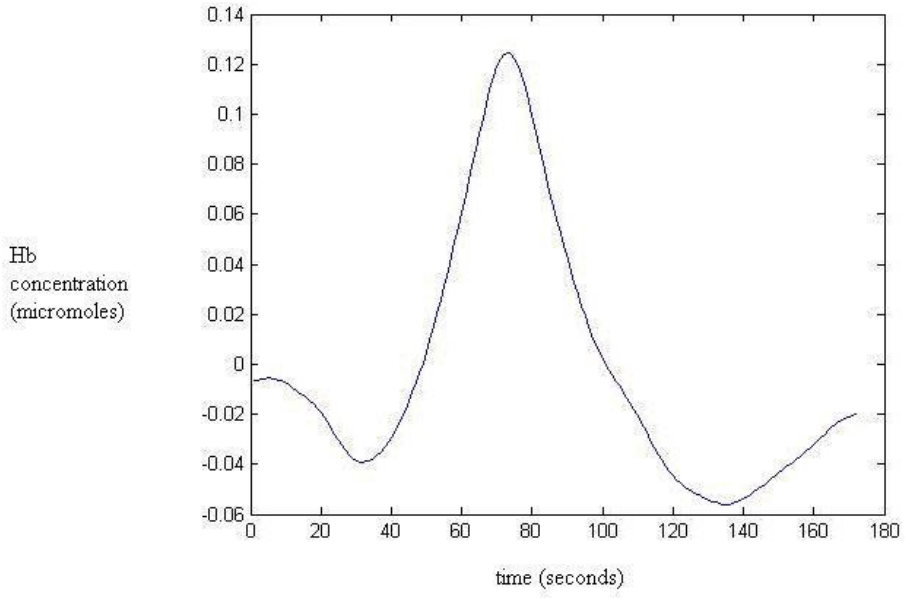

Figure 4.10. A healthy subject's hemoglobin concentration versus time graph.

The difference between a healthy subject and a migraineur comes from the absence of the serotonin hormone in migraineurs. It is a hormone that regulates the blood vessels, i.e. serotonin dilates vessels when a stimulus is given and contracts when there is no more stimulus. So, as a result, the blood vessels of a migraineur could not be dilated and the blood volume does not increase as much as it does in a healthy subject. The reason of the initial dip occurring in a healthy subject is that, when a stimulus is applied, the serotonin

hormone dilates the brain vessels and the volume of the vessels increase. Therefore, the Hb concentration decreases per volume of blood.

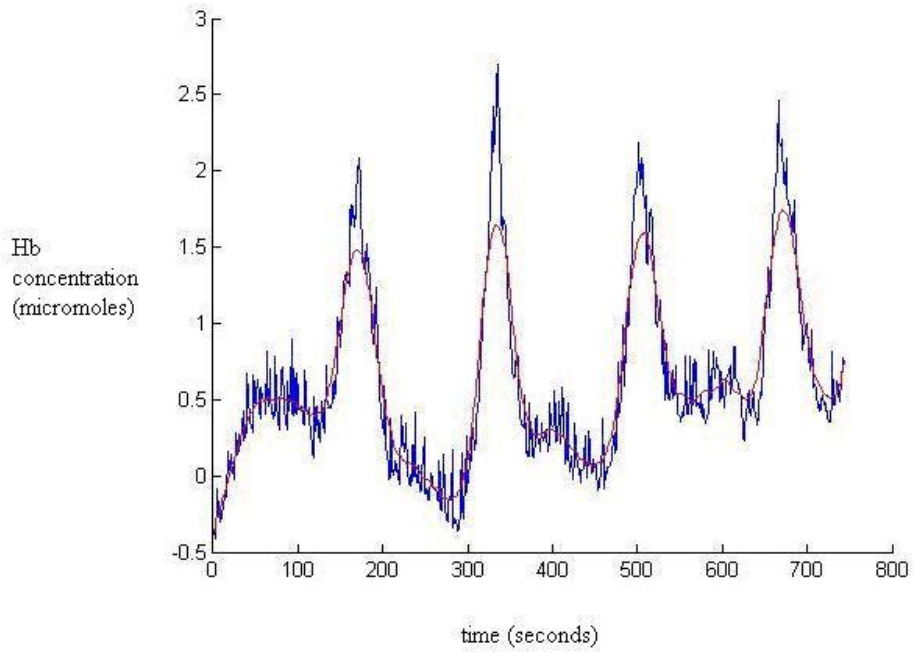

Figure 4.11. A migraineur's hemoglobin concentration versus time graph.

As the trapezoidal time values have an importance on the physiological explanation of the change in the brain hemodynamics, the standard deviations of each trapezoidal time values of the healthy and migraineur subjects are calculated separately (Table 4.1). It is evident that the time values are characteristic to the subjects. The first time value of the trapezoidal function is the time elapsed at rest position (normal breathing is succeeded), which depends on the experimental protocols. The main difference comes from the second time value, which shows the duration that the brain hemodynamic changes take place. It is not yet known how long it takes the brain to regulate itself to the stimulus. This time value includes both the time spent during regulation and the time to get to the saturation value. Furthermore, the third time value, which indicates the time spent to get to the normal value (baseline value), is an unknown in the brain hemodynamics. Therefore, the least squares curve fitting is used to characterize the unknown trapezoidal time values.

As it can be seen from Table 4.1, the standard deviation values of the migraineur subject is at least two times that of the healthy subject's. That can be explained by the regulation problem in the brain blood vessels of the migraineur. It cannot be regulated as quickly as it was in the healthy one because of the absense of the serotonin hormone in migraineurs.

Table 4.1. Trapezoidal Time Value Comparison of Healthy and Migraineur Subjects

	Trapezoidal time values for healthy and migraineur subjects	Standard deviation t_1	Standard deviation t_2	Standard deviation t_3	Standard deviation t_4
Healthy subject (1st breath holding)	[354.7735 360.5704 362.3079 384.1565]	1.5117	2.3655	2.5136	1.8480
Healthy subject (2nd breath holding)	[352.1234 360.0115 362.3902 379.9149]				
Healthy subject (3rd breath holding)	[352.2093 365.2857 367.6809 380.6665]				
Migraineur (1st breath holding)	[91.5598 114.7428 113.9390 134.1226]	6.1063	4.6463	5.7351	5.1100
Migraineur (2nd breath holding)	[101.4680 111.9891 119.0211 132.0294]				
Migraineur (3rd breath holding)	[86.8102 103.8025 105.1379 122.3887]				

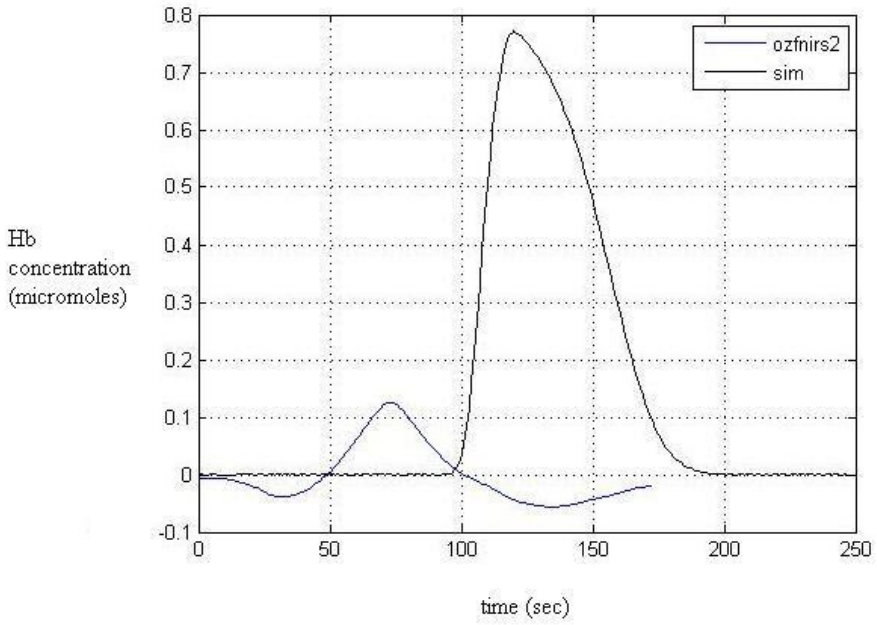

Figure 4.12. Healthy subject's and the simulated Hb graphs versus time.

The experimentally obtained Hb data of the healthy subject are lower than the simulated data obtained by the Balloon Model (Figure 4.12). The dynamics observed in real data are far different than the simulated data. Hence we resort to least squeares method to be able to estimate the parameters that will make the difference minimum. The lagging between the data occurs as a result of the experimental protocol. This is the first study on migraine, therefore there can not be any comparison with the literature data.

Figure 4.13 compares average value of ten migraineurs' and ten healthy subjects' Hb data. The blue time profile, the average of ten healthy subjects' Hb data, has higher values with an initial dip and a post undershoot which are the main differences from the migraineurs' data.

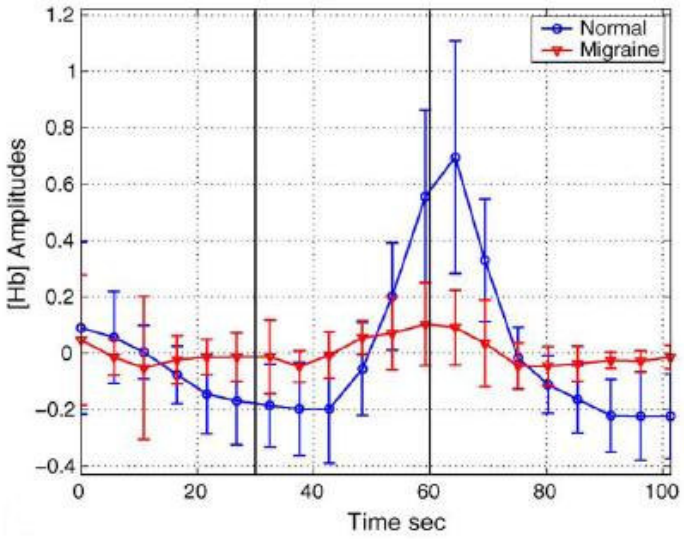

Figure 4.13. The average of ten migraineurs' and ten healthy subjects' Hb data [29].

4.4. Sensitivity Analysis

4.4.1. Effect of Trapezoidal Window

In order to investigate the effect of size and corner values of trapezoidal window on the curve shapes, twelve different trapezoid windows are chosen.

Trapezoid01 = [90sec 118sec 120sec 210sec] (original window)

Trapezoid02 = **[60 118 120 210]**

Trapezoid03 = **[70 118 120 210]**

Trapezoid04 = **[110 118 120 210]**

Trapezoid05 **= [90 108 120 210]**

Trapezoid06 **= [90 98 120 210]**

Trapezoid07 **= [90 118 150 210]**

Trapezoid08 **= [90 118 170 210]**

Trapezoid09 **= [90 118 200 210]**

Trapezoid10 **= [90 118 120 150]**

Trapezoid11 **= [90 118 120 180]**

Trapezoid12 **= [90 118 120 250]**

This window parameter caused significant changes in the time profiles of v, q, BOLD, f_{in}, HbO_2 and O_2 (Figures 4.14, 4.15, 4.16, 4.17, 4.18 and 4.19). Although the shapes of the curves remained similar, the profiles shifted in time. There is no change in the saturation values of these time profiles while the shape was varying through window length or incremental size between trapezoid corners.

The first value of the trapezoidal function does have an effect on the time spent at rest position. If it is increased and all the other values of the trapezoidal function are kept constant, it results with an insufficient saturation time. The increment or decrement in the second corner value of the trapezoidal function results in a nonrealistic pattern of the saturation time profile. The third corner value of the trapezoidal function indicates the time that the blood flow is regulated. The increment or decrement in this value shows how it is rapid to regulate the flow. It must show a realistic pattern. The decrement or increment of this value results with a smoother or a steeper pattern, respectively.

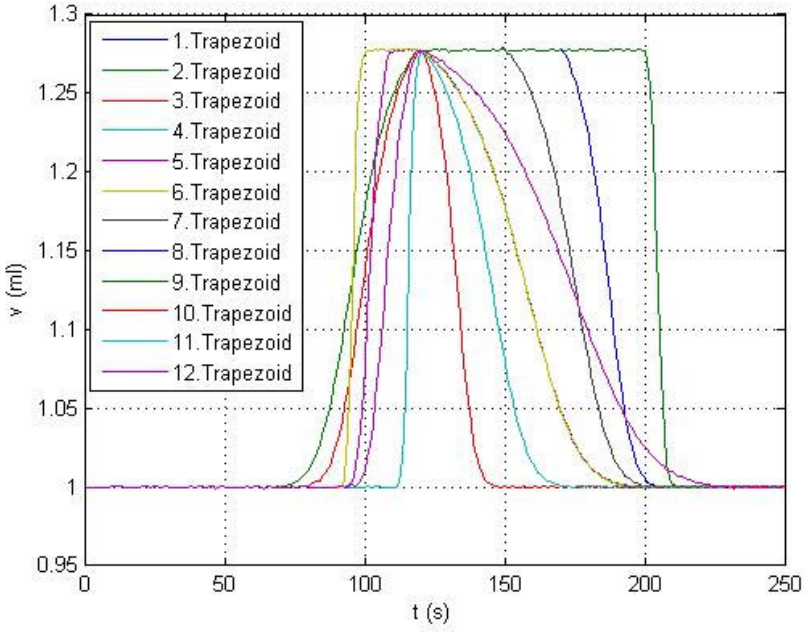

Figure 4.14. Volume versus time at different window parameters.

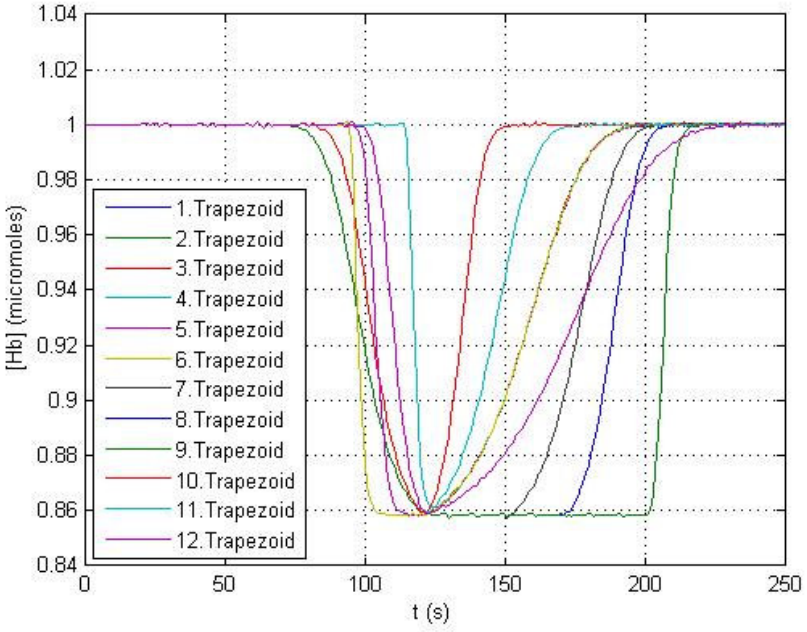

Figure 4.15. Deoxyhemoglobin concentration versus time at different window parameters.

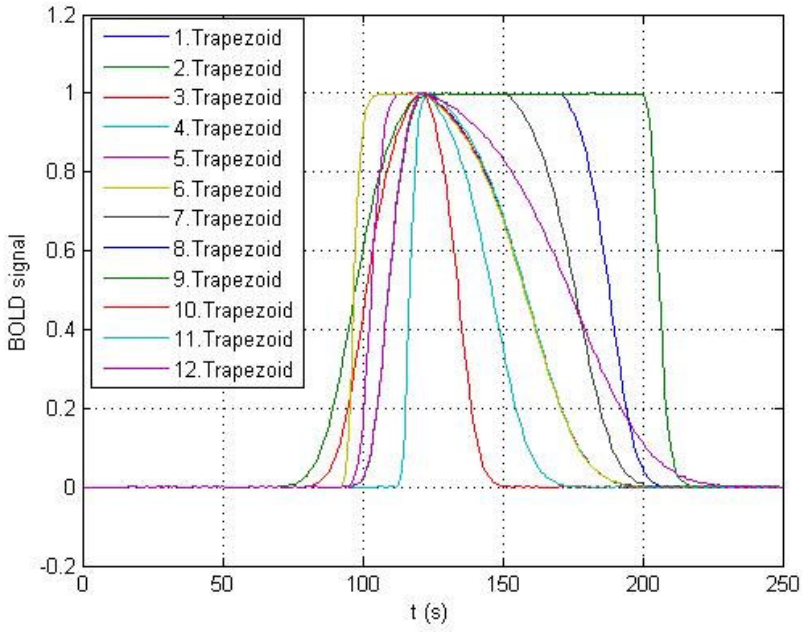

Figure 4.16. BOLD signal versus time at different window parameters.

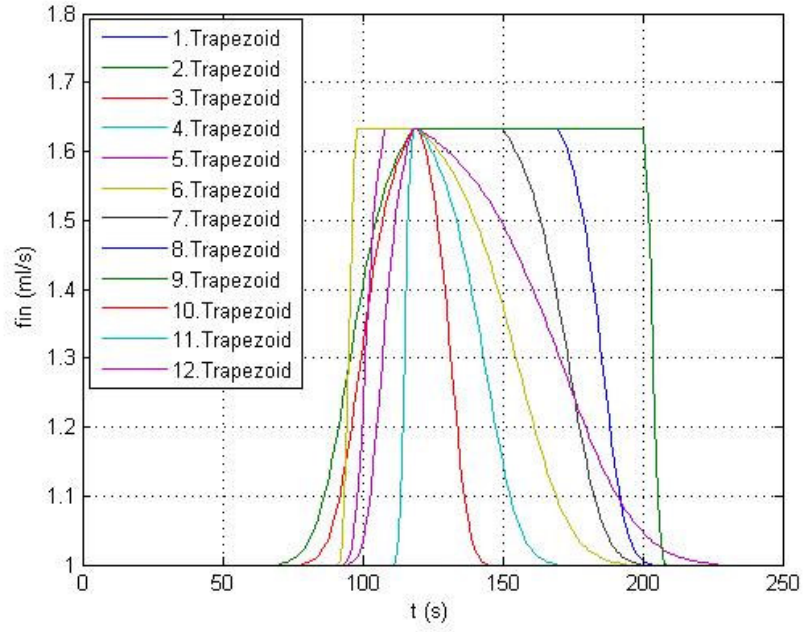

Figure 4.17. f_{in} versus time at different window parameters.

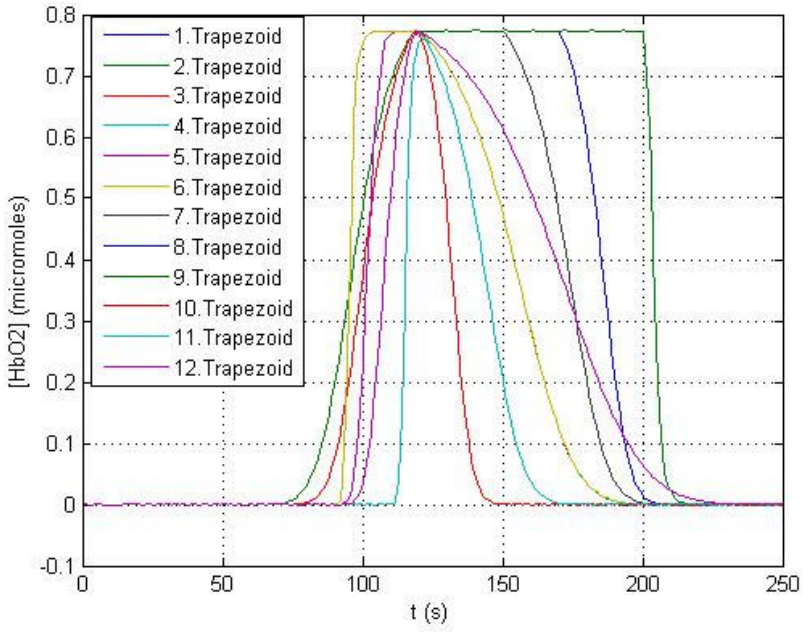

Figure 4.18. HbO_2 concentration versus time at different window parameters.

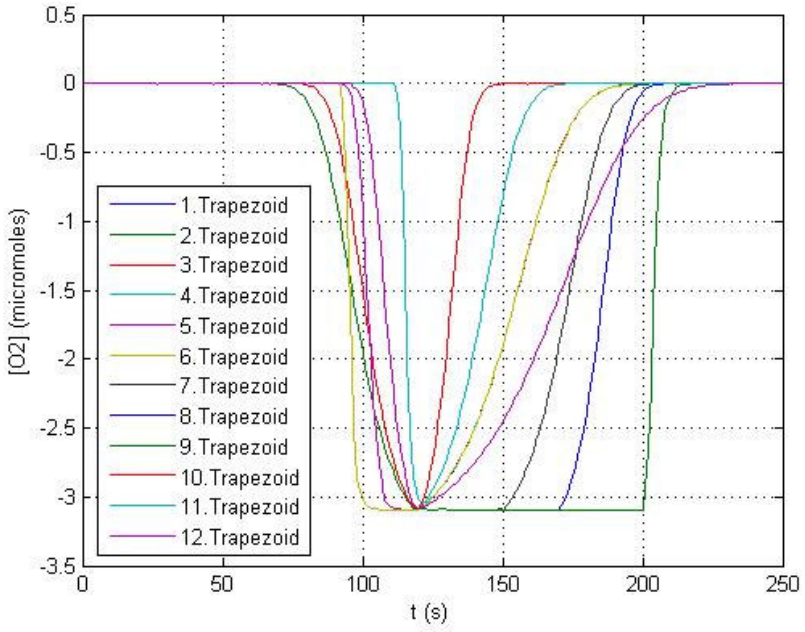

Figure 4.19. O_2 concentration versus time at different window parameters.

4.4.1.1. ANOVA Analysis Results

ANOVA compares the means of two or more groups of data. It returns the p-value for the null hypothesis that the means of the groups are equal. Here it is used to find the most significant parameter in the trapezoidal function time values. A parameter is considered as significant only if p-value is less than or equal to 0.05. The below graphs (Figures 4.20, 4.21, 4.22, 4.23) show the ANOVA analysis results of the trapezoidal function time values. The number (1) is the used for the control, i.e. healthy subject, where the number (2) is used for the migraineur data. The standard deviations indicated with the short lines above the double trapezoidal shapes belonging to the healthy subject and the migraineur data. Each line at the middles of these double trapezoidals are the mean values of the time values. As it can be seen from Table 4.2, the trapezoidal time value t_1 is the most significant whereas t_3 is the least significant parameter. In addition to this, t_2 and t_4 have similar significances. t_1 is the time elapsed at rest position where the normal breathing is performed which causes the binding reaction of oxygen to hemoglobin. If the time is not long enough for binding of oxygen to hemoglobin in migraineurs, the data on hemoglobin concentration indicate the regulation problem occuring in the brain hemodynamics.

Table 4.2. P-values of ANOVA Analysis

Trapezoidal Time Values	P- values
t_1	0.0009
t_2	0.0752
t_3	0.7180
t_4	0.0975

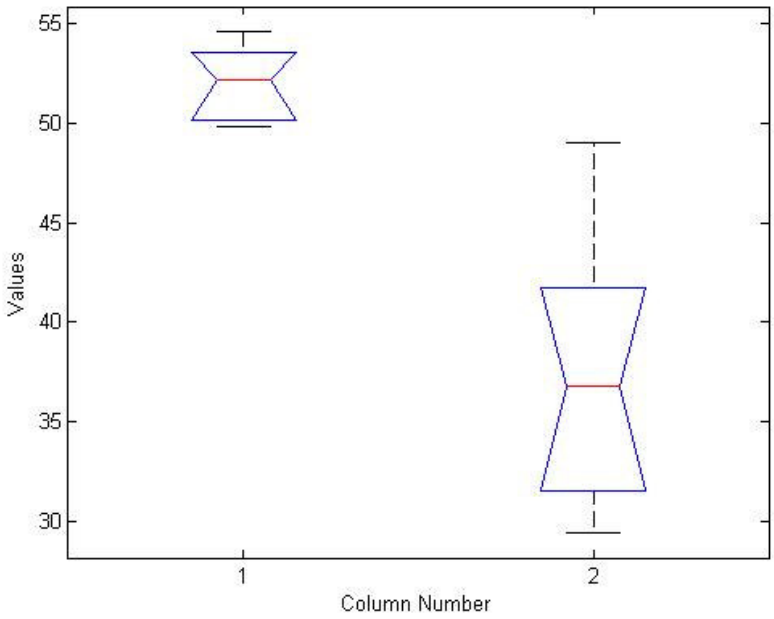

Figure 4.20. t_1 time value ANOVA analysis.

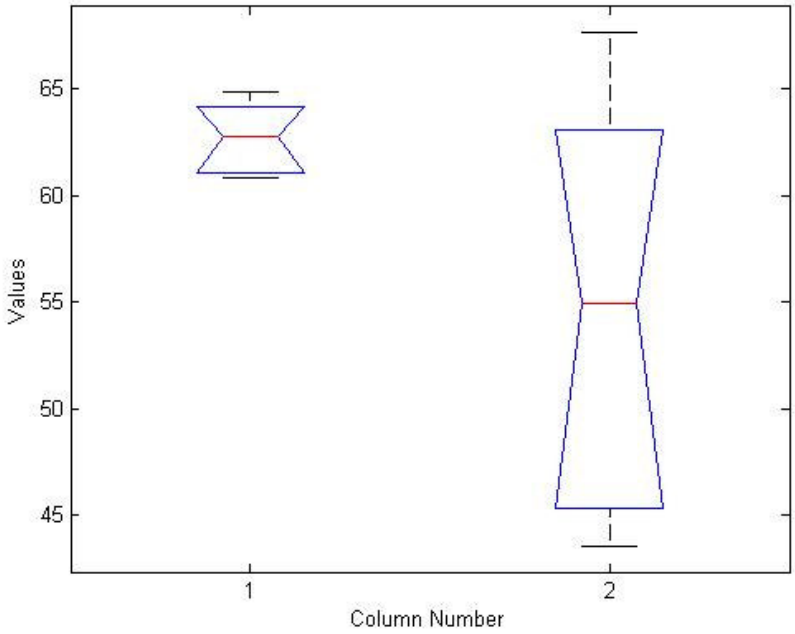

Figure 4.21. t_2 time value ANOVA analysis.

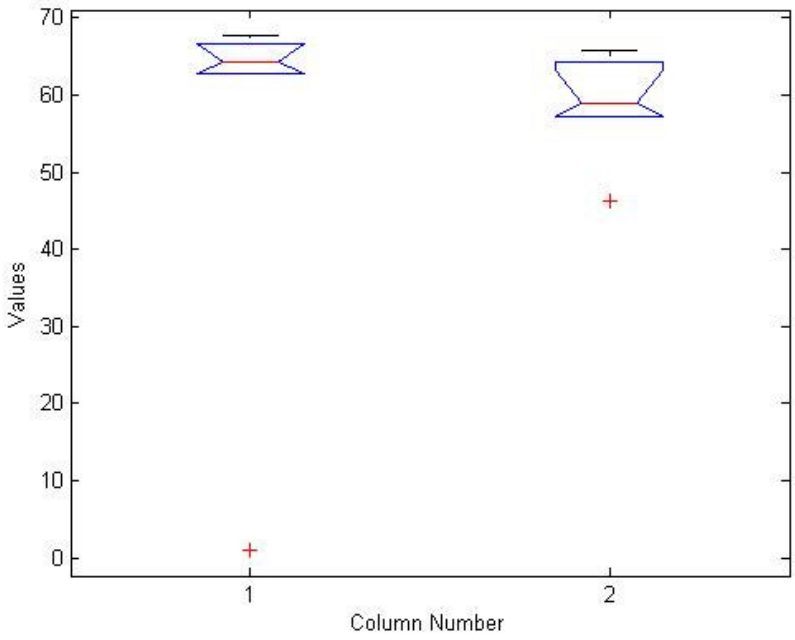

Figure 4.22. t_3 time value ANOVA analysis.

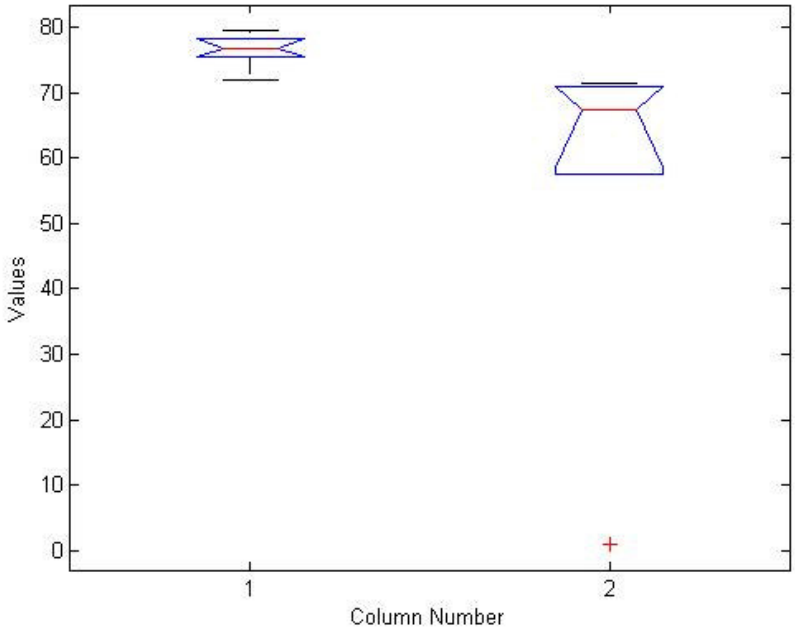

Figure 4.23. t_4 time value ANOVA analysis.

4.4.2. Effect of Oxygen Extraction Factor (E_0)

E_0 is the baseline value of the OEF and the local oxygenation of the venous blood depends directly on E. The critical value of E_0 is found to be equal to 0.4. Oxygen extraction fraction is a potentially important factor in determining the nature of evoked fMRI responses because it may be sensitive to the nature of the baseline that defines the resting state.

The change in the value of E_0 has an effect on the plots of Hb (Figure 4.24), BOLD signal (Figure 4.25), HbO_2 and O_2 concentrations (Figures 4.26 and 4.27) with respect to time. Increases in this parameter can have profound effects on the shape of the response that bias it toward an early dip. The increment or the decrement in this value causes a stability problem. Even though there has not been anything performed in the first 10 seconds, the change in E_0 causes a change in this time interval. An important point to mention in this analysis is that a change in E_0 causes the maximal points of the plots to change except the BOLD signal. BOLD signal equation can tolerate this effect of E_0 with the coefficients of k_1, k_2 and k_3 and with the volume term, v (Figure 4.25).

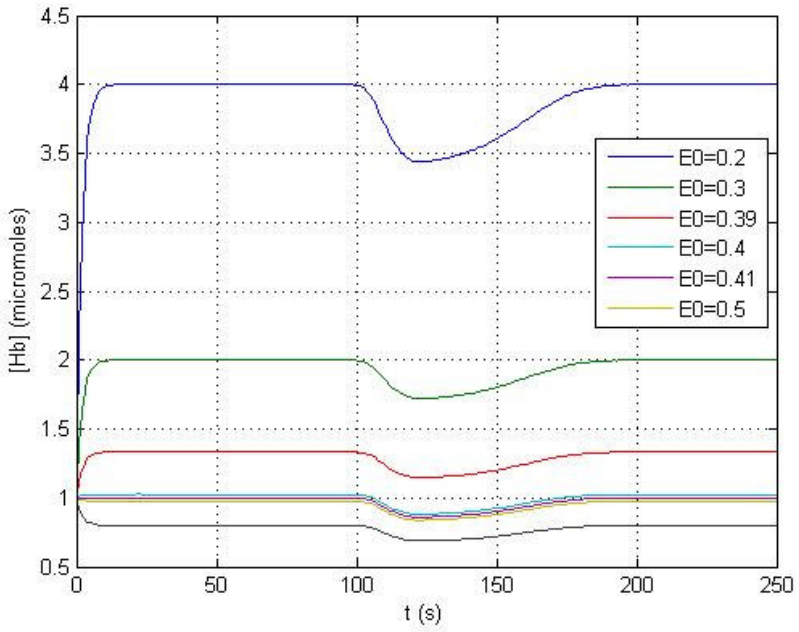

Figure 4.24. Deoxyhemoglobin concentration versus time at different E_0 values.

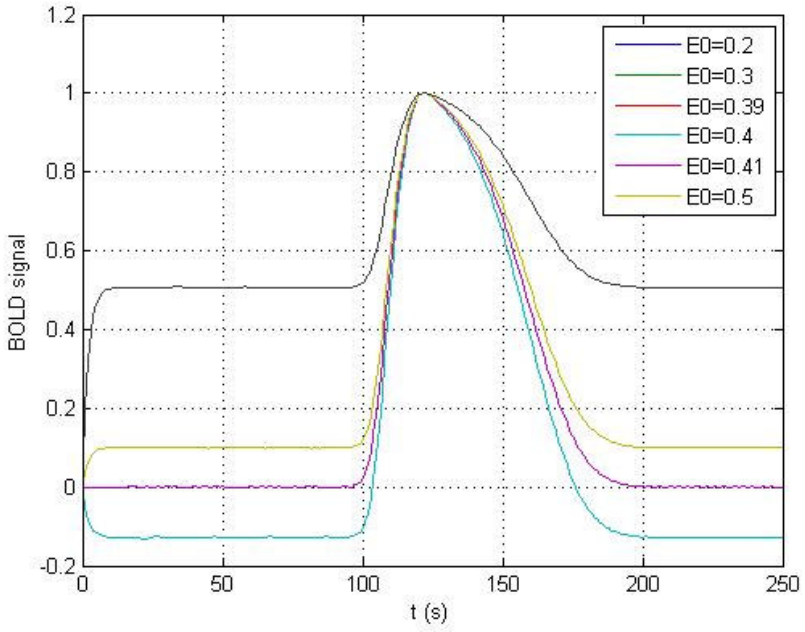

Figure 4.25. BOLD signal versus time at different E_0 values.

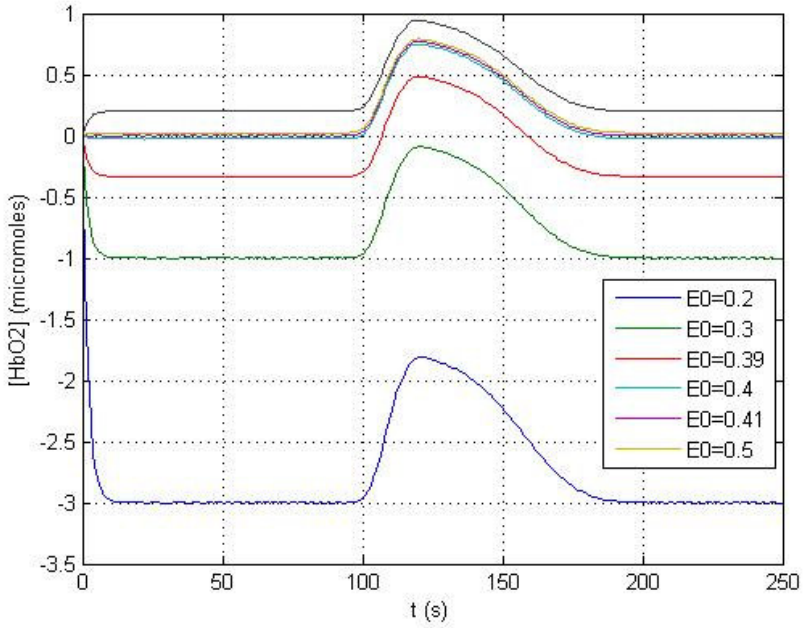

Figure 4.26. HbO_2 concentration versus time at different E_0 values.

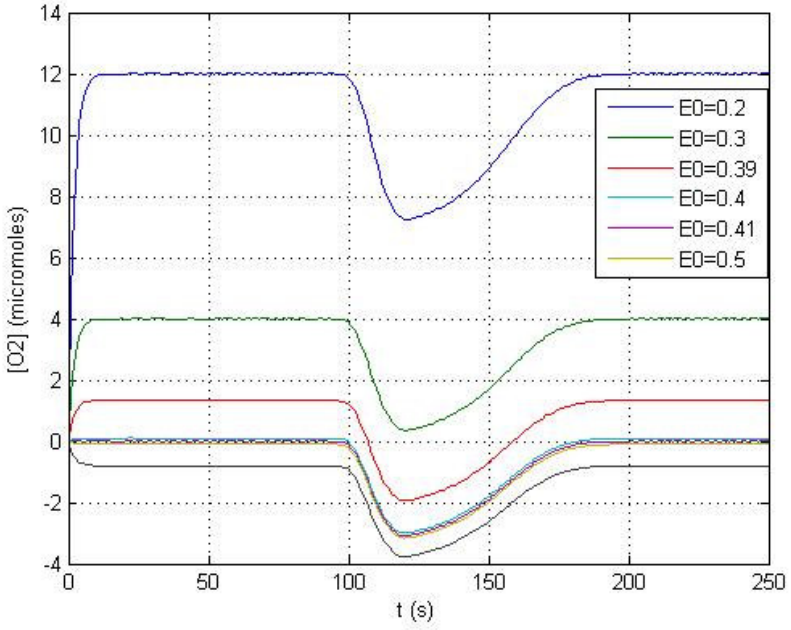

Figure 4.27. O_2 concentration versus time at different E_0 values.

4.4.3. Effect of mean transit time (τ)

Tau (τ) is an important parameter that determines the dynamics of the signal. It is the mean transit time through the venous compartment at rest and the effects of the change in this value are significant as shown in the figures 4.28, 4.29, 4.30, 4.31, 4.32 and 4.33. The effect of increasing mean transit time is to slow down the dynamics of the BOLD signal with respect to the flow changes. The shape of the response remains same but it is expressed more slowly. The original value of τ is 2.

Mathematically the effect of τ_0, τ value at rest, on volume and Hb concentration can be explained by the equations 2.4 and 2.5 showing inverse proportions. The increment in mean transit time results in a decrement in volume and Hb concentration values with longer delay times. The delay time shows how slow the blood flow is regulated.

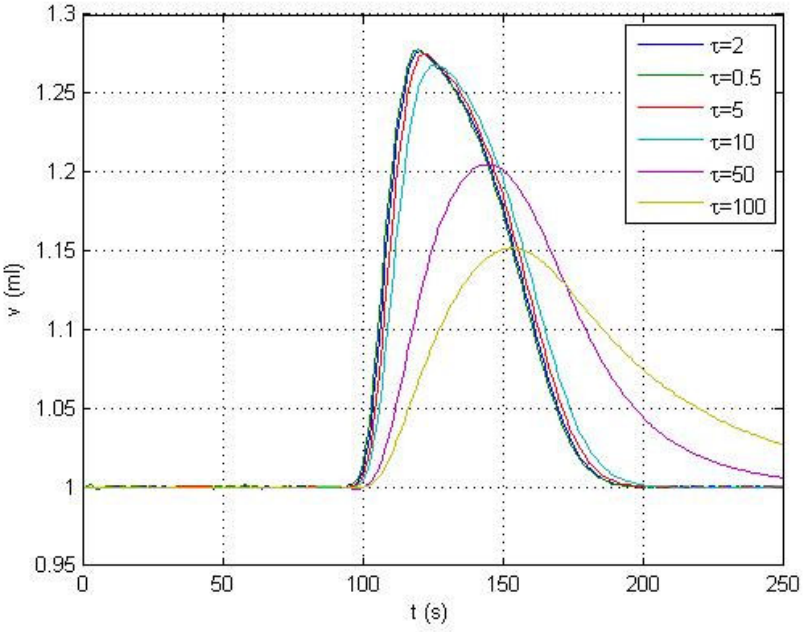

Figure 4.28. Volume versus time at different tau values.

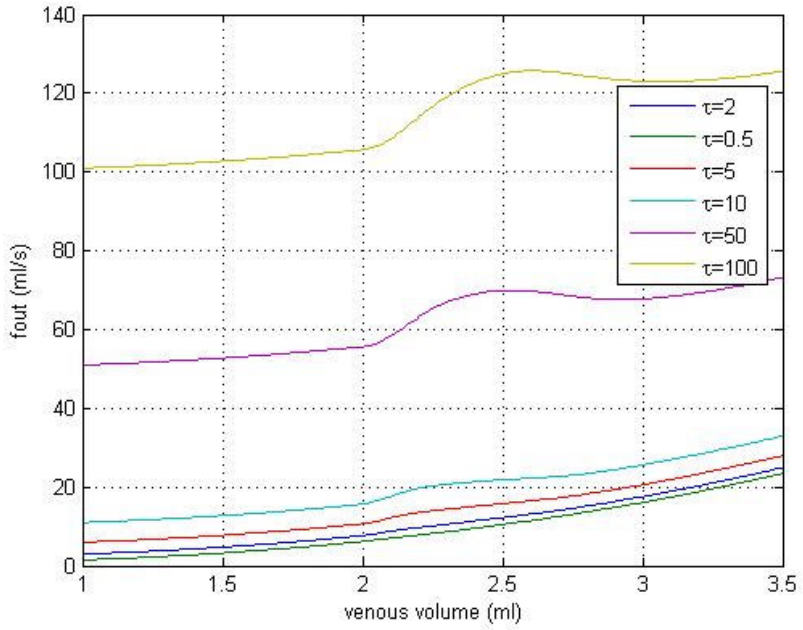

Figure 4.29. f_{out} versus venous volume at different tau values.

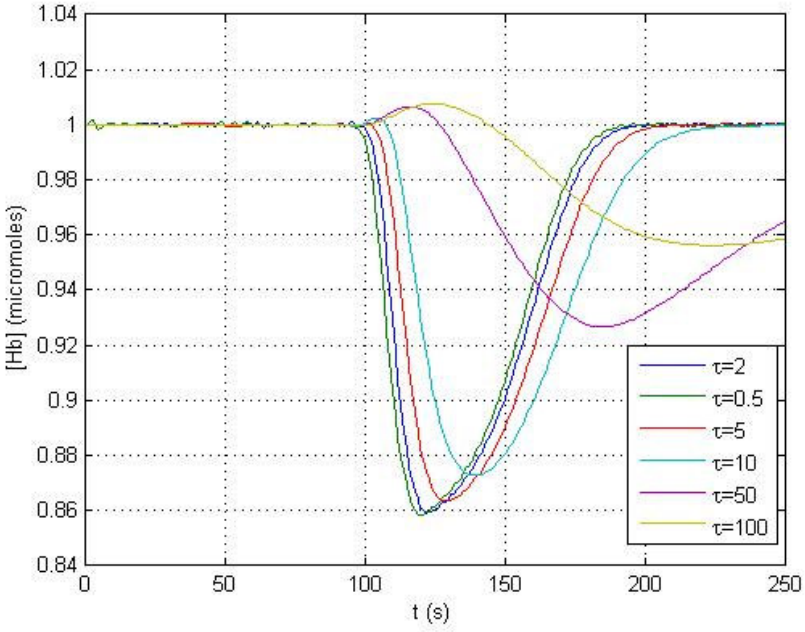

Figure 4.30. Deoxyhemoglobin concentration versus time at different tau values.

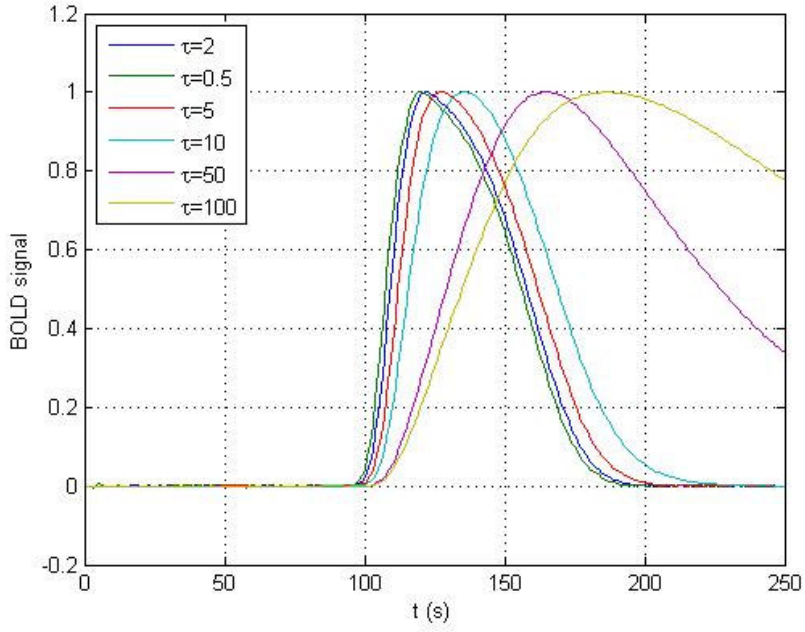

Figure 4.31. BOLD signal versus time at different tau values.

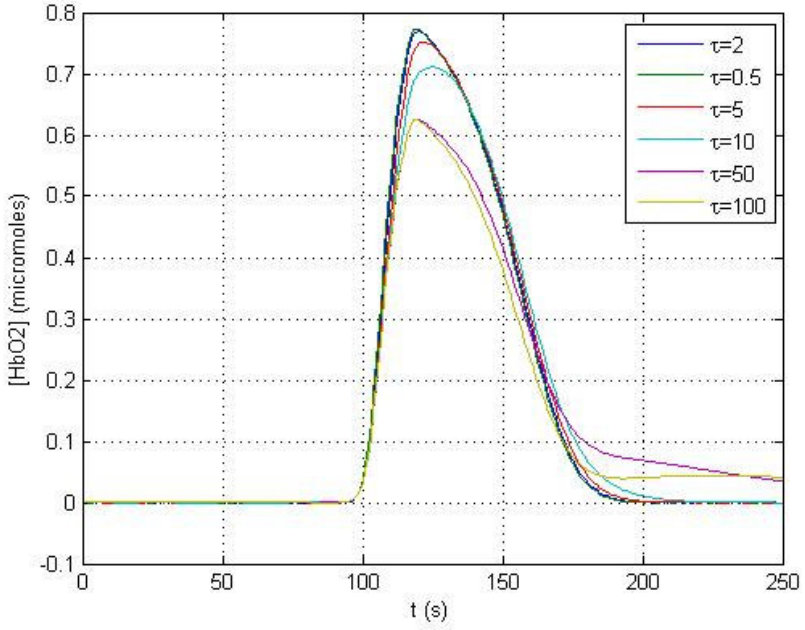

Figure 4.32. HbO_2 concentration versus time at different tau values.

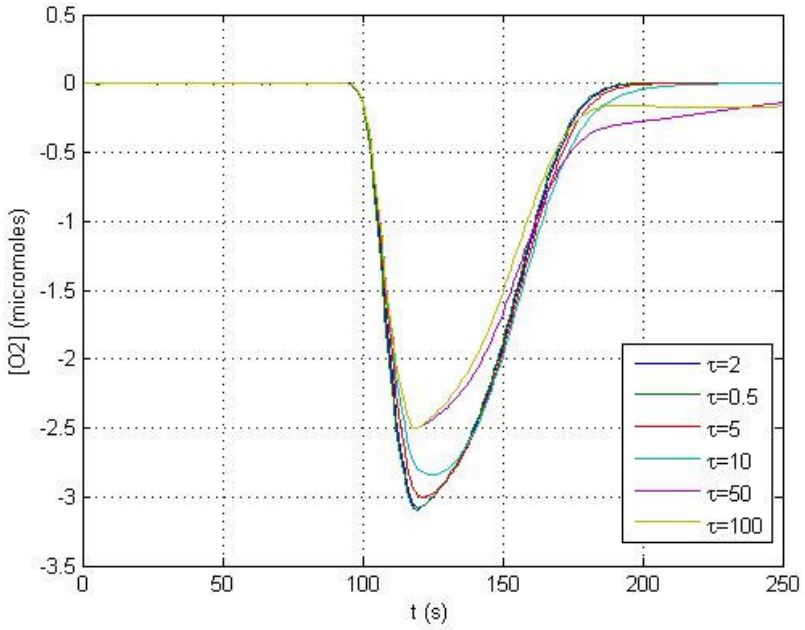

Figure 4.33. O_2 concentration versus time at different tau values.

4.4.4. Effect of Stiffness Parameter (α)

Stiffness parameter, α, appears in the steady-state relationship of blood flow and volume and the transient relation $f_{out}(v)$ that controls the transition from one steady state to another (Equation 3.1). Therefore; the change in the value of α only affects the value of f_{out} exponentially (Figure 4.34). Increasing this parameter increases the degree of nonlinearity in the flow-volume behavior of the venous balloon that underpins the nonlinear behaviors.

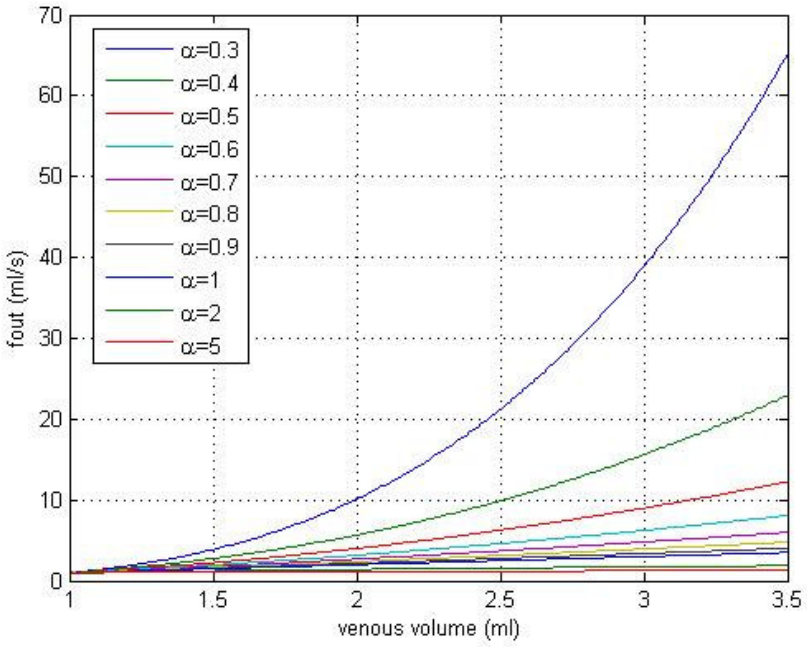

Figure 4.34. f_{out} versus venous volume at different α values.

5. CONCLUSIONS AND RECOMMENDATIONS

5.1. Conclusions

Neural activity in the brain is accompanied by changes in cerebral blood flow (CBF) and blood oxygenation that are detectable with functional magnetic resonance imaging (fMRI) techniques. The recent mathematical models of this hemodynamic response are described for: (1) the blood oxygenation level dependent (BOLD) signal as a function of changes in cerebral oxygen extraction fraction (E) and cerebral blood volume (CBV); (2) the transient dynamics of CBV and deoxyhaemoglobin (Hb) and how they affect the BOLD signal, the Balloon Model; (3) neurovascular coupling, relating the responses in CBF and cerebral metabolic rate of oxygen ($CMRO_2$) to the neural activity response; and (4) the temporal nonlinearity of the neural response itself. However, the modeling of the changes during brain activation needs further improvements as the blood flow from the arteries to the capillaries are so far not taken into consideration.

In this present work, the cerebral blood flow from the arteries to the capillaries is incorporated into conventional Balloon Model. When a stimulus is applied (i.e. when the breath is hold) the cells in the brain tissues continue to do their own work (i.e. break the carbohydrates into its monomers), and hence they need oxygen. Since they keep consuming the oxygen in the cerebral blood, the concentration of CO_2 will be increasing. When the CO_2 comes to a saturation level in the blood, the volume of the blood will increase. It can be assumed that the partial pressure of CO_2 is the driving force of the mechanism in the brain hemodynamics and thus it is used as the input to the conventional NVC Model (Figure 4.35). The relation between $PaCO_2$ and f_{in} is given as an input function in the integrated model. Hence, one of the main contributions of the present study to Buxton's Balloon Model is the addition of the CO_2 kinetics, which is in the form of a sigmoid function. The set of differential equations describing oxygen kinetics are also integrated to NVC model (Figure 4.35) and the changes in blood volume, arterial oxygenation, capillary transit time, rate of O_2 uptake and hemoglobin concentration are estimated and the hemoglobin concentrations of a healthy subject are also compared with a migraineur's Hb data (my own data).

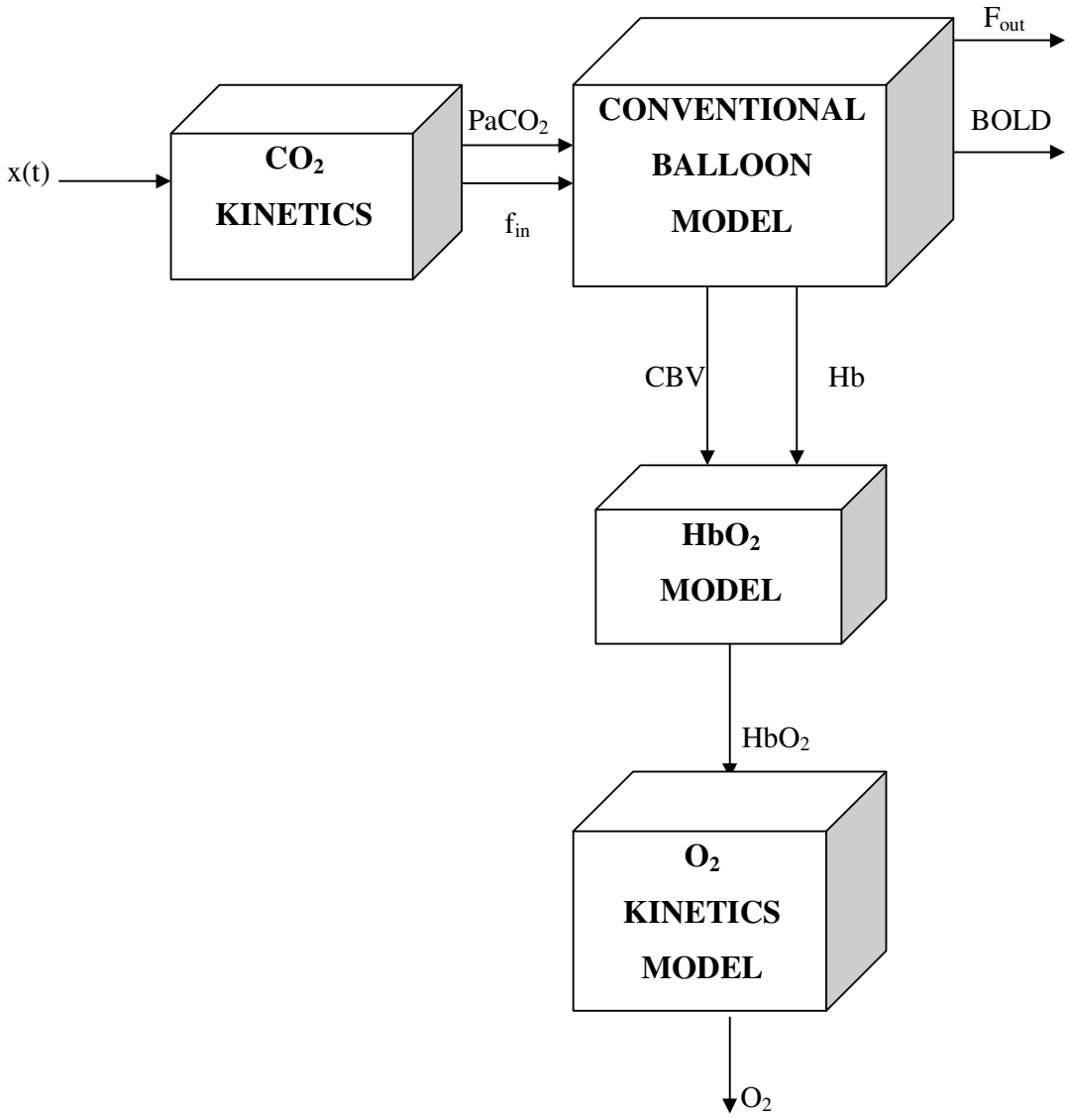

Figure 4.35. Block Diagram of Integrated Neurovascular Model.

Among the four phases of migraine (prodrome, aura, attack, postdrome), a decrease in CBF is observed in aura phase. The release of neuronal activator serotonin, from platelets cause an increase in plasma serotonin, which in turn causes constriction of cerebral blood vessels and a reduction in CBF in aura phase. That leads to a depletion or drop in serotonin level which is followed by vasodilatation (swelling of blood vessels) causing pain and an increase in blood flow. The results of the present modeling study indicate that during migraine, f_{in} (CBF) and concentration of oxyhemoglobin (HbO_2) increase, but concentrations of deoxyhaemoglobin (Hb) and oxygen (O_2) decrease which

are in agreement with the literature data. During a breath holding task (in analogy to the condition of a migraineur), there is no additional oxygen gained, but there is an increase in the consumption rate of oxygen which then causes a decrease in the concentration of oxygen. A comparison of the time profiles of deoxy-Hb concentration between a healthy subject and a migraineur indicates a regulation problem in the blood vessels related to the serotonin level.

The above findings indicate that the present integrated NVC model successfully predicts the changes in deoxy-Hb, HbO_2 and O_2 concentrations together with those in the venous compartment volume, v, and BOLD signal during brain activation and enables us to undersand the facts underlying the migraine illness and its pathophysiology to distinguish a migraineur from a healthy subject.

5.2. Recommendations

- In the present model, the brain hemodynamics is not regulated strictly in the model and therefore, the output graphs of the Integrated Neurovascular Coupling Model is weak at the oscillations. There should be an initial dip followed by a post undershoot mechanism after the stimulus. In this respect, further studies may include the mechanisms of these oscillations.

- It is predicted that the initial value of the partial pressure of CO_2, $PaCO_{2i}$, is an important data in brain hemodynamics. But it is still unknown and cannot be personalized to each human. A relation can be developed to include $PaCO_{2i}$ in further studies.

- The relation between $PaCO_2$ and f_{in} are developed for a healthy subject. A further study may include the derivation of a relation for a migraineur data.

6. APPENDIX

6.1. Additional Results of Sensitivity Analysis

6.1.1. Sensitivity Analysis on Trapezoidal Window

Figure 6.1 shows how the trapezoidal window affects the function parameters. Any significant change is not observed in the patterns of these variables.

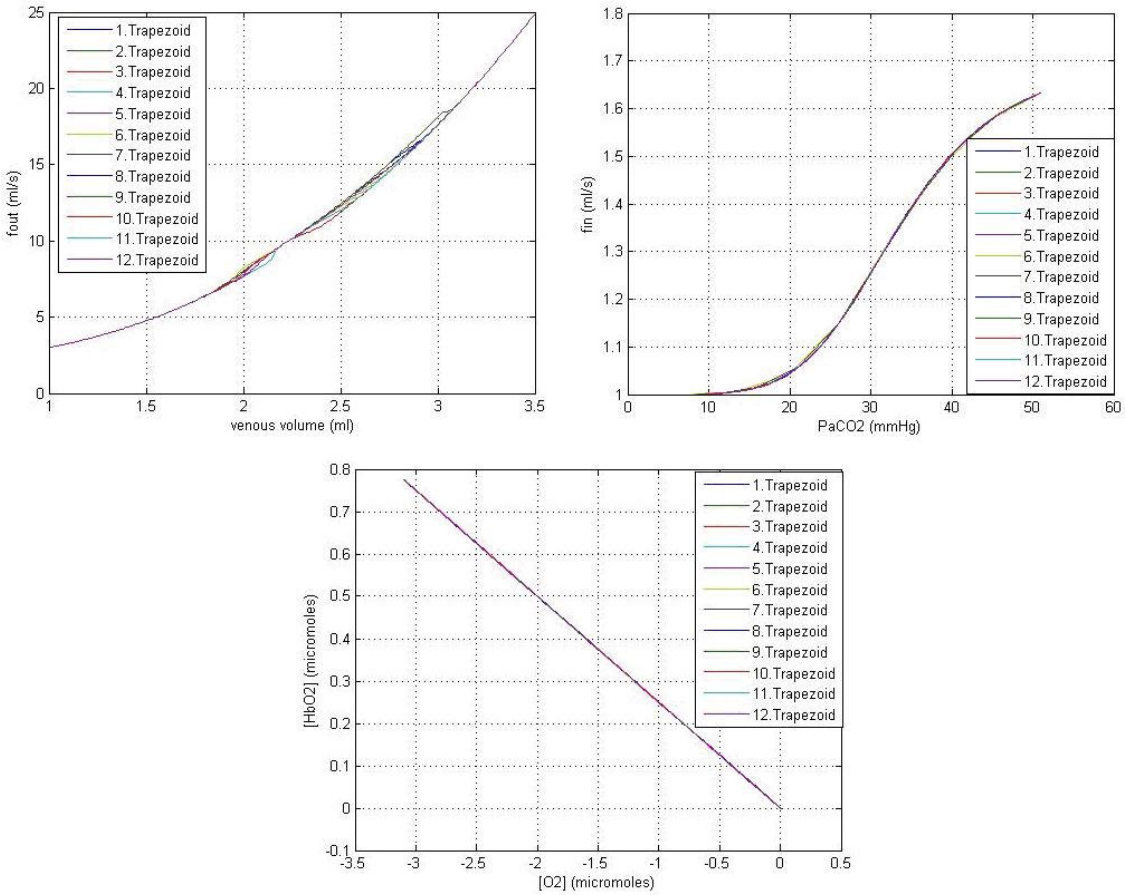

Figure 6.1. Integrated NVC Model at different window values.

6.1.2. Sensitivity Analysis on E_0

OEF is a parameter related to the rate constant of the separation of O_2 from HbO_2. So, it is a parameter related to the concentration of Hb and therefore it does not make any sense in the other physiological parameters (Figure 6.2).

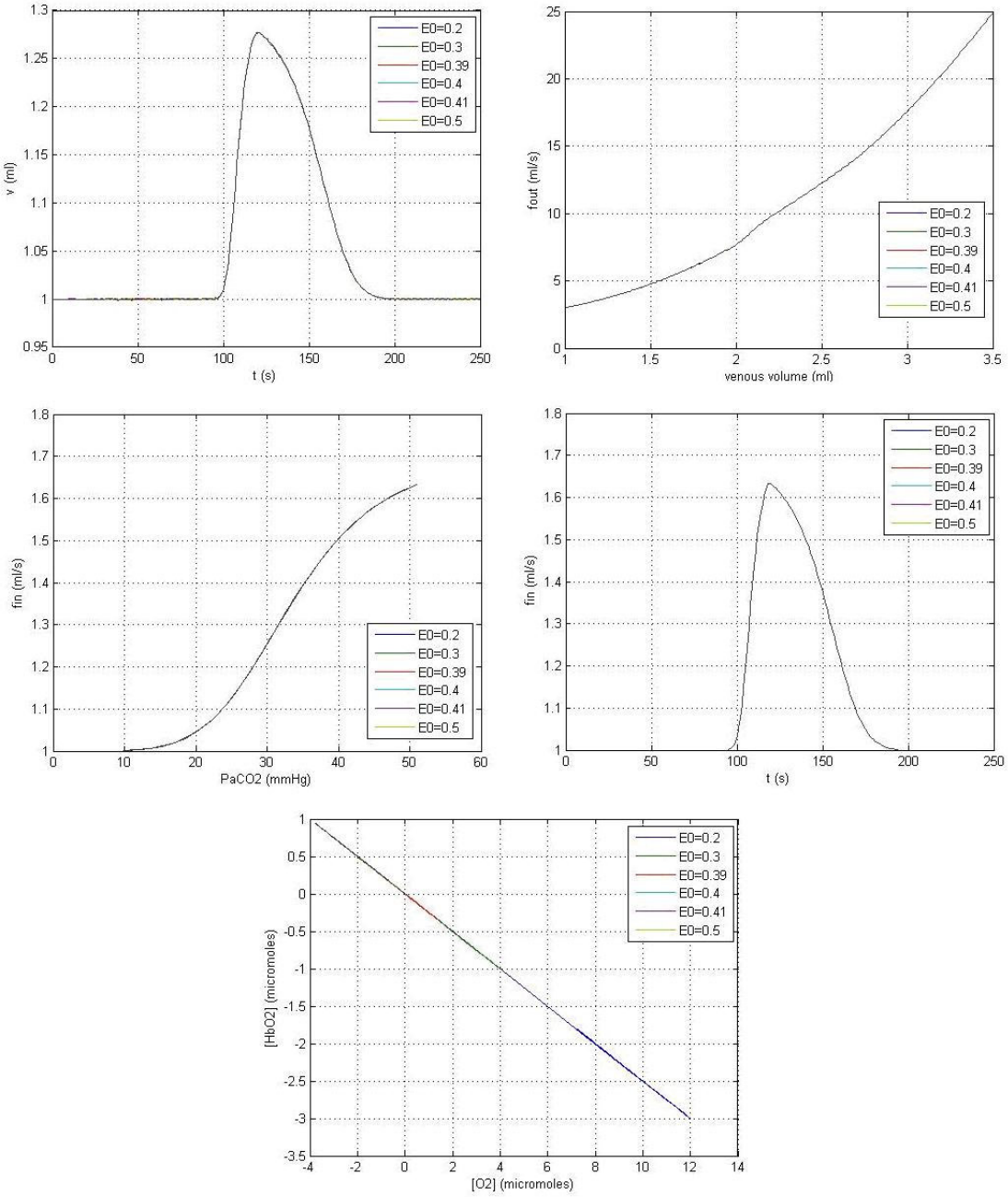

Figure 6.2. Integrated NVC Model at different E_0 values.

6.1.3. Sensitivity analysis with respect to Tau (τ)

Figure 6.3 gives the effect of tau parameter on f_{in}, $PaCO_2$, HbO_2 and O_2 concentrations. Since τ is an important parameter on the time elapsed to reach the steady state value, any effect could not be observed from the plots independent of time. f_{in} versus time plot is dependent only on the trapezoidal time values which do not change with time.

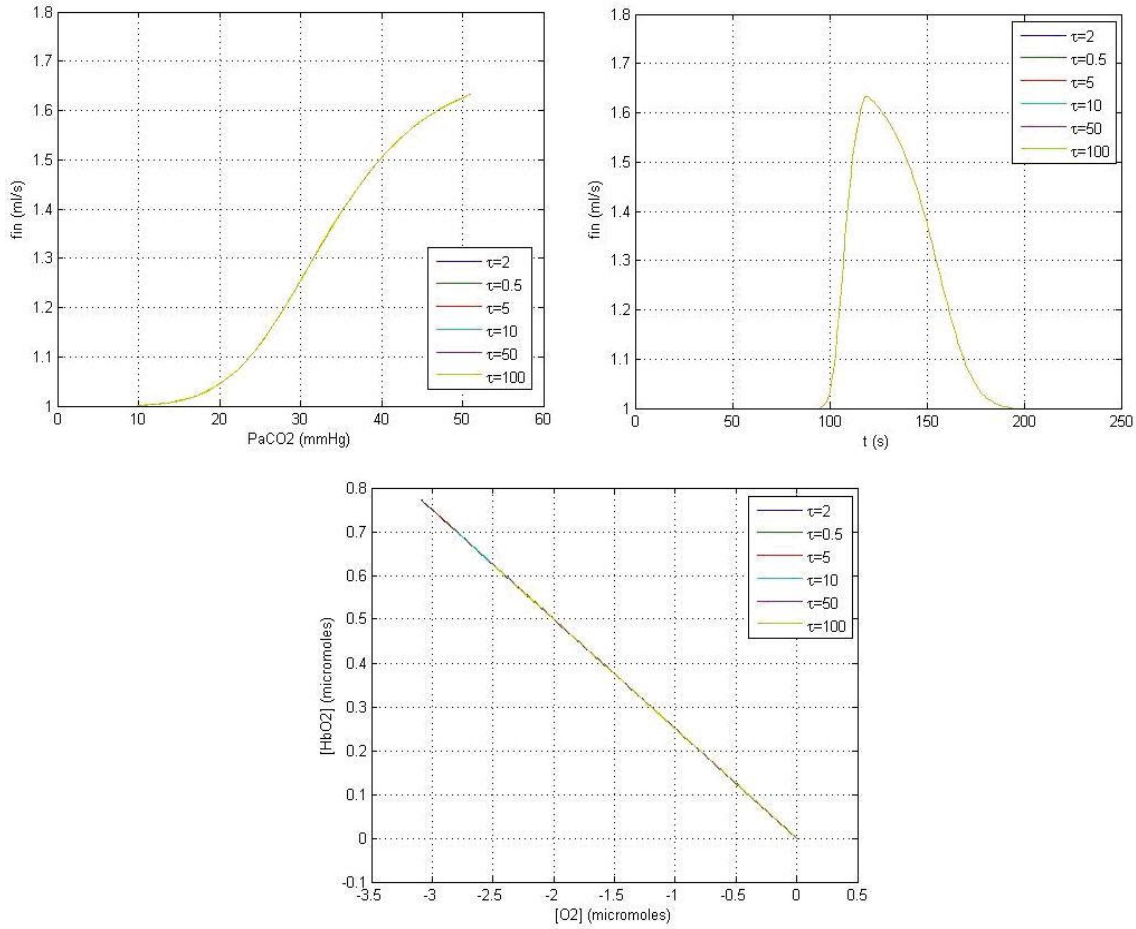

Figure 6.3. Integrated NVC Model at different tau values.

6.1.4. Sensitivity analysis with respect to the coefficients in BOLD signal expression

The sensitivity analysis on the coefficients of the BOLD signal (k_1, k_2 and k_3) indicated that these coefficients do not have any effect on the Integrated NVC Model (Figure 6.4, 6.5, 6.6).

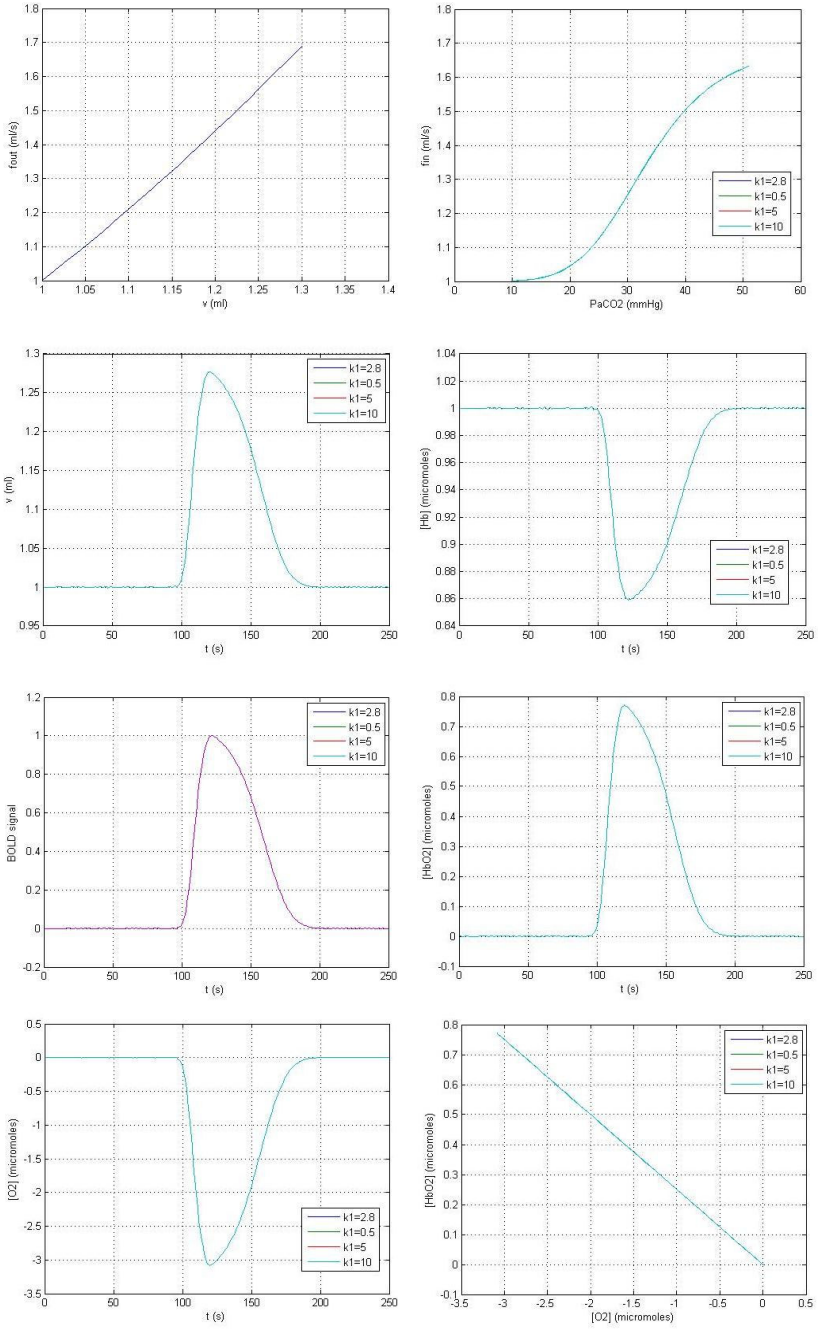

Figure 6.4. Integrated NVC Model at different k_1 values.

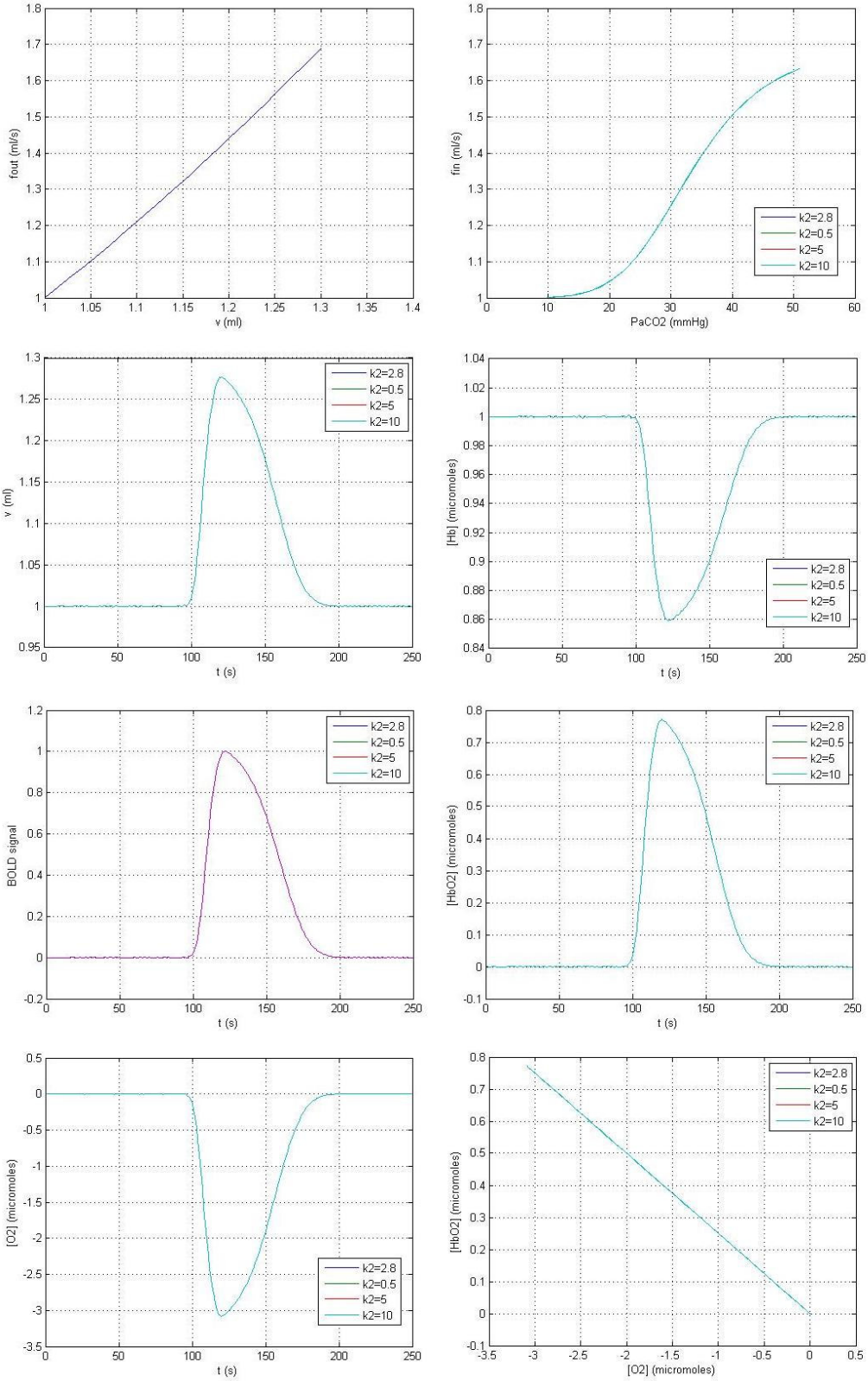

Figure 6.5. Integrated NVC Model at different k_2 values.

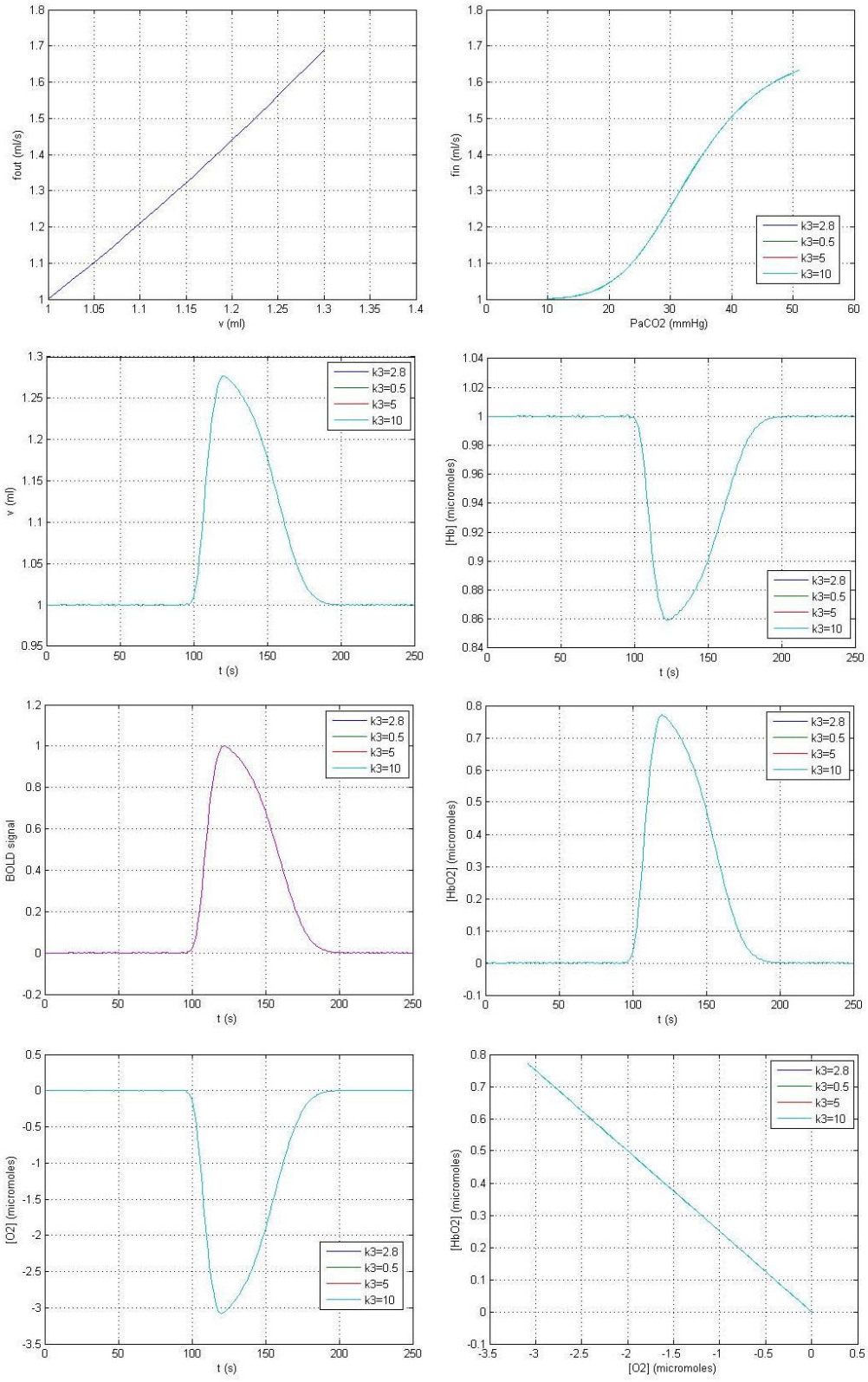

Figure 6.6. Integrated NVC Model at different k_3 values.

6.2. Trapezoidal Time Value Estimation by Trapezoidal Function Fitting of a Healthy Subject

The trapezoidal time values are found by the least squares curve fitting method which solves non-linear least squares problems. The Matlab® command *lsqcurvefit* automatically draws the trapezoidal shape of the function (Figure 6.7). The best trapezoidal function giving the real deoxy-Hb data is estimated. The r-square value of the trapezoidal function fitting is 0.9741.

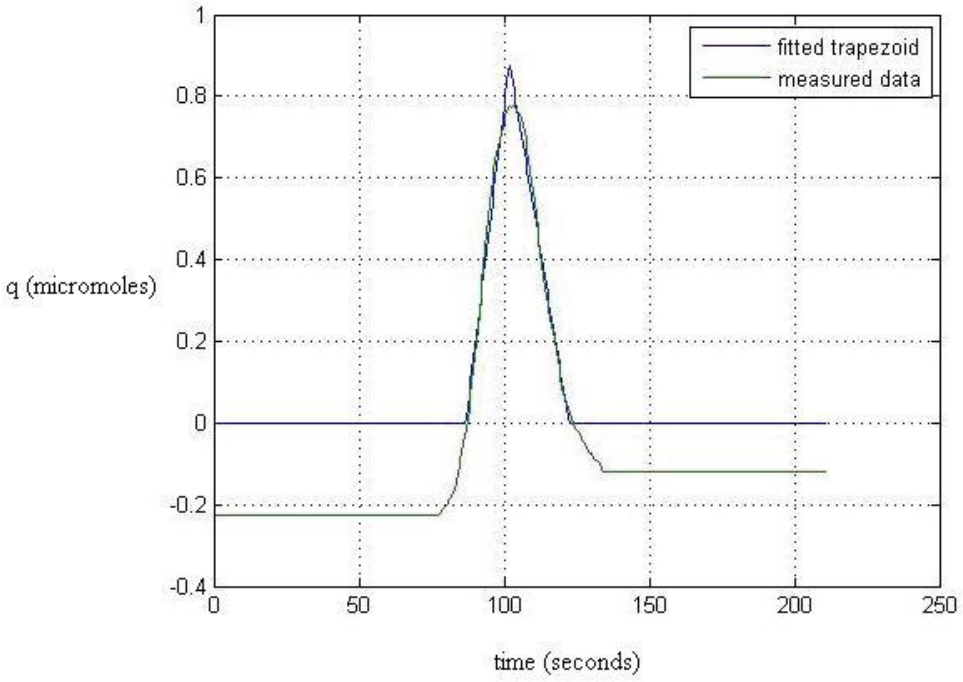

Figure 6.7. Least squares curve fitting to a healthy subject data.

REFERENCES

1. Moskowitz, M. A., H. Bolay and T. Dalkara, “Deciphering Migraine Mechanisms: Clues from Familial Hemiplegic Migraine Genotypes”, American Neurological Association, Vol. 55, No. 2, February 2004.

2. Hargreaves, R. J. and S. L. Shepheard, “Pathophysiology of Migraine - New Insights”, Canadian Journal of Neurological Sciences, Vol. 26, Suppl. 3, pp. 12-19, 1999.

3. Loder, E., “What is the Evolutionary Advantage of Migraine?”, Cephalalgia, Vol. 22, pp. 624–632, 2002.

4. Siniatchkin, M., N. Averkina, F. Andrasik, U. Stephani and W.D. Gerber, “Neurophysiological Reactivity Before a Migraine Attack”, Neuroscience Letters, 2006.

5. Headache Classification Committee of the International Headache Society, “Classification and Diagnostic Criteria for Headache Disorders, Cranial Neuralgias and Facial Pain”, Cephalalgia, Vol. 8, Suppl. 7, pp. 13-96, 1988.

6. Campbell, J. K. and R. J. Caselli, “Headache and Other Craniofacial Pain: Neurology in Clinical Practice”, Vol. 2, Butterworth-Heinemann, 1991.

7. Lauritzen, M., “Cerebral Blood Flow in Migraine and Cortical Spreading Depression”, Acta Neurol Scand Suppl., Vol.76, pp. 1-40, 1987.

8. Lauritzen, M., “ Cortical Spreading Depression in Migraine ”, Cephalalgia, Vol. 21, Issue 7, pp. 757, 2001.

9. Wolf, T., U. Lindauer, H. Obrig, J. Dreier, T. Back, A. Villringer and U. Dirnagl, “Systemic Nitric Oxide Synthase Inhibition Does Not Affect Brain Oxygenation During Cortical Spreading Depression in Rats: A Noninvasive Near-Infrared Spectroscopy and Laser-Doppler Flowmetry Study”, Journal Cerebral Blood Flow Metabolism, Vol. 16, pp. 1100-1107, 1996.

10. Bolay, H., U. Reuter, A. K. Dunn, Z. Huang, D. A. Boas and M. A. Moskowitz, "Intrinsic Brain Activity Triggers Trigeminal Meningeal Afferents in a Migraine Model", Nature Medicine, Vol. 8, No.2, pp. 136-142, February 2002.

11. Lauritzen, M., T. S. Olsen, N. A. Lassen and O.B. Paulson, "Regulation of Regonal Cerebral Blood Flow During and Between Migraine Attacks", Ann Neurology, Vol. 14, pp. 569-572, 1983.

12. Shinoura, N. and R. Yamada, "Decreased Vasoreactivity to Right Cerebral Hemisphere Pressure in Migraine Without Aura: A Near-Infrared Spectroscopy Study", Clinical Neurophysiology, Vol. 116, pp. 1280–1285, 2005.

13. Friston, K. J., A. Mechelli, R. Turner and C. J. Price, "Nonlinear Responses in fMRI: The Balloon Model, Volterra Kernels, and Other Hemodynamics", NeuroImage, Vol. 12, pp. 466–477, 2000.

14. Buxton, R. B., E. C. Wong and L. R. Frank, "Dynamics of Blood Flow and Oxygenation Changes During Brain Activation: The Balloon Model", Magnetic Resonance in Medicine, Vol. 39, pp. 855-864, 1998.

15. Zheng, Y., D. Johnston, J. Berwick, D. Chen, S. Billings and J. Mayhew, "A Three-Compartment Model of the Hemodynamic Response and Oxygen Delivery to Brain", NeuroImage, Vol. 28, pp. 925 – 939, 2005.

16. Buxton, R. B., K. Uludağ, D. J. Dubowitz and T. T. Liu, "Modeling the Hemodynamic Response To Brain Activation", NeuroImage, Vol. 23, pp. 220–233, 2004.

17. Akgül, C. B., B. Sankur and A. Akın, "Extraction of Cognitive Activity Related Signals from Functional Near-Infrared Signals", submitted to EUSIPCO 2006.

18. Toronov, V., S. Walker, R. Gupta, J. H. Choi, E. Gratton, D. Hueber and A. Webb, "The Roles of Changes in Deoxyhaemoglobin Concentration and Regional Cerebral Blood Volume in the fMRI BOLD Signal", NeuroImage, Vol. 19, pp. 1521–1531, 2003.

19. Fantini, S., “A Haemodynamic Model For the Physiological Interpretation of In Vivo Measurements of the Concentration and Oxygen Saturation of Haemoglobin”, Phys. Med. Biol., Vol. 47, pp. 249–257, 2002.

20. Grubb, R. L., M. Raichle and J. O. Eichling, Ter-Poggosian, M. M., “The Effects of Changes in $PaCO_2$ on Cerebral Blood Volume, Blood Flow, and Vascular Mean Transit Time”, Stroke, Vol. 5, 1974.

21. Fletcher, J. E., “A Model Describing the Unsteady Transport of Substrate to Tissue From the Microcirculation”, J. App. Math., Vol. 29, No. 3, November 1975.

22. Gutierrez, G., “The Rate of Oxygen Release and Its Effect on Capillary O_2 Tension: A Mathematical Analysis”, Respiration Physiology, Vol. 63, pp. 79-96, 1986.

23. Lodi, C. A., M. Ursino, A. T. Minassian and L. Beydon, “A Mathematical Model of Intracranial Pressure and Cerebral Hemodynamics Response to CO_2 Changes”, Transactions on Biomedicine and Health, Vol. 4, 1997.

24. Gutierrez, G., “A Mathematical Model of Tissue–Blood Carbon Dioxide Exchange during Hypoxia”, Am J of Respir Crit Care Med, Vol. 169, pp. 525–533, 2004.

25. Dash, R. K. and J. B. Bassingthwaighte, “Simultaneous Blood–Tissue Exchange of Oxygen, Carbon Dioxide, Bicarbonate, and Hydrogen Ion”, Annals of Biomedical Engineering, Vol. 34, No. 7, pp. 1129–1148, July 2006.

26. Izzetoglu, K., S. Bunce, M. Izzetoglu, B. Onaral and K. Pourrezaeil, “ fNIR Spectroscopy As a Measure of Cognitive Task Load ”, Proceedings of the 25th Annual lnternational Conference of the IEEE EMBS Cancun, Mexico, 3431-3434, . September 17-21,2003.

27. Chance, B., E. Anday, S. Nioka, S. Zhou, L. Hong, K. Worden , C. Li, T. Murray, Y. Ovetsky, D. Pidikiti and R. Thomas, “A novel method for fast imaging of brain function, non-invasively, with light”, *Optics Express,* 1998.

28. Villringer A. and B. Chance, “Non-invasive optical spectroscopy and imaging of human brain function”, *Trends in Neuroscience*, Vol. 20, 435-442, 1997.

29. Akın, A., D. Bilensoy, U. E. Emir, M. Gülsoy, S. Candansayar and H. Bolay, "Cerebro-vascular dynamics in patients with migraine: Near-infrared spectroscopy study", Neuroscience, Vol. 400, pp. 86–91, 2006.

30. Lippincott's Biochemistry, Illustrated Review Series, pp. 28, 1997.

31. Bilensoy, D., "Cerebrovascular Dynamics In Migraine Measured with fNIRS", M.S. Thesis, Boğaziçi University, 2005.

32. Kemper, R., "Modelling Trigeminovascular Pain in the Unrestrained Rat: An Approach to a Better Understanding of Migraine Headache", Ph.D. Thesis, Groningen University, 1999.

33. Gersten, A., "Evaluation of the Extension of the Cerebral Blood Flow and its Main Parameters", Department of Physics, Ben-Gurion University of the Negev, Unit of Biomedical Engineering, Zlotowski Center for Neuroscience,

34. http://www.merckmedicus.com/

35. http://www.migraine.ie/

36. http://www.headachecare.com/

37. http://neuro.med.harvard.edu/

38. http://www.neurologie.uni-duesseldorf.de/

39. http://www.wikipedia.com/